

Elisabet Syverud

Axial Compressor Performance Deterioration and Recovery through Online Washing

Thesis for the degree of doktor ingeniør

Trondheim, May 2007

Norwegian University of
Science and Technology
Faculty of Engineering Science and Technology
Department of Energy and Process Engineering

NTNU
Norwegian University of Science and Technology

Thesis for the degree of doktor ingeniør

Faculty of Engineering Science and Technology
Department of Energy and Process Engineering

©Elisabet Syverud

ISBN 978-82-471-1870-2 [printed ver.]
ISBN 978-82-471-1884-9 [electronic ver.]
ISSN 1503-8181

Theses at NTNU, 85

Printed by Tapir Uttrykk

Elisabet Syverud

***Axial Compressor Performance Deterioration
and Recovery through Online Washing***

Abstract

Gas turbine performance deterioration can negatively affect overall production capacity of power plants and cause major economic losses. Gas turbines deteriorate from fouling in the compressor section, and online washing is often applied to recover their performance. The success of online washing depends on site-specific issues, and current systems are inconsistent in use and their effectiveness is difficult to test. The objective of this work is to determine the fundamental mechanisms of axial compressor performance deterioration and recovery through online washing.

Empirical data from online washing of RB211-24G at an offshore site were analyzed in the initial phase of research. Empirical data from accelerated salt deterioration and online water washing of a GE J85-13 jet engine were unique to this project. First overall compressor deterioration and single stage performance deterioration were measured using inter-stage gas path instrumentation. Secondly, salt deposits were analyzed to characterize the stage surface roughness and fouling distribution. Finally, recovery through online washing was evaluated. Quasi-one-dimensional models were developed for the GE J85-13 to aid in the test data analysis and to verify the applicability of deterioration loss models to fouled compressors.

The study shows that detection of compressor deterioration can be hampered by nonlinear sensitivities to fouling. Engine control modes must be accounted for to avoid misreading the deterioration rate and production capacity. Flow rate was found as the most sensitive deterioration parameter in the GE J85-13. Fouling affected all parts of the stage characteristics reducing flow, pressure and head. The models successfully reflected the deterioration mechanisms although the effects of deterioration were under-predicted. This study shows the importance of applying Reynolds corrections to deteriorated compressors.

Online washing efficiency is predominantly affected by the water flow rate. Small droplets and low flow rates increase the fouling in the aft stages, and increased injection time cannot compensate for low flow rates. For effective water washing of the entire compressor section the recommended water-to-air ratio is between 0.8 to 2%.

The major contributions of this work are presented in four papers contained in the Appendices.

Acknowledgements

The project is part of a long-term initiative by Statoil and NTNU for optimized offshore gas turbine operations. The project is financed by Statoil ASA and Dresser-Rand Norwegian Operations in a 6:1 split, respectively. The Royal Norwegian Air Force allowed access to their Kjeller test facilities and a GE J85-13 jet engine. The Royal Norwegian Navy supported the experimental work and the presentation of the work at international conferences. The work would not have reached conclusion without the combined efforts of these organizations.

I thank my advisor Professor Lars E. Bakken who in strenuous times celebrated my accomplishments and searched for future challenges, without dwelling on lost opportunities. His great sense of humor combined with professionalism has often left me lighthearted and highly motivated.

Statoil is graciously acknowledged for their financial support and for giving access to operational data from offshore installations. I thank Kyrre Langnes who introduced me to the subject and gave vital support throughout the work.

I thank Dresser-Rand for allowing access to their workshop resources. Hans Haugen and Stein Aanensen helped me with the design and building of test equipment. I also thank Dresser-Rand for allowing me a part time position after my financial well dried out.

The Royal Norwegian Air Forces generously allowed access to their test facilities. I express my gratitude to Hans K. Henriksen for his heartfelt enthusiasm. His in-depth knowledge of the test facilities was invaluable.

I thank Geraldine Jordet, of the Technological Institute Laboratory Services, who taught me methods for non-destructive testing of salt deposits.

I thank my co-authors and fellow students who have challenged me and pushed my work forward. Olaf Brekke, with his operational background and structured mind, was essential in the planning of the tests and in the publication of the work.

I thank my colleagues and friends for their continued interest and support which have motivated me to finish this thesis. Peter M. Campbell read the manuscript and gave valuable feedback in the final stages.

Finishing a PhD dissertation is a lone climb. Although I've tried to minimize the strains on my family, I know that I have been absent-minded with my mind stuck in the world of gas turbines. I thank my husband Pål and our sons Espen, Håkon and Andreas for their patience and support. My gratitude also goes to my family who always believe in me.

List of Papers

- I. Syverud, E., Bakken, L.E., Langnes, K. and Bjørnås, F., 2003
“Gas turbine operation offshore; Online compressor wash at peak load”,
Proc. ASME Turbo Expo: Land, Sea & Air, 16-19 June 2003, Atlanta, GA,
USA, ASME Paper No. 2003-GT-30871.

- II. Syverud, E., Brekke, O. and Bakken, L.E., 2007
“Axial compressor deterioration caused by saltwater ingestion”,
J. of Turbomachinery, Vol.129, No.1, pp. 119-126, January.
 - Presented at the ASME Turbo Expo 2005 on 8 June 2005 in Reno NV,
USA. Printed in the Proceedings of ASME Turbo Expo 2005, ASME
Paper No. GT2005-68701.
 - Presented by O. Brekke at the 35th Turbomachinery Symposium on
27September 2006 in Houston, TX, USA. Published in the 35th
Turbomachinery Symposium Proceedings.

- III. Syverud, E. and Bakken, L.E., 2007
“Online water wash test of GE J85-13”,
J. of Turbomachinery, Vol.129, No.1, pp. 136-142, January.
 - Presented at the ASME Turbo Expo 2005 on 8 June 2005 in Reno NV,
USA. Printed in the Proceedings of ASME Turbo Expo 2005, ASME
Paper No. GT2005-68702.
 - Presented by O. Brekke at the 35th Turbomachinery Symposium on
27September 2006 in Houston, TX, USA. Published in the 35th
Turbomachinery Symposium Proceedings.

- IV. Syverud, E. and Bakken, L.E.
“The impact of surface roughness on axial compressor performance
deterioration”,
Proc. GT2006 ASME Turbo Expo: Power for Land, Sea and Air 2006, 8-11 May
2006, Barcelona, Spain, ASME Paper No. GT2006-90004, 2006.
 - Presented at the ASME Turbo Expo 2006 on 8 May 2006 in Barcelona,
Spain.

Contents

Abstract.....	i
Acknowledgements	iii
List of Papers.....	v
Contents.....	vii
List of Figures	ix
List of Tables.....	xiii
Nomenclature	xiv
1 Introduction	1
1.1 Axial compressor performance deterioration.....	3
1.2 Online compressor cleaning.....	6
1.3 Scope of work	8
1.4 Work outline.....	9
1.5 Limitations	10
1.6 Thesis outline	11
2 Compressor deterioration mechanisms	13
2.1 Fundamental compressor loss mechanisms	13
2.2 Surface roughness on fouled surfaces.....	18
2.3 Influence of fouling on compressor loss mechanisms.....	20
2.4 Overall compressor loss model.....	25
2.5 Quasi-one-dimensional compressor model.....	25
2.6 Conclusions	27
3 Online compressor washing mechanisms	29
3.1 Fluid flow rate (water-to-air ratio).....	30
3.2 Fluid temperature	31
3.3 Droplet size	33
3.4 Droplet velocity and slip.....	36
3.5 Duration and washing frequency	37
3.6 Spray pattern	38
3.7 Conclusions	38
4 Test equipment and methods.....	41
4.1 Test of RB211-24G gas turbine	41
4.2 Test of GE J85-13 jet engine.....	41
4.3 Methods for characterizing compressor fouling	50
4.4 Conclusions	54

5	Performance Deterioration and Recovery.....	55
5.1	Quantify fouling distribution and surface structure.....	55
5.2	Validity of stage performance deterioration models.....	56
5.3	Compressor performance deterioration signature.....	56
5.4	Recovering performance with online washing.....	58
6	Conclusions and Recommended work.....	63
6.1	Conclusions.....	63
6.2	Recommended work.....	65
7	Perspectives of online washing.....	67
8	References.....	69
	Appendix A Paper I on Online washing at Heidrun.....	77
	Appendix B Paper II on Compressor Deterioration.....	91
	Appendix C Paper III on Online Washing of GE J85-13.....	101
	Appendix D Paper IV on Modeling Losses Due to Surface Roughness.....	111
	Appendix E GE J85-13 Measurement Error Analysis.....	125
	Appendix F GE J85-13 Test Matrix and Test Repeatability.....	133
	Appendix G GE J85-13 Compressor Geometry and Stage Characteristics.....	137
	Appendix H GE J85-13 Compressor Performance in Clean Conditions.....	143
	Appendix I GE J85-13 Deteriorated Stage Performance.....	147
	Appendix J GE J85-13 Recovered Stage Performance.....	157

List of Figures

Figure 1 Example of heavy dust fouling in axial compressor [62].....	4
Figure 2 Reported gas turbine degradation	4
Figure 3 Relative gas turbine capacity with online wash [44].....	7
Figure 4 Howell’s breakdown of losses [24]	14
Figure 5 Boundary layer development on suction side of compressor blade	15
Figure 6 Moody diagram of resistance [81].....	16
Figure 7 Definition of surface roughness parameter [80].....	19
Figure 8 Comparison of the Koch&Smith data to the Moody diagram.....	21
Figure 9 Momentum thickness of NACA 65-(6)10 profile [65].....	22
Figure 10 Correlation for blockage	24
Figure 11 Effect of roughness on three stage compressor [14]	26
Figure 12 Wet gas path [103].....	29
Figure 13 Measured temperatures at inlet an outlet of a six stage compressor [96]...	32
Figure 14 Calculated temperature variations along compressor mean-line [96].....	32
Figure 15 Motion of droplets in a rotor row [103].....	33
Figure 16 Droplet sizes applied in washing and fogging systems	35
Figure 17 GE J85-13 stage work characteristics.....	42
Figure 18 GE J85-13 with test equipment mounted in the inlet screen.....	42
Figure 19 GE J85-13 casing with extra temperature sensors (top view).....	46
Figure 20 GE J85-13 compressor cross-sectional view with temperature sensors.....	46
Figure 21 Stage six temperature measurements during water injection	48
Figure 22 Salt deposits on the third stage stator vanes	51
Figure 23 Microscope images of second stage leading edge deposits.....	51
Figure 24 Application of Struer’s replicas to collect salt grains.....	53
Figure 25 Dissolving salt on the first stage stator vanes.....	53
Figure 26 Temperature change from dry to wet conditions at different flow rates	59
Figure 27 Temperature change from dry to wet conditions at different droplet sizes	61
Figure 28 Gas path temperature profiles [40]	128

Figure 29 Effect of variation in temperature recovery factor on the stage work.....	130
Figure 30 Salt deposits on first stage temperature sensor	130
Figure 31 Repeatability of clean and degraded condition.....	134
Figure 32 Repeatability of stage work coefficient, stages one to four.....	135
Figure 33 Repeatability of stage work coefficient, stage five to eight	136
Figure 34 GE J85-13 compressor geometry.....	138
Figure 35 GE J85-13 mean-line geometry	138
Figure 36 GE J85-13 mean-line rotor blade geometry	139
Figure 37 GE J85-13 mean-line stator vane geometry	139
Figure 38 GE J85-13 mean-line rotor blade solidity and thickness-to-chord ratio ..	140
Figure 39 GE J85-13 mean-line stator vane solidity and thickness-to-chord ratio ..	140
Figure 40 Stage efficiencies	141
Figure 41 Stage total pressure coefficients	141
Figure 42 Gas properties (air and vapor mixture).....	143
Figure 43 GE J85-13 compressor temperatures (clean condition).....	144
Figure 44 GE J85-13 compressor pressures (clean condition)	144
Figure 45 GE J85-13 compressor air velocities (clean condition).....	145
Figure 46 GE J85-13 Reynolds number and Mach number (clean condition)	145
Figure 47 Stage one deteriorated performance	148
Figure 48 Stage two deteriorated performance	149
Figure 49 Stage three deteriorated performance	150
Figure 50 Stage four deteriorated performance	151
Figure 51 Stage five deteriorated performance	152
Figure 52 Stage six deteriorated performance	153
Figure 53 Stage seven deteriorated performance	154
Figure 54 Stage eight deteriorated performance	155
Figure 55 Dataset 1, stage one to four.....	158
Figure 56 Dataset 1, stage five to eight.....	159

Figure 57 Dataset 2, stage one to four.....	160
Figure 58 Dataset 2, stage five to eight.....	161
Figure 59 Dataset 3, stage one to four.....	162
Figure 60 Dataset 3, stage five to eight.....	163

List of Tables

Table 1 Equivalent sand roughness of regularly spaced spheres [81]	19
Table 2 Recommended water-to-air-ratios for aeroderivative gas turbines.....	30
Table 3 Minimum water droplet velocity.....	37
Table 4 Limits for online washing parameters.....	39
Table 5 Online washing system data.....	44
Table 6 Parameters for detecting GE J85-13 compressor deterioration [18].....	50
Table 7 Summary of methods to quantify compressor salt deposits	54
Table 8 Measurement uncertainties	126
Table 9 Gas path blockage due to temperature sensors	127
Table 10 Temperature profile error.....	128
Table 11 GE J85-13 test matrix.....	133
Table 12 Specification of datasets for recovered performance.....	157

Nomenclature

<u>Symbol</u>	<u>Description</u>	<u>Unit</u>
A	Flow area	m ²
B	Blockage	--
c	Chord length	m
D	Droplet size	μm
k	Peak roughness parameter, grain size	μm
k _s	Equivalent sand roughness	μm
<i>m</i>	Mass flow rate	kg/s
M	Mach number	--
N	Shaft speed	rpm
p	Pressure	kPa
R	Blade radius	m
R _a	Average value of all roughness elements, Figure 7	m
Re	Reynolds number	--
T	Temperature	K, °C
U	Blade velocity	m/s
V	Air velocity	m/s
w/a	Water-to-air ratio (mass based)	kg/kg
We	Weber number	--
y	Roughness parameter, see Figure 7	m

Greek symbols

<u>Symbol</u>	<u>Description</u>	<u>Unit</u>
η	Isentropic efficiency	--
λ	Darcy friction factor	--
θ	Momentum thickness	m
ρ	Air density	kg/m ³
Ψ ^T	Stage work coefficient, defined in Paper II	--
Ψ ^P	Stage pressure coefficient, defined in paper IV	--
Φ	Flow coefficient, defined in Paper II	--
σ	Surface tension	dyne/cm

Subscripts

<u>Symbol</u>	<u>Description</u>
s	Static condition
t	Total condition
v _{0.9}	90 % of the total liquid volume is in drops of smaller diameter
x	Axial velocity component

Compressor numbering system

<i>Symbol</i>	<i>Description</i>
2.1	Compressor stage 1
2.3	Compressor stage 3
2.4	Compressor stage 4
2.5	Compressor stage 5
2.6	Compressor stage 6
3	Compressor discharge

Acronyms

<i>Symbol</i>	<i>Description</i>
ASME	American Society of Mechanical Engineers
GE	General Electric
IGV	Inlet guide vanes
ISO	International Organization for Standardization
LE	Leading edge of blade or vane
OGV	Outlet guide vanes
NACA	National Advisory Committee for Aeronautics
NASA	National Aeronautics and Space Administration
PS	Pressure side (concave) of blades and vanes
RNoAF	Royal Norwegian Air Force
RTD	Resistance temperature detector
SS	Suction side (convex) of blades and vanes
TE	Trailing edge of blade or vane
VMD	Volume median diameter

1 Introduction

Global energy needs will grow steadily for at least the next 25 years. The world's primary energy demand is expected to be more than 50% higher in 2030 than in 2005. More than two-thirds of this growth is expected to come from developing countries, and fossil fuels are expected to meet more than 80% of the projected increase in primary energy demand. The natural gas demand, which is primarily driven by power generation, will have the fastest growth rate, overtaking coal as the world's second-largest primary energy source before 2015. Oil will remain the single largest fuel with two-thirds of the increase coming from the transport sector [15].

Analysis of power plant data compiled by the World Energy Council has shown a substantial gap between the worldwide average performance and that being achieved by top performing plants. It has been estimated that eliminating this gap would result in savings of US\$80 billion per year. Since the existing plants could operate with higher performance and availability, there would be less need for additional capacity. Moreover, this improvement is expected to reduce annual emissions by 1 billion ton carbon dioxide, which is approximately 4 % of annual global emissions [104].

Industrial gas turbines, first demonstrated by Ægidius Elling in 1903 [11], are the prime movers of power plants. Gas turbines are also used for aircraft engines, ship propulsion systems, and in industrial applications as prime movers of gas compressors, liquid pumps, and electric generators. Currently, close to 200 gas turbines are serving the Norwegian oil and gas industry. In 2004, the authorities and the industry collaborated on a study of the potential for more efficient power supply on the Norwegian continental shelf. The study concluded that a realistic, although ambitious, estimate of potential emission reductions was between five and ten percent over a period of ten years. This can be achieved if the industry systematically develops, tests, and implements new technology and energy management in all aspects of the operations [25].

Gas turbines involved in offshore oil and gas production have a large economic potential to keep performance and availability at the highest level possible. For the Statoil Heidrun field, a power loss of 1 % reduces the annual production by USD \$34 million [Paper I, updated with data from reference 71 and 88].

All gas turbines experience loss of performance over time. Performance deterioration is caused by many different factors such as erosion of blade surfaces due to particle ingestion, fouling due to airborne pollution or oil vapors, blocking of cooling holes and labyrinth seals, and foreign object damage. Deterioration is generally referred to as either recoverable by routine maintenance actions or non-recoverable except by replacement of degraded engine components. Recoverable performance loss is associated with loss of axial compressor performance due to the fouling of internal surfaces by airborne contaminants. These contaminants are deposited on the front

surfaces of the inlet shroud and the internals gas path of the axial compressor, causing an overall reduction in the power capacity, an increase in the specific fuel consumption and emissions production, and a reduction in time between overhaul. In this study, considerations of axial compressor deterioration are restricted to the removable deposits which do not cause any permanent damages to the internal surfaces.

Historically, compressor cleaning was first attempted by injecting solid particles such as nutshells or rice. Since the introduction of coated compressor blades, this method has been avoided due to concerns of pitting corrosion [86].

The state-of-the art method for removing fouling is a liquid wash in which a wash fluid is injected at the front end of the gas turbine. The wash fluid penetrates the gas path where it dissolves and removes the fouling. There are presently two washing methods in use for liquid washing: offline wash and online wash.

In offline washing, the gas turbine is run at sub-idle shaft speeds while a cleaning solution is injected into the engine. This method is well-proven and effective in removing deposits not only in the axial compressor but also on the interior surfaces of the entire gas path. Before an offline wash, the gas turbine unit must be shut down and cooled to avoid excessive thermal loading of the internal gas turbine components. This causes loss of availability and possibly production losses. For the Statoil Heidrun field, the six hours production shutdown associated with an offline wash will cost the operator on the order of US \$2.3 million [Paper I, 71, 88].

Online washing is done during gas turbine operation by injecting the cleaning solution into the compressor section while the engine is running in normal operation, hence avoiding the associated down-time cost. The potential savings that can be gained from efficient online compressor cleaning have led a number of companies to install such systems. Online washing is often combined with off-line washing to optimize uptime while maintaining an acceptable thermal efficiency. Cost of fuel and lost production are the predominant economic factors in determining the time between off-line washes.

Manufacturers and operators of gas turbines have tried to quantify the effect of online water wash systems with respect to reduced degradation, increased regularity and increased production. However, field testing is challenging, and the degradation rates are continuously changing due to environmental conditions, over which the operator has limited influence. Hence, the test results are often difficult to compare and provide limited conclusions to the overall phenomena of deterioration mechanisms and performance restoration.

The success of online cleaning appears to depend on site-specific issues such as the gas turbine operating profile and the nature of the deposits. Improper use of online

cleaning may further deteriorate gas turbine performance and increase fouling, both in the gas path and in the cooling air passages.

This doctoral project was initiated from a need to understand when and how to use online cleaning on offshore gas turbines to avoid power losses and to ascertain maintenance intervals that optimize energy use. Fundamental issues concerning gas turbine deterioration and online washing are emphasized in this study.

1.1 Axial compressor performance deterioration

Axial compressors are an integrated part of the gas turbine. The compressor consists of several stages of airfoils circumferentially positioned on a rotor driven by a turbine. The purpose of the compressor is to increase the total pressure of the gas stream with minimum power absorbed. Axial compressors consume up to 60 % of the produced turbine power, therefore maintaining the compressor at its optimum performance during operation is of major importance.

During operation, the axial compressor will be deteriorated by airborne particles adhering to the internal surfaces. The first stages of an axial compressor will normally be the ones most heavily fouled, although deposits will have different characteristics depending on the nature of the contamination. Dry particles in dry atmospheres are likely to deposit in different areas depending on the location of sticky material and oily compounds. At high inlet humidity, the drop in static pressure during acceleration of the air through the compressor will increase dust adhesion on the blades because of the condensing water.

Fouling restricts flow and causes increased boundary layer thickness both on the blades and along the endwalls of the annulus and hub. Figure 1 shows an example of the deposits found in the air intake of an industrial engine [62]. Offshore installations typically have less fouling than seen in Figure 1. Blockage of the air path and increased frictional losses reduce the compressor head and flow, causing an overall reduction in the power capacity and an increase in the specific fuel consumption.

The deterioration rate will depend on the level of airborne contaminants present at the installation site and the efficiency of the air intake filters. Experience indicates a tendency for the degradation rate to be highest during initial operation, declining exponentially with operating hours and stabilizing after a given time. Figure 2 illustrates the large spread in reported data on degradation rate within the first 4000 operating hours. The inconclusive degradation trends seen in Figure 2 are caused by different environmental conditions in which gas turbines operate. Recoverable losses, attributable to compressor fouling, typically account for 75 % to 80 % of the total performance losses [12]. Up to 20% permanent degradation is claimed for industrial gas turbine engines over a 30000 hours operating time [62], although 2 % 6 % degradation is more typical [9].



Figure 1 Example of heavy dust fouling in axial compressor [62]

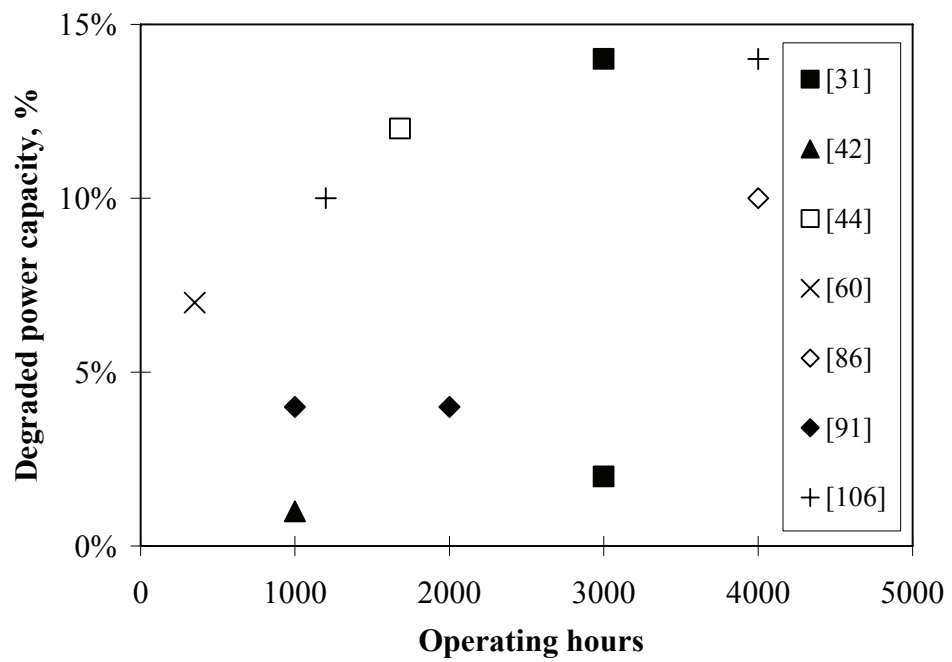


Figure 2 Reported gas turbine degradation

Ambient humidity and lengthy operation in saturated conditions may influence the degradation rate. Varying ambient humidity is found to be the main cause for a widespread disparity in measured power from a 3.1 % loss to a 0.5% gain for the same gas turbine unit over 70 operating hours [86]. On the other hand, long term operation in saturated conditions may cause a natural washing effect due to condensation in the bellmouth and inlet guide vanes.

Fouling is traditionally seen in one or more of the following performance parameters:

- Reduced compressor discharge pressure
- Reduced compressor efficiency
- Increased compressor discharge temperature
- Reduced power output
- Slowing of shaft speed in multi-spool engines
- Onset of compressor stall or surge

Simple monitoring of these parameters reveals unstable trends which are difficult to interpret. Comparative testing in which the data are compared using engine baselines is a minimum requirement for monitoring [47], still the results may be challenging to interpret.

This report will show that fouling changes all aspects of the stage characteristics, causing non-linear shifts in compressor efficiency which hampers decision making. For operation at maximum power, the engine control lines will affect the deterioration rate. If engine mode is not taken into account, the deterioration rate will be misinterpreted.

Filter systems

All industrial and marine gas turbines are equipped with air intake filters that remove most of the airborne particles, but it is common for offshore filter systems to let through particles smaller than 2 μm . The lack of common standards for gas turbine filter system testing makes it very difficult to compare filter systems on an equal basis. State-of-the-art filtration systems are designed to catch even smaller particles using three stage filters with liquid separation, but such systems are not commonly available for offshore retrofit due to the larger cross-sectional area and the substantial weight penalty. It is essential to all filter systems that the air is completely dry when entering the last filter stage. If this is not the case, water soluble dirt will be washed out from the filters and subsequently entered into the gas turbine regardless of the filter efficiency. Stalder has shown that salt can travel through the air filters and will increase the alkali metals in the hot section with subsequent possibility of hot corrosion [87].

To illustrate the problem, the salt load is calculated for a 22 MW gas turbine engine in an offshore environment. The sub 2 μm dry salt particles of air adds to 7.2 kg salt being ingested in the gas turbine in one year, or 20 g salt per day [53]. The

significance of ingesting 20 g salt per day became evident in the initial phases of the GE J85-13 tests: Even 6 g of salt caused significant performance deterioration of the GE J85-13 jet engine while 30 g salt reduced the available power by 10 %. Clearly, the gas turbine would benefit if this salt was removed by the filter system.

1.2 Online compressor cleaning

Wet cleaning of gas turbines is not a new concept: Since 1953, more than 40 patents have been filed related to compressor wet cleaning, two during the first two months of 2007. All major gas turbine manufacturers have recommended practices for wet cleaning and there are standards for use on helicopter engines. Systems are often supplied through the Original Equipment Manufacturers (OEM); in addition there are several independent suppliers of washing equipment [23, 27, 33, 35, 75, 76, 98]. In-house, proprietary research is often limited to nozzle position and wash nozzle design. Review of patents and proposals, and face-to-face discussions with wash system manufacturers are ways to gain insight into the state-of-the-art. Two surveys of online washing systems give good overview of the history and state-of-the art of online washing [67, 86].

Several different wet cleaning philosophies are applied in industry: Some installations limit the wet cleaning to the well established offline washing. Other installations use online washing in addition to offline washing in an attempt to lower the downtime costs of critical installations. Review of the information provides no consensus for online washing of gas turbines. Systems properties such as pressure, temperature and fluid injection rate vary from one system to another. Each system's benefits are backed up with reference to sites where the particular system works. This makes it difficult for operators to choose between the different systems and to find the optimum online cleaning system for their application.

Early work on online compressor washing showed significant improvement in the overall gas turbine performance [44, 72, 94]. A classical example of deterioration rate in a gas turbine with and without online washing is given in Figure 3.

A Statoil-supported study reported potential yearly earnings increases of 4 to 7 times the cost of the wash system [17]. In 1992, Statoil conducted tests of online detergent washing of a GE LM2500 at an offshore installation [22]. The results were not conclusive. Although online washing was partly successful, the associated costs were too large to recommend online washing. Later, Statoil recommended the use of online wash on their gas turbines after extensive laboratory testing showed promising results [32, 42]. However, implementation and use at offshore installations showed no improvements and the results in Figure 3 are not reported on Statoil power plants.

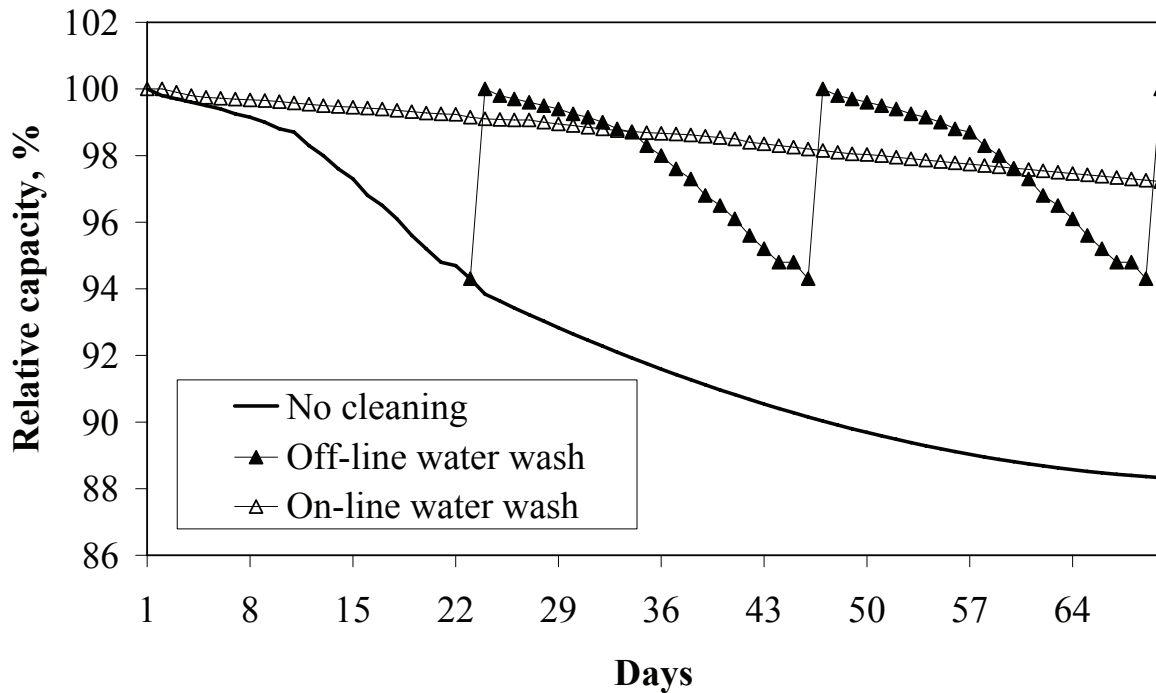


Figure 3 Relative gas turbine capacity with online wash [44]

Chemical additives in the wash fluid dissolve carbonaceous fouling and aid in the solubility of salt deposits. These detergents affect the surface tension and specific gravity of the washing fluid and influence the droplet size and droplet evaporation rate affecting the penetration of the fluid in the axial compressor. There are numerous brands of cleaning detergents and their performances are discussed in several studies. Current wash fluid selection is not conclusive and varies from one operator to another, even for comparable sites and gas turbine types. In a ranking of 44 detergents applied to soil made from engine oil mixed with carbon black, de-ionized water came out number 6 from the top. While water removed 96 % of the fouling, the worst detergent removed only 71 % [105]. De-ionized water should be used for online washing because water residues are shown to cause deposit build-up and increase deterioration rate [39].

This study shows that online washing can be applied effectively if tailored to the axial compressor type. Online washing efficiency is predominantly affected by the water flow rate, and the flow rate should be significantly increased from the currently applied levels. Droplet size is less important. Moreover, the duration of online washing can in many cases be lowered because the fouling will dissolve within the first one to two minutes of cleaning. Longer durations cannot compensate for reduced flow rates.

1.3 Scope of work

The lack of consistency among online washing systems and the difficulties of testing such systems call for a closer look at the different aspects of fouling and online washing of axial compressors.

The objective of this work is to determine the fundamental mechanisms of axial compressor performance deterioration and recovery through online washing.

The objective is broken down in the following goals:

- A** Determine the fundamental compressor deterioration mechanisms by reviewing the literature and standards. Develop models to simulate stage performance deterioration due to fouling. Validate the deterioration loss models using empirical data from the GE J85-13 jet engine.
- B** Determine overall and stage-wise compressor performance deterioration signature by analyzing empirical data from the RB211-24G gas turbine and the GE J85-13 jet engine.
- C** Quantify the compressor fouling by analyzing salt deposits found after accelerated salt testing of the GE J85-13 jet engine.
- D** Determine the fundamental parameters for online compressor washing from a review of the literature and industry practice. Determine the sensitivity of online wash parameters to performance recovery from empirical data of the RB211-24G gas turbine and the GE J85-13 jet engine.

1.4 Work outline

This work is mainly empirical. Quasi-one-dimensional models are developed to aid in the test data analysis and to verify the applicability of deterioration loss models to fouled compressors.

The empirical data is taken from two sources:

- a) Online washing of an RB211-24G offshore installation provided by the operator
- b) Deterioration testing and online washing of a GE J85-13 jet engine in a test cell

The accelerated salt deterioration tests of a GE J85-13 jet engine were unique to this project: Firstly, overall compressor deterioration and single stage performance deterioration were measured using additional gas path instrumentation. Secondly, salt deposits were analyzed to characterize the surface structure and distribution. Finally, recovery through online washing was evaluated. The test planning, instrumentation set-up, data collection, and data analysis comprise the major efforts.

Quasi-one-dimensional models are developed for the GE J85-13. The compressor geometry, stage characteristics and performance data are found in literature. This provides an excellent data source that's usually unavailable. The impact of fouling on stage performance is calculated by applying the measured changes in surface roughness to the loss models. The results are compared to the measured stage performance losses of the fouled compressor to verify the applicability of the models.

The work is presented in four papers, all presented at international conferences and published in conference proceedings or in journals. The papers are attached in the Appendices and contain the major contribution of the work.

Contribution by others

Several people have contributed to this study, and the following clarifies the contributions of the co-authors.

Paper I is based on test data for the RB211. Bakken and Langnes initiated the work and planned the tests at the offshore installation. Parts of the data were analyzed by Bjørnås [16]. My contribution was data validation based on stable operation criteria and measurement uncertainty, and data analysis based on influence of engine controls on deterioration rate.

Paper II contains data from both the initial phase and the main test program of the GE J85-13 tests. The planning of the GE J85-13 tests was done in close cooperation with Brekke who was responsible for the test procedure, data analysis, and documentation of the initial salt deterioration tests. Brekke's thesis [18] is complementary to this work and should be consulted for details on data acquisition, pre-test measurement

uncertainty, and data handling. Brekke's stage models are not used in the present work.

All laboratory analyses of the salt deposits were done in close cooperation with Technological Institute Laboratory Services as part of the present study.

Paper III and IV contain data collected in full in the present study.

1.5 Limitations

This work is limited by the following issues:

- Axial compressor deterioration is restricted to removable fouling which will not cause any permanent damage to the gas turbine.
- All flow measurements are done with standard instrumentation for gas phase properties, while two-phase flow measurements are not covered.
- Two-phase flow of online water washing is studied purely empirically. Two-phase flow theory is not covered in this work.
- Tap water was used for the GE J85-13 online wash experiments. The available tap water was of sufficient quality for the GE J85-13 experiments because of the short time frame involved in these accelerated deterioration tests, where the engine was deteriorated and thoroughly cleaned twice a day.
- The use of chemical additives in the washing fluid is not covered. One of the unresolved issues in the selection of additives is the propagation and temperature increase of the liquid into the axial compressor during operation. This will be studied with the hope that extrapolation to other liquids should be relatively straightforward.
- Degradation models that apply techniques like fuzzy logic are not considered, although modern research is successfully applying these models. The results often lack validation by experimental data.
- Computational fluid dynamics is not covered in this work. These are powerful tools for calculating flow phenomena that are currently being extended to multi-fluid phenomena. The success of these simulations depends on empirical data for model validation. The hope is that the empirical database collected in this study can be used in future models to extend the understanding of fundamental phenomena and to simplify the scaling of data to other gas turbines and operating conditions.

1.6 Thesis outline

The thesis gives the background for the papers, details the experimental setup and summarizes the results. This thesis is written with sufficient documentation to verify, challenge, or disqualify the conclusions.

Chapter 1 introduces the subject of the thesis and defines the scope of work.

Chapter 2 determines the axial compressor deterioration mechanisms and loss models from a review of the literature.

Chapter 3 determines the fundamental parameters of online washing from reviewing the literature and industry practice.

Chapter 4 summarizes the test equipment and methods used in the experimental work and outline the methods used to characterize salt fouling.

Chapter 5 summarizes the findings of the performance deterioration tests, the salt fouling tests, the loss model validation, and the online wash tests as presented in the papers and Appendices.

Chapter 6 gives conclusions and recommendations.

Chapter 7 gives perspectives for the future of online washing.

Appendix A contains **Paper I**. This paper reports the findings of a large test program of online wet cleaning of the RB211-24G gas turbine engine at the Statoil Heidrun offshore installation.

Appendix B contains **Paper II**. This paper reports the findings of the GE J85-13 salt deterioration testing.

Appendix C contains **Paper III**. This paper reports the GE J85-13 online water washing experiments.

Appendix D contains **Paper IV**. This paper reports on the applicability of the loss models to predict the fouling losses in the GE J85-13 compressor.

Appendix E contains the error analysis for the GE J85-13 tests.

Appendix F contains the test matrix and repeatability data for the GE J85-13 tests.

Appendix G contains the GE J85-13 compressor geometry and stage characteristics.

Appendix H contains the GE J85-13 performance data in clean conditions.

Appendix I contains the data on GE J85-13 deteriorated stage performance.

Appendix J contains the data on GE J85-13 recovered stage performance.

The solution to online washing is better filter systems.

(D-R project engineer, fall 2001)

2 Compressor deterioration mechanisms

The purpose of this chapter is to determine the fundamental deterioration mechanisms and the related models from a review of the literature and standards. This supports goal A. This chapter contains the background information for Paper IV.

The chapter reviews fundamental loss mechanisms, discusses surface roughness of fouled surfaces, describes the influence of fouling on the loss mechanisms, and describes the loss models used in the study.

2.1 Fundamental compressor loss mechanisms

Flow in axial compressors is inherently unsteady, turbulent, and fully three-dimensional. Traditional preliminary design practices use one-dimensional models and introduce three-dimensional effects through semi-empirical correlations from cascade testing and full scale compressor design. This gives axial compressors the greatest number of design parameters of all gas turbine components. The preliminary design process is laid out in several books [8, 24, 73, 101] and gives quick results although not very innovative designs. Modern three-dimensional computational fluid dynamic models integrate viscous forces and secondary flow patterns in the calculations and the resulting designs are characterized by advanced three-dimensionally curved blades [66].

Compressor stage performance is defined by the combination of head and efficiency over the flow range. Theoretical stage performance is defined by the Euler equation which is purely a function of geometrical flow turning with no regard to the losses. Losses come from small scale viscous shearing effects in the gas path and cause reduction in the stagnation pressure and increases in the entropy compared to the ideal case. Although physically inseparable, losses are normally treated independently as profile, annulus (or endwall), tip clearance, and secondary losses. Howell's classical breakdown of losses from 1945 is seen in Figure 4 and is still valid. In the following sections, the profile losses are discussed separately while other loss sources are lumped together and discussed as secondary loss sources.

In this work, the axial compressor flow is analyzed in the mean-line blade-to-blade surface in the mid-span meridional plane using preliminary design methods. This is essentially a one-dimensional flow regime although the axis-symmetrical flow has tangential components. Three-dimensional effects are introduced using semi-empirical loss factors applicable to fouled conditions making the models quasi-one-dimensional. Note that in Paper IV, the applied models are described as two-dimensional, but to avoid confusion with traditional notions of two-dimensional throughflow analyses, quasi-one-dimensional is considered a better description and is used in this thesis.

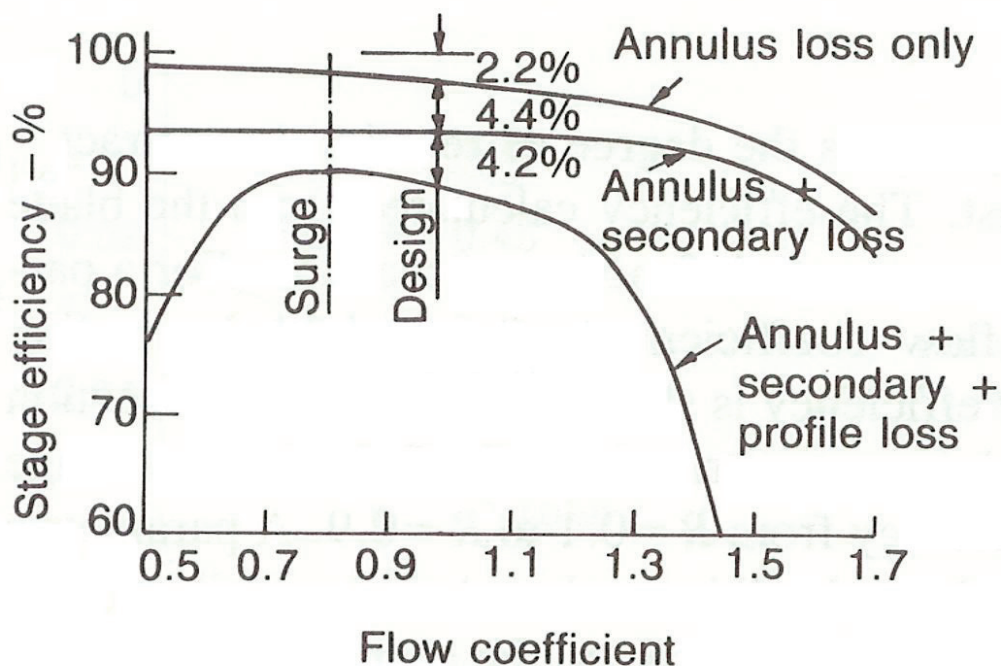


Figure 4 Howell's breakdown of losses [24]

2.1.1 Profile losses

The compressor converts work to head by non-uniform, high velocity flow across the curved blade profiles. The profile losses grow from viscous dissipation by shear work in the flow field. Skin friction sets up boundary layers which normally separate due to flow deceleration and shock formation on the suction side of the curved blade surfaces. The non-uniform flow from the separation process must be mixed out to reduce the wakes and allow proper usage of energy in the downstream flow.

For the simple case of flat plates in steady flow, the boundary layers are characterized by laminar, transitional or turbulent flow. The non-dimensional Reynolds number is used as indicator of the flow condition, and the same general picture is applied to other cases like pipe flow.

The boundary layers are more complex for compressor blades: The flow near the leading edge is quasi-laminar with wake-induced transitional strips extending well into the laminar region as seen in Figure 5. For highly loaded blades, wake induced turbulence can extend to the leading edge [41].

The composite picture found in Figure 5 is simplified in preliminary compressor design by assuming laminar boundary layers at the front of the blade and attached turbulent boundary layers at the aft. The boundary layer condition affects the compressor behavior. For hydrodynamically smooth surfaces the profile losses are found to vary by Re^{-n} , where Re is Reynolds number and n is an empirical correlation depending on Mach number and the mean stage aspect ratio [102]. Further increases to the Reynolds number cause the roughness elements to protrude the laminar sublayer of the turbulent layer. In this hydrodynamically rough condition, losses

become independent of the Reynolds number [80]. This is physically the same phenomenon as seen for rough flat plates and pipes where the friction coefficient is constant at high Reynolds numbers.

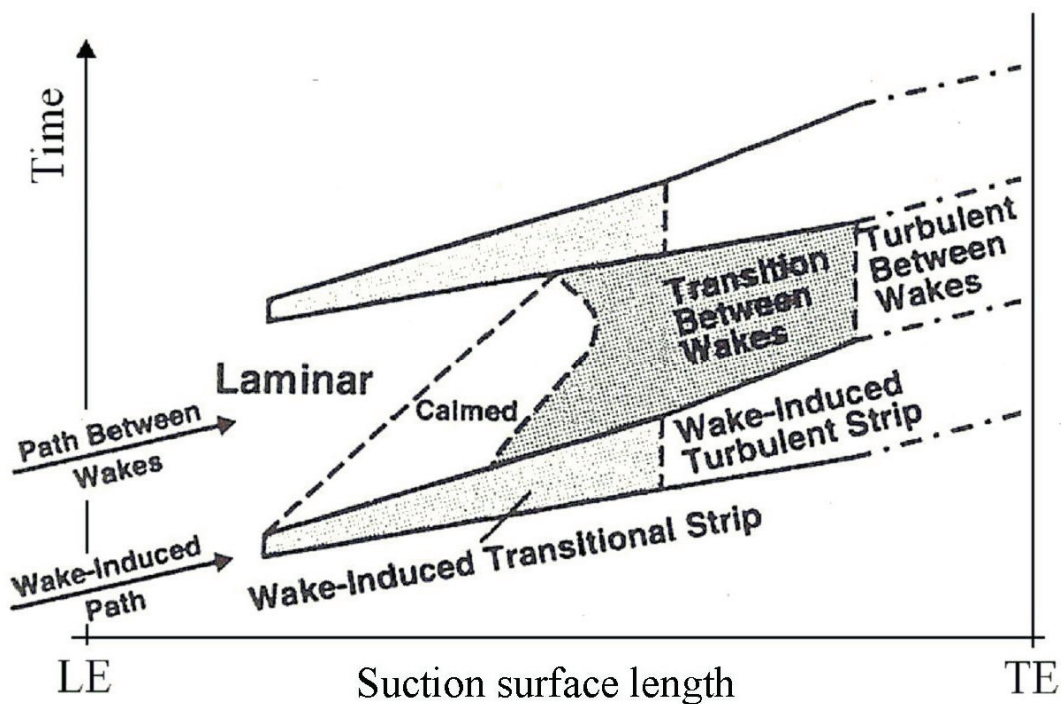


Figure 5 Boundary layer development on suction side of compressor blade (at design point) [41]

The internal hydraulic losses of pipes due to surface roughness were determined in the classic work by Nikuradse [70]. Experiments showed that pipe friction correlated on a scale of relative roughness (which for pipe flow is the ratio of surface roughness height to the pipe inner diameter). Moody converted Nikuradse's data for artificially roughened surfaces to commercial pipes and the results were presented in the Moody diagram seen in Figure 6.

The Moody diagram is applied to axial compressors by replacing the representative length of hydraulic diameter with chord length, and using blade inlet velocity in the Reynolds number. Consequently, in Figure 6, the relative roughness, k_s/c , is defined by the ratio of equivalent sand roughness to chord length which is consistent with axial compressor design. The change in application may alter the relative onset of flow conditions and the challenge is to define the Reynolds number beyond which the surface is hydrodynamically rough and the frictional losses are independent of the Reynolds number, indicated by the stippled line in Figure 6.

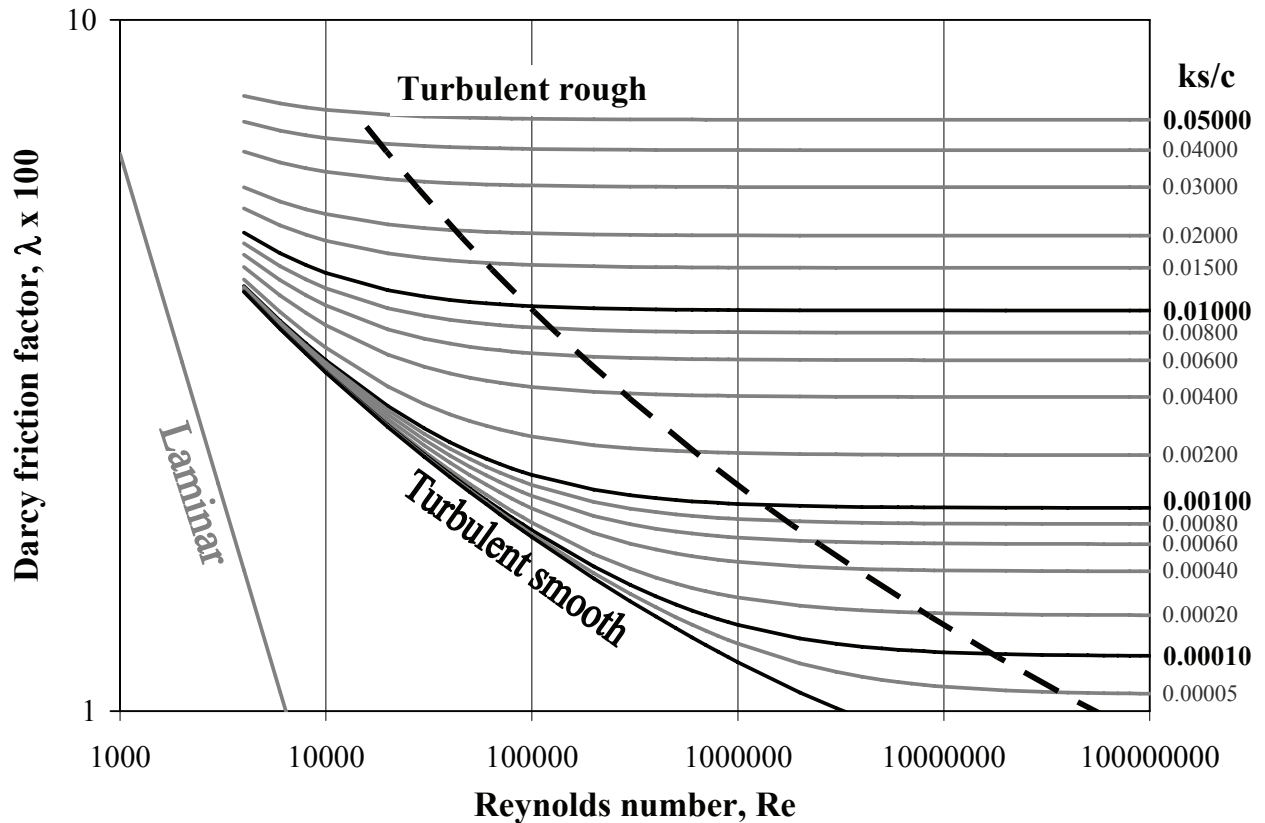


Figure 6 Moody diagram of resistance [81]

Independent studies of axial compressors show that the onset of turbulent rough flow is dependent on surface roughness and flow velocity, but independent of compressor geometry. This is discussed in Paper II, and it was found that the first stage of the GE J85-13 jet engine experiences turbulent rough flow for relative roughness above 0.0002.

Preliminary calculations of blade profile losses rely on Lieblein's empirical correlations of blade profile loss data by the momentum-thickness ratio and the form factor of the wake based on two-dimensional incompressible flow in cascades [55]. Koch&Smith [51] extended the Lieblein correlations to include effects of surface roughness valid for roughness levels associated with manufacturing. The change in momentum thickness was given in a chart that resembles the turbulent part of the Moody diagram.

Paper IV defines the profile loss correlations applied in this work. When applying empirical correlations based on two-dimensional cascade flow to describe a three-dimensional flow field it is essential to choose correlations that are determined using similar blade geometries as used in the compressor. All correlations applied in this work are based on NACA 65-Series profiles.

Flow turning

Flow turning in a compressor passage evolves from the pressure distribution around the blade profiles by which the blade loading balances the centrifugal forces in the flow. Deviation is defined as the difference between the blade trailing edge angle and the mass averaged outlet flow velocity and is normally a small number for unstalled blades. In inviscid flow theory, deviation evolves from the trailing edge condition where pressure must gradually decrease and the blade loading must be zero in order to have a continuous flow field. This results in deviation in the outlet flow for profiles with non-axial camber at the trailing edge.

Although small, the development of the boundary layer will affect the deviation for unstalled blades. Calculations including the boundary layer development for smooth surfaces (design condition), show that deviation is affected by 2-3 degrees for axial-velocity-density ratios below 1.0 [24]. In preliminary compressor design, the deviation angle is determined from the blade geometry and the incidence angle using empirical correlations [69].

In this work, changes to the deviation angle are modeled as changes to the mean-line compressor velocity diagram at the design point.

Shock losses

Profile losses also include shock losses which are characterized by Mach numbers. Mach number effects become evident in high speed flows where the increased air speed on the suction surface reaches sonic speed at the point of maximum diffusion. For high Reynolds number flows, the loss coefficient is unaffected by changes to the Mach number as long as the flow is free of shock waves. When shocks start to form, the profile loss coefficient rises dramatically. In gas turbine performance analysis, data are compared at similar Mach numbers by applying correction factors. Engine control also applies Mach number similarities for variable geometry schedules. Mach number corrections are commonly used, and their theoretical background is described by Volponi [100].

In this work, all test data are compared using corrected data to compare test points at similar Mach numbers and thereby avoiding changing conditions due to shock waves in the flow.

2.1.2 Secondary losses

The presence of a hub and annulus influences the flow across the blade profile and causes secondary flows in the span-wise direction. Both the endwall boundary layers as well as secondary flows are very difficult to predict analytically. Viscous effects in the endwall shear layers are responsible for reductions to the mass flow capacity as well as limiting the maximum pressure rise of the stage.

Endwall losses

Adverse pressure gradients in the compressor set up a boundary layer along the endwalls. The complex flows in the endwall boundary layers are coupled with tip clearance effects which further complicate the calculations, and compressor designers are normally relying on empirical correlations to account for the reduced area available for throughflow. Two different design practices are common: In the British tradition, the work-done factor is used to account for the reduced work input to the stages [46, 73], while the American tradition defines a blockage factor to calculate the area reduction [8]. Blockage is used in this work because the GE J85-13 is an American design and the empirical data exists for blockage only [63].

Blockage is defined by $B = \dot{m} / \int (\rho V_x) dA$ where \dot{m} is the total air mass flow, ρ is the free-stream air density, V_x is the free stream axial air velocity and A is the annulus cross-sectional area. With the notion of free-stream air properties, the flow is assumed to be uniform from hub to tip, neglecting the presence of endwall boundary layers. Blockage is therefore a fraction of the area available for through-flow after subtracting the hub and annulus boundary layer displacement thickness from the overall span length [8, 24].

In this work, blockage is defined as the ratio of actual flow area to the geometric flow area which agrees with GE J85-13 practice [63]. This is 1-blockage as defined above.

3D separation

The endwall boundary layers influence the spanwise flow field and may lead to spanwise separation on the blades and vanes. These effects are influenced by the hub and tip clearances and by surface roughness. Compressors with rising hubs (like the GE J85-13) are especially prone to 3D separations along the hub due to the strong radial forces unloading the hub region of the blades.

In this work, the effects of 3D separation are included as part of the endwall loss mechanisms and covered by the blockage model.

2.2 Surface roughness on fouled surfaces

Fouling alters the surface microstructure. Surface roughness is defined as either the arithmetic average value of all roughness elements, Ra , or the peak roughness parameter, k , defined as the difference between the arithmetic average of the ten highest peaks and the ten deepest grooves per unit length. This is illustrated in Figure 7 [80].

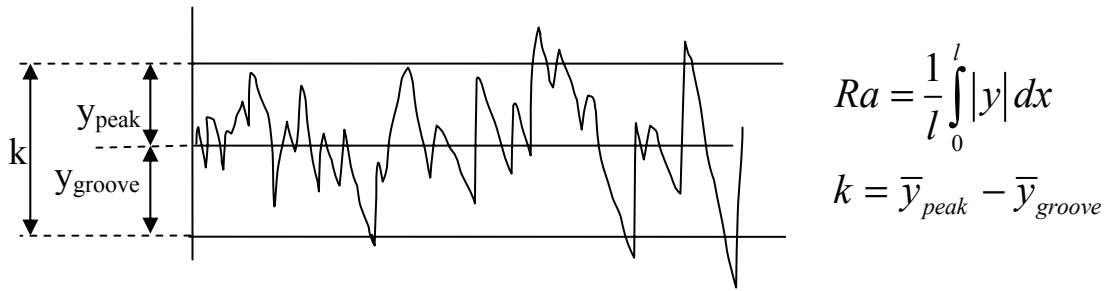
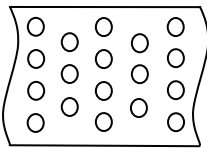


Figure 7 Definition of surface roughness parameter [80]

Two separate studies show that for a forged and electrochemically machined compressor blade the peak roughness parameter is on average 6.2 to 8.9 times larger than the arithmetic average value of all roughness elements [51, 80]. The values are considered to agree due to the difficulties involved in measuring surface roughness [80]. No similar data are found for fouled surfaces. Because the crystal structure found on fouled surfaces is much larger than the grooves and peaks associated with new and clean blades, the actual height of protrusion is assumed equal to the arithmetic average of all crystals found on the surface.

The scale of equivalent sand roughness used in the Moody diagram is challenging to adapt to the distributed crystal structures. In Nikuradse's research on friction, the artificial roughness applied using emery grains is of maximum density [70]. Schlichting [81] adapted Nikuradse's work to applications where the roughness density is much smaller by testing a channel with regularly arranged roughness elements and correlating the results on a scale of equivalent sand roughness. Table 1 gives the result for regularly spaced spheres. Because these data is based on roughness elements glued to the surface, the data should be applicable to situations where the fouling is found as distributed crystals on the surface.

Table 1 Equivalent sand roughness of regularly spaced spheres [81]

<i>Roughness pattern</i>	<i>Distance between spheres (cm)</i>	<i>Diameter of spheres (cm)</i>	<i>Actual height of protrusion, k (cm)</i>	<i>Equivalent sand roughness, k_s (cm)</i>
	4	0.41	0.41	0.093
	2	0.41	0.41	0.344
	1	0.41	0.41	1.26
	0.6	0.41	0.41	1.56
	Densest	0.41	0.41	0.257
	1	0.21	0.21	0.172
	0.5	0.21	0.21	0.759

In this work, the distributed crystal structures found on fouled surfaces correlate to the equivalent sand roughness scale using Table 1 and assuming the actual height of protrusion to be the average height of all roughness elements.

2.3 Influence of fouling on compressor loss mechanisms

In this section, the fundamental compressor loss mechanisms determined in section 2.1 are reviewed to find the influence of fouling in the gas path.

The added surface roughness with fouling influences the boundary layer condition and causes increased skin friction, reduced flow turning, and reduced effective throughflow area. Fouling is assumed to be completely removable and not cause any permanent damages to the geometry, for example leading or trailing edge bluntness, chord changes, or increased tip clearances.

For fouled compressors, the challenge is to find ways to calculate the additional losses imposed in the deterioration process. Deterioration changes the stage mass flow rate, pressure ratio and efficiency. In addition, increased surface roughness may cause narrowing in the operating range through early onset of stall and surge.

Fouling may increase the turbulence in the axial compressor due to unequal distribution of deposits along the circumference. In this work, the turbulence level for clean conditions is assumed to be above critical conditions, and the additional effect of deterioration on turbulence is therefore negligible.

2.3.1 Added profile losses

Surface roughness affects the momentum thickness and thereby the total pressure losses of the blades. The correlations are given in paper IV with the background given below.

Koch&Smith [51] showed the effect of surface roughness and chord Reynolds number on momentum thickness. The data are validated at minimum loss incidence. The data are given in a form similar to the Moody diagram but with marked differences for the effect of relative roughness. Figure 8 compares the Koch&Smith data to the Moody diagram of Figure 6 for similar relative roughness. Above a relative roughness of 0.0005 the difference becomes evident, and the relative change in losses is higher with the Koch&Smith data.

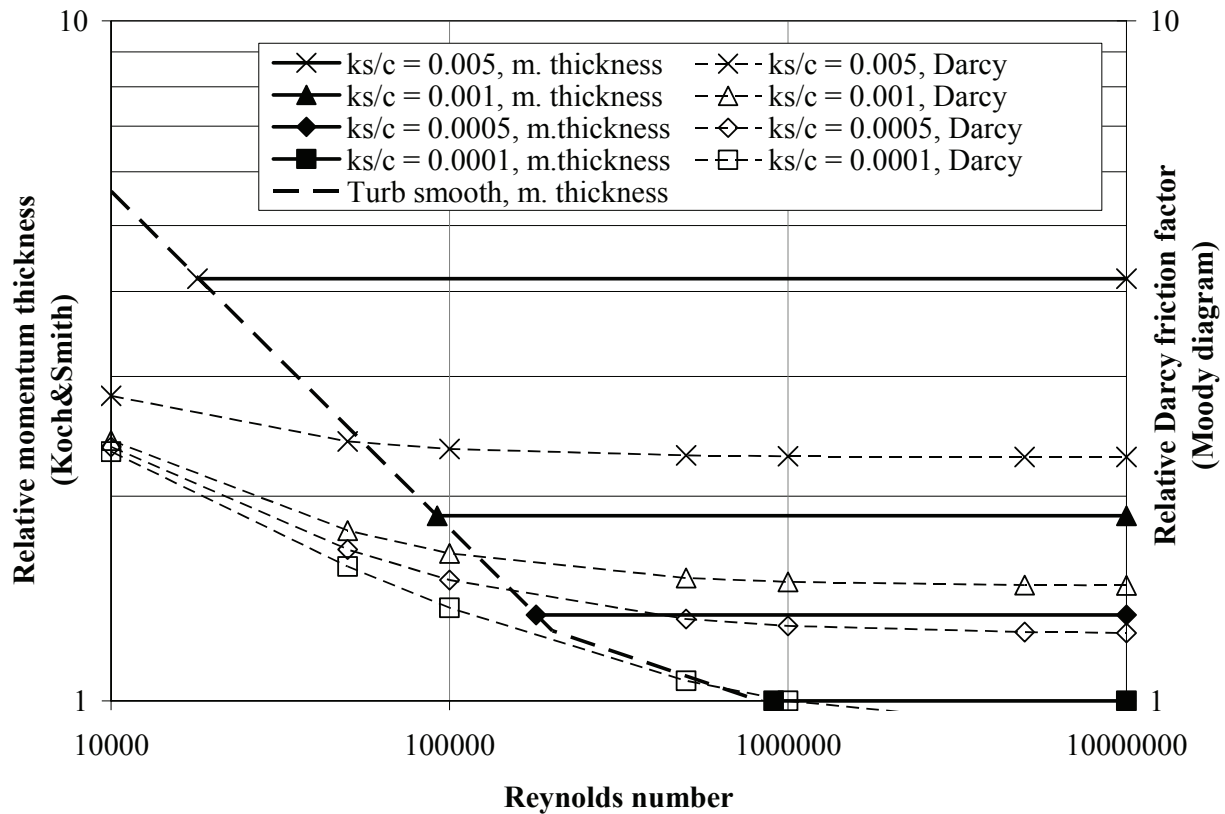


Figure 8 Comparison of the Koch&Smith data to the Moody diagram

The effect of roughness on the momentum thickness of artificially fouled NACA 65-Series cascades was tested by Milsch [65]. Relative roughness ranging from 0.056 to 0.00556 was applied uniformly and completely on the cascade profiles using emery grains. All tests were at low Mach numbers and at minimum loss incidence. Figure 9 shows the momentum thickness related to blade chord for a NACA 65-(6)10 cascade with solidity of 1.33 which resembles the compressor rotor blades of the GE J85-13 jet engine. The momentum thickness is measured at the pressure side and the suction side [13, 65]. In classic boundary layer theory the flow in the laminar regions is independent of roughness. In contrast, Milsch's data [65] shows that the laminar boundary layer thickness depends on the surface roughness because vortices shedding off the roughness grains are sufficiently strong to increase the boundary layer thickness but too weak to cause early transition.

In Paper IV, Milsch's data [65] are compared to the Koch&Smith data and the Darcy friction factor (Moody diagram) for NACA cascades and at roughness levels applicable to the GE J85-13. Milsch's data for pressure side momentum thickness follows the data of the Darcy friction factor, while the suction side momentum thickness follows the Koch&Smith relations for the low camber airfoil.

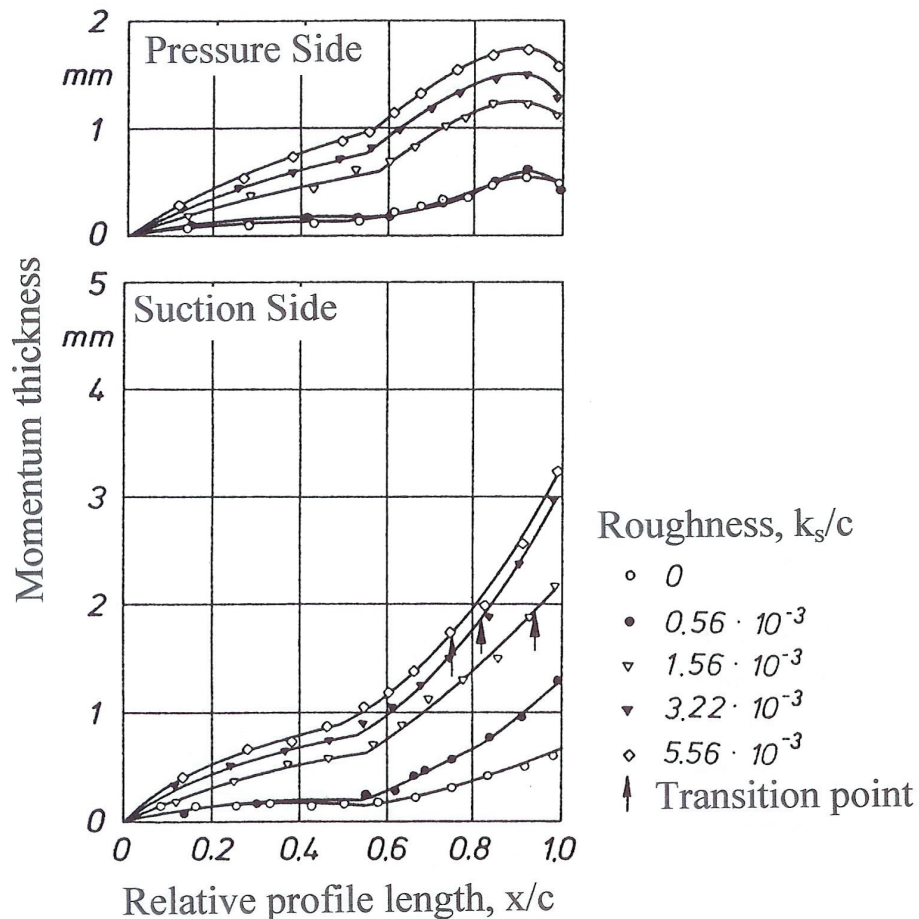


Figure 9 Momentum thickness of NACA 65-(6)10 profile [65]

In this work, the overall change in momentum thickness is modeled using the data from Koch&Smith [51] for the suction side roughness, and the Darcy friction factor for the pressure side. The overall momentum thickness is the sum of the calculated momentum thickness for both surfaces. The correlations are given in Paper IV.

The correlations are used to modify existing stage characteristics based on the additional profile losses calculated for the fouled condition. Hence, it was not necessary to apply the loss equations to establish the stage characteristics for the clean conditions.

Concluding remarks on the profile losses

Calculating profile losses due to deterioration using a quasi-one-dimensional model is not new. Similar models are applied to loss calculations with surface roughness changes [37, 84], geometry changes [38], and manufacturing deviations (including roughness) [59]. This study differs from others by the following factors: firstly, the momentum thickness correlations are different for the suction and pressure side, secondly, the model is applied to existing stage characteristics, and finally, the deviations from clean to fouled conditions are calculated using a measured level of surface roughness (also in [59]).

2.3.2 Deviation changes

Increased surface roughness will affect the pressure distribution, thicken the boundary layers, and thus alter the deviation angle.

Two sources for effect of deviation are found in the literature. The first dataset is based on cascade tests where uniform roughness was added to NACA 65-Series profiles [65], while the second dataset is based on roughness added at the back of an unknown profile [58]. The data are compared and discussed in Paper IV.

Milsch's data [65] represents the best source for modeling deviation in NACA 65-Series profiles and is used in this work. The data applies only to the design point.

2.3.3 Secondary losses

Surface deposits will cause secondary losses by increased endwall boundary layers, changing tip clearances, increased profile thickness and increased 3D separations. These effects are accounted for by blockage which reduces the effective annulus area.

Endwall boundary layers

Surface deposits along the hub and annulus will increase the endwall boundary layer thickness, change the hub-to-tip velocity profile and reduce the volume flow through the compressor.

In this work, the blockage model covers the effect of endwall boundary layers.

3D separation

Increased roughness is known to cause significant 3D separation at the design point of a single stage compressor with inlet guide vanes and controlled diffusion airfoils. Roughness applied in strips of emery paper at the leading edge to peak suction significantly affected the deviation, caused a larger deviation along the hub and a slight reduction at the outer span. For rough surfaces, large 3D separations were found at the design point while for smooth surfaces, 3D separation occurred only at lower flow coefficients [36]. Additional losses due to 3D separations should be expected in fouled axial compressors due to the increased surface roughness.

In this work, the blockage model covers the effect of 3D separation.

Tip clearance losses

Increased tip clearance is one of the first problems an axial compressor is exposed to and is often considered the main cause of the initial performance loss facing new engines. After this initial wear, tip clearance losses will not be further affected by soft fouling. Deposits along the endwalls may cause blockage of the tip clearance with subsequent reduction of the tip clearance losses. Changes to the tip clearance losses are not separated in this work, but are included in the blockage model.

Blockage model

Bammert&Woelk [14] studied the influence of added surface roughness on changes to the suction volume flow. Roughness was added uniformly by adhering emery grains to the NACA 65-Series profiles of a three-stage compressor. The data for full speed is given in Figure 10. In the Figure, a correlation on the data for 10% pressure reduction is superimposed on the original data.

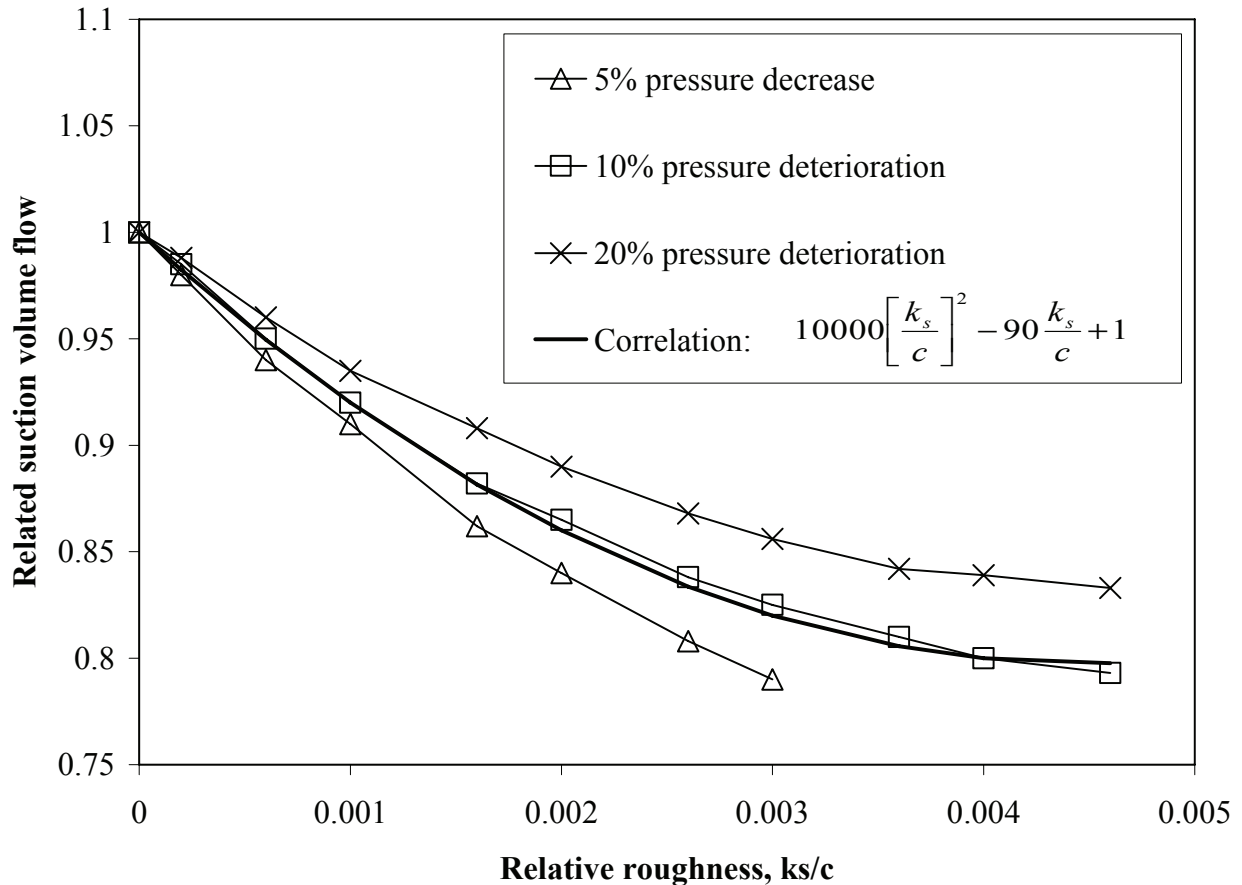


Figure 10 Correlation for blockage

In this work, blockage effects due to surface roughness are accounted for by reducing the suction volume flow rate using the correlation of experimental data given in Figure 10. The change in suction volume flow causes a horizontal shift in the flow coefficient of the stage characteristics.

2.3.4 Equivalent Reynolds correction model

The equivalent Reynolds correction model [89] takes on a different approach than the profile loss model for predicting increased frictional losses in a fouled compressor. In this approach, the ratio between the internal hydraulic losses and the changes to the friction factor is constant for a given compressor. A reference Reynolds number is defined for the hydraulic losses, and the effect of increased surface roughness is modeled equivalent to changes in Reynolds number for clean surfaces. The model accounts for sub-critical boundary layer flows and is therefore not restricted to the completely rough flow regime. Knowing the surface roughness and the reference Reynolds number, the Darcy friction factors are read directly off the Moody diagram

of Figure 6, or by applying an explicit equation as in Paper IV. Changes to isentropic head and flow coefficients are found from empirically validated relationships for centrifugal compressors [89] and is adapted to axial compressors in Paper IV.

The equivalent Reynolds correction procedure is included in the ASME test code [2]; however, the correction to flow coefficient is not included in the latest revision of the standard.

Although the polytropic head and efficiency are used in the original work, the isentropic head and efficiency are considered here. Applying the equations to a single stage, the end results should not be affected. To gain confidence in the data, the relations should be carefully reviewed with data on axial compressors; however, with the lack of such data, the equations for centrifugal compressors are applied in this work without further adaptation.

2.4 Overall compressor loss model

Additional roughness is expected to narrow the stability range of the compressor. Figure 11 shows the overall compressor performance map for a three stage axial compressor at four speeds with roughness elements applied uniformly and completely on the axial compressor and vanes [14]. The Figure shows the narrowing in range for the constant speed lines and a strong influence on the flow coefficient with increasing roughness.

The data presented in Figure 11 are not very practical for fouled compressors because these will rarely see uniform distribution of the surface roughness on all stages. The data are used in Paper IV for comparison of overall performance losses due to surface roughness.

2.5 Quasi-one-dimensional compressor model

A quasi-one-dimensional multi stage model is used in this work. The model calculates the flow conditions and velocity diagrams at the mean-line inlet and outlet from each blade row, assuming constant axial velocity in the stage. The model applies the measured gas path data to obtain the best fit for the available measurements, calculating the missing flow parameters. The results are compared to stage characteristics available in the literature. The model is given in Papers II and III.

In Paper IV, the change in compressor losses due to fouling are modeled using the correlations found in section 2.3. The model applies the data from the quasi-one-dimensional model of the clean condition and adjusts the stage characteristics by applying the measured surface roughness to the loss correlations found in this work.

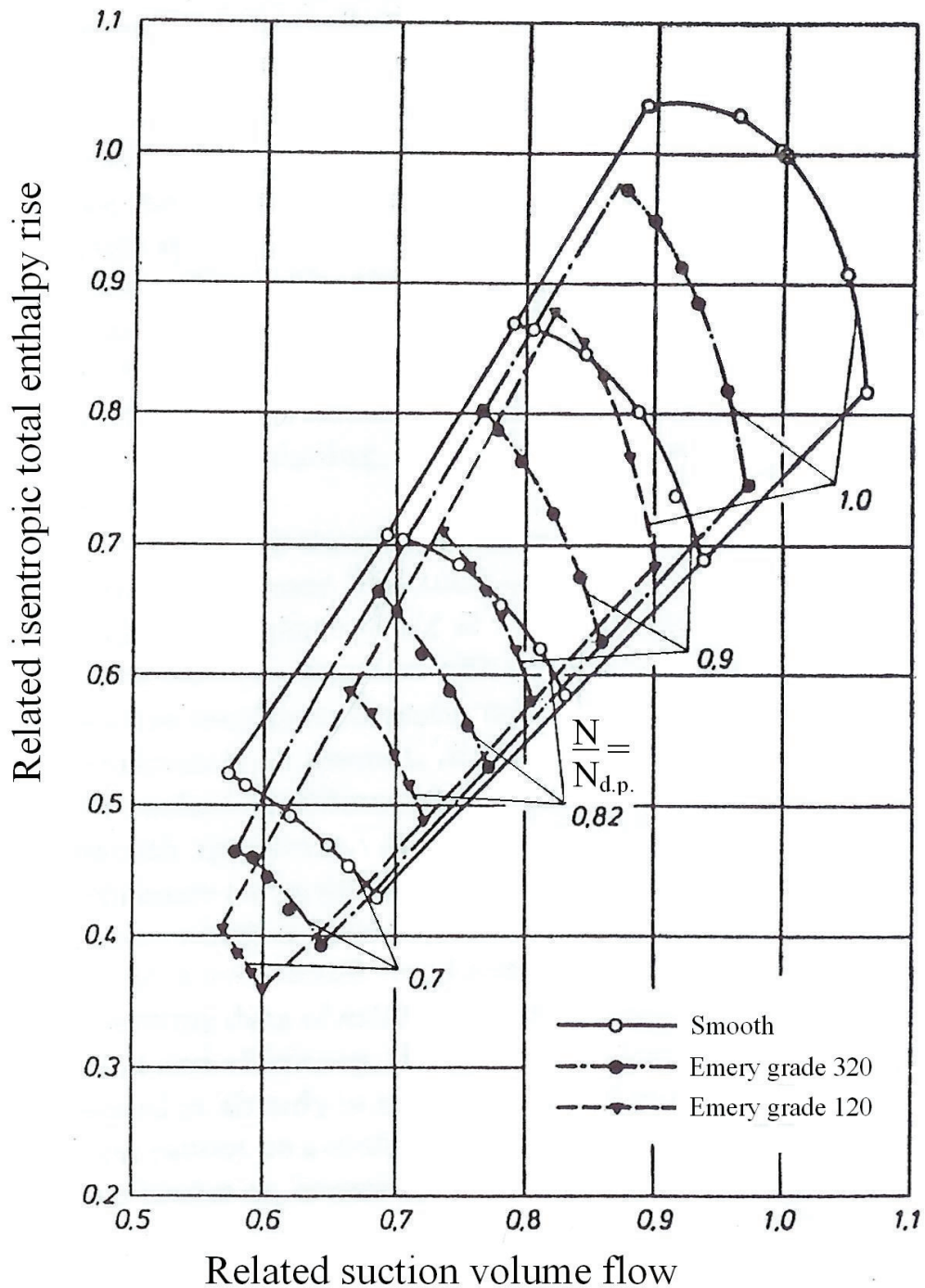


Figure 11 Effect of roughness on three stage compressor [14]

No adjustments are made to account for off-design effects. The correlations presented are therefore valid in the vicinity of the design point. If the stage characteristics are known, the effects of roughness should be valid for similar flow regimes: i.e. subsonic and turbulent flow regimes should, in principle, react in the same way to increased roughness. One should, however, be careful when applying the correlations to flow regimes close to boundary layer separation and for transonic flows.

2.6 Conclusions

This chapter supports goal A by determining the fundamental compressor deterioration mechanisms and loss models associated with fouling.

Increased profile losses, changes in deviation, increased blockage, and 3D separation are identified as the main deterioration mechanisms for fouled axial compressors. Sufficient data have been found to model the effect of fouling on profile loss, blockage and deviation. These data are used in Paper IV.

Two different models were applied for the increased frictional losses due to surface roughness: One model adjusts the momentum thickness factors of the classic two-dimensional profile loss correlations, while the other model applies a correlation for surface roughness on hydraulic losses verified for centrifugal compressors. The first model allows for separation of the effect of roughness on the suction and pressure sides of the blades. Blockage and deviation models are based on data found in the literature. All loss models are described in Paper IV.

Quasi-one-dimensional models are used in this work to calculate the inlet and outlet conditions of each blade row. All models are described in Papers II, III and IV.

Helicopter engines are vulnerable to salt fouling during heavy storms at sea. When power is way down you better find the nearest cloud to rinse the engines.

(Air force test pilot, Kjeller 2004)

3 Online compressor washing mechanisms

The purpose of this chapter is to determine the fundamental parameters for online compressor washing from reviewing the literature and industry practice. This chapter contains the background information for Paper III and supports goal D.

Performance recovery depends on the success of fouling removal and is determined by fouling solubility, surface wetting, fluid evaporation rate and wetting time. In addition, the removal of fouling must not impose secondary damage to the surfaces such as erosion. The surface must be left clean without increased adhesion of airborne fouling, which could cause increased deterioration rates after washing.

Inlet condensation can occur in high humidity conditions due to air acceleration and subsequent static temperature reduction in the bellmouth. Condensation may increase the rate of deposit build up because surface wetting of the bellmouth and inlet guide vanes may increase surface adhesion.

It is difficult to calculate the complex three-dimensional flow field in a compressor with water ingestion. Although one may have good control of the wet gas properties at the compressor face, the flow field becomes more complex after the first rotor. Centrifugal forces cause droplets to move toward the annulus and coalesce. In addition, the water film on the blade will re-enter the flow after the blades in different droplet sizes. Figure 12 illustrates the complexity of the flow field through the compressor as observed in low speed compressor tests. In the rotor, the droplets are forced toward the annulus, while in the stator the liquid is fanned out toward the centerline. The water sheet from the stator row is observed to cover about one third of the blade span [103]. Although the droplet path in the initial stage may be influenced by the droplet size, droplet size may have less importance in the wetting of the final stages.

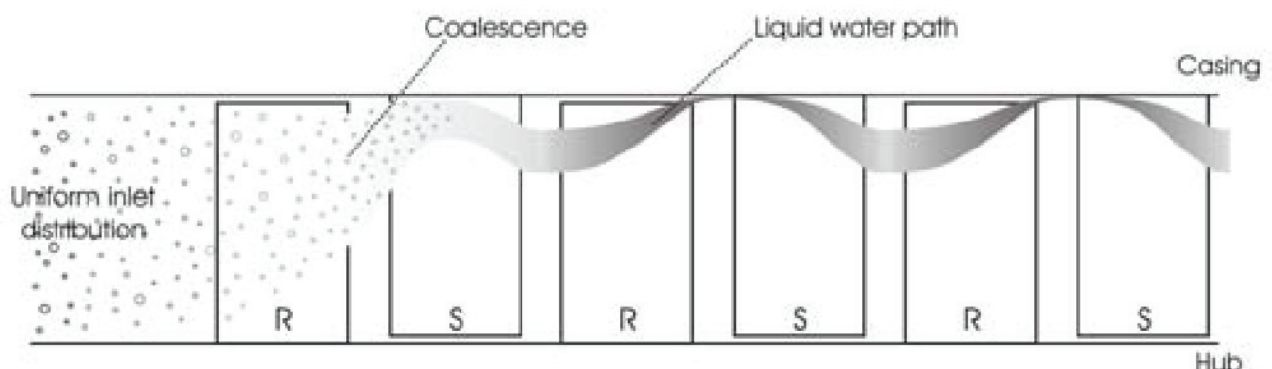


Figure 12 Wet gas path [103]

This work studies the influence of wet gas properties on fouling removal. The wet gas properties are defined at the compressor face to simplify specification of the spray.

The following properties are discussed:

- Fluid flow rate
- Fluid temperature
- Droplet size
- Droplet velocity and slip
- Duration and washing frequency
- Spray pattern

Fluid density is an important property for determining the spray characteristics from a nozzle. This work is based on water, and the effect of changing fluid density is not covered.

3.1 Fluid flow rate (water-to-air ratio)

The fluid flow rate will directly influence the liquid content of the flow inside the axial compressor. Higher fluid flow rates increases the surface wetting of the gas path and improves the wash efficiency. Fluid flow rate is assessed as a mass-based water-to-air ratio which is a non-dimensional parameter for the liquid content of the compressor air.

Current online washing systems are sometimes limited in flow rate by the gas turbine manufacturers. Table 2 lists recommended water-to-air ratio for online washing of aeroderivative gas turbine engines from two different manufacturers.

Table 2 Recommended water-to-air-ratios for aeroderivative gas turbines

<i>Gas turbine type</i>	<i>Water-to-air ratio for online wash</i>
Twin shaft, <50MW	0.46% at full load
	0.73 % at part load
Twin shaft, <50MW	0.42 % at full load
	0.95 % at part load
Three shaft > 50MW	1.2 % at full load

Review of available information gives a range of water-to-air ratio from 0.2 % to 0.7 % for aeroderivative engines up to 50MW output [5, 22, 30, 32, 67]. Although Mund [67] found that heavy duty engines generally had lower water-to-air ratios, flow rates up to 2 % water-to-air ratio are reported for the GE Frame 9 heavy duty engine [50, 97].

The present certification requirement for aircraft engines requires testing of engines at water-to-air ratios of 3 %. This requirement has been applied to all new engines since 1998 [99].

Axial compressors have been successfully tested at water-to-air ratios up to 15 % [95]. This indicates a potential for increased injection rates for online washing.

In this work, the water-to-air ratio ranges from 0.4 % to 3 %. While 0.4 % resembles the online washing systems commercially available for aeroderivative engines, the increase in water-to-air ratio is tested to analyze the effect of increased flow rates.

3.2 Fluid temperature

The solubility of deposits increases with increasing water temperature, and for offline wash it is common to heat the wash fluid to 60° to 70°C [32, 52]. Engine manufacturers typically recommend the cleaning solution and rinse water temperature to be between 38°C and 66°C.

The work input in the compressor causes an increase in both pressure and temperature. The air temperature increases rapidly and typically reaches 100°C after five or six stages. Some assume that the wash fluid inside a compressor will evaporate as the air temperature reaches the boiling point. Based on the observation that fouling is at its worst in stages five and six, reports have concluded that an online water wash can only be effective at air temperatures below the boiling point [22, 42].

Temperature measurements of two-phase water/air flow in a six stage axial compressor show that the temperature along the annulus at exit stayed unchanged regardless of the amount of water injected [96]. The test results are given in Figure 13. This shows that a water film flowed along the annulus and remained in liquid form at exit regardless of the liquid fraction. This is supported by the observations given in Figure 12.

Calculations of wet gas flow in axial compressors indicate that the liquid phase has a slower temperature increase compared to the air. Figure 14 shows the temperature increase of wet gas flow along the mean-line of a six stage axial compressor. The data are calculated using a stage model for dry conditions [96]. The boiling point of water increases with the pressure increase in the compressor. However, water temperature is significantly lower than the boiling point, indicating a slower evaporation rate inside the compressor.

Numerical investigations of the two-phase flow field of the compressor inlet of industrial engines during washing indicates that the fluid will quickly approach the temperature of the surrounding air before the droplets enters the compressor, and that the benefits of heating the fluid disappears due to this energy transport between the phases [26, 68].

In this work, fluid temperature was considered of minor importance in the compressor recovery. In addition, tests of 20°C and 40°C fluid temperature showed

no changes to the measured gas path temperatures. Hence, the fluid temperature was kept between 15°C and 20°C in the experimental program.

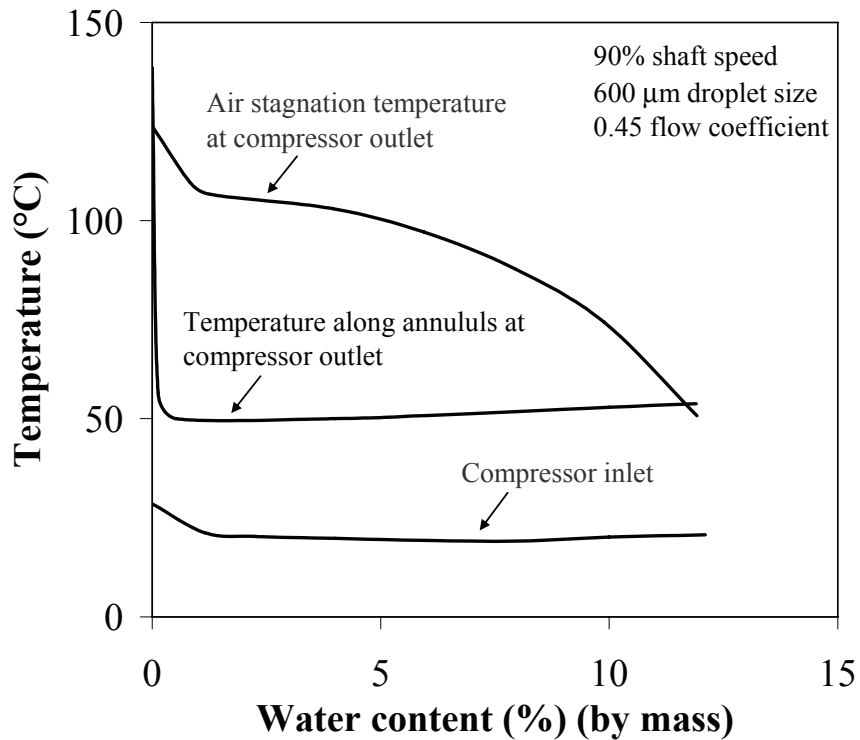


Figure 13 Measured temperatures at inlet an outlet of a six stage compressor [96]

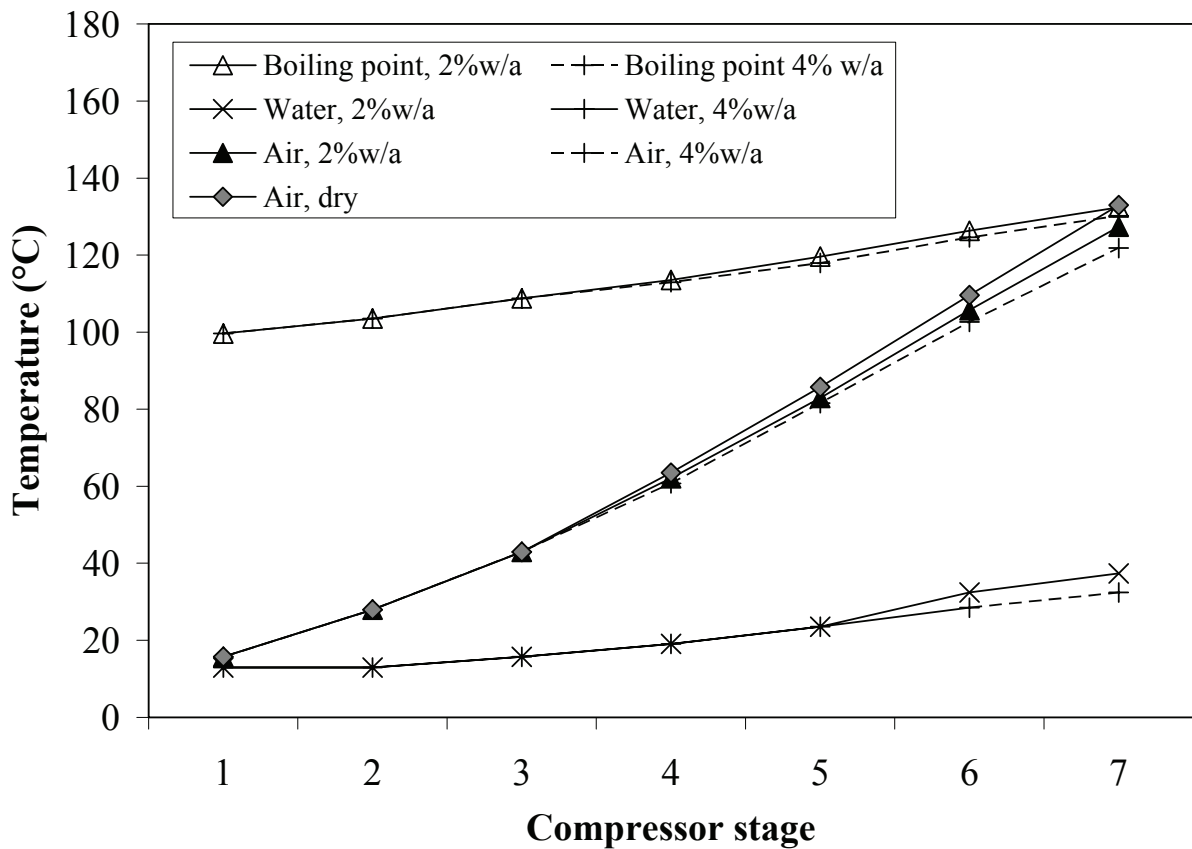


Figure 14 Calculated temperature variations along compressor mean-line [96]

3.3 Droplet size

In this section droplet size is discussed from a practical point of view by looking at the droplet size found in compressor wet gas applications and comparing these to droplets occurring naturally in the atmosphere. From this information a set of droplet size ranges are selected for testing of the online washing system.

In online washing systems, droplet size is considered important for performance recovery in the aft compressor stages because smaller droplets tend to follow the flow and therefore penetrate deeper into the gas turbine, thereby improving the aft stage wetting. Studies of the fundamental effects of water droplet motion inside axial compressors show trajectories of solid spherical particles calculated from the particle's equation of motion. Figure 15 presents the results of a numerical study of a compressor. A maximum droplet size of $10\ \mu\text{m}$ is defined to allow dispersion of the droplet in the rotor stage [103]. Similar calculations are used to determine the maximum droplet size for online washing systems [6]. Small droplets will penetrate the first compressor stage better than large droplets but because of the three-dimensional flow field and the wet film flowing along the blades, it is difficult to calculate the full flow field through the compressor.

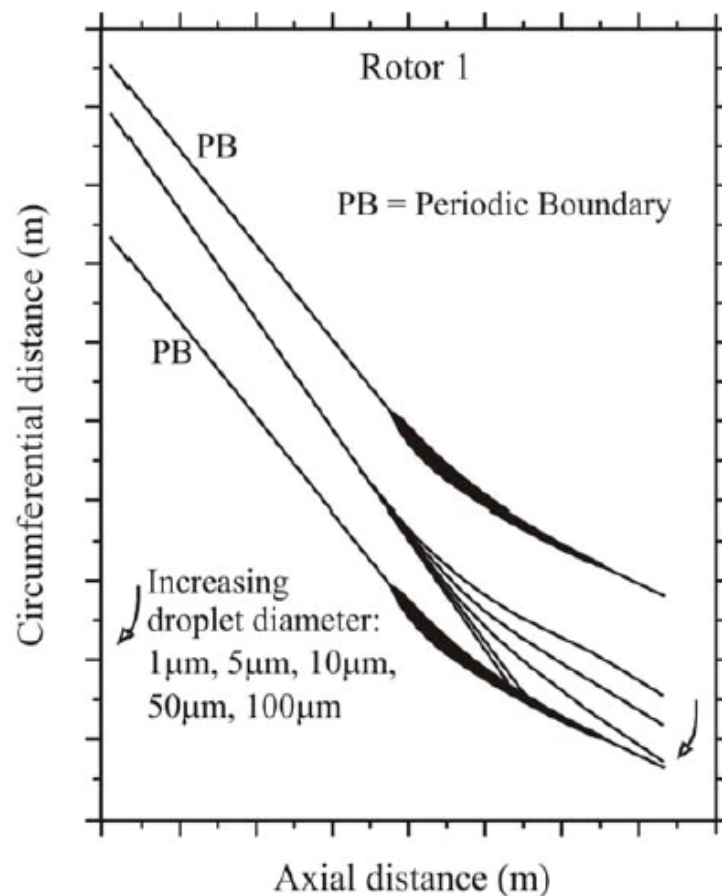


Figure 15 Motion of droplets in a rotor row [103]

The droplet size depends on the spray nozzle design. Gas-assisted atomizing nozzles will produce smaller droplets than single phase nozzles. The same nozzle will generate larger droplets at lower system pressures; however, increasing the pressure

will only produce smaller droplets up to a certain threshold [85]. Today's online washing equipment can be categorized in two main pressure ranges: Fluid pressures below 10 bar are considered low pressure systems while high pressure systems have fluid pressure above 50 bar. Single phase low pressure systems will produce droplets with diameters ranging from 100 μm to 1000 μm . Air assisted low pressure nozzles and single phase high pressure systems will produce smaller droplets of volumetric median diameter less than 100 μm . [6, 30, 67, 97] R-MC claims different droplet sizes clean different areas of the engine and has patented a system where the droplet sizes are varied from 80 μm to 500 μm to clean different parts of the gas path [45].

Erosion will depend on droplet size and droplet velocity. Gas turbine manufacturers do not specify droplet size for online washing systems except for requiring droplet size to be sufficiently small so as not to cause erosion inside the compressor.

According to GE, solid particles below 10 μm do not cause erosion, whereas particles larger than 20 μm may cause erosion when present in sufficient quantities [56]. No information is given for liquid droplets, although the kinetic energy of the droplet, the droplet size, droplet number impinging per unit time, impingement angle, and the material properties of the eroded material are all important erosion properties.

Water droplet erosion and subsequent fatigue cracks have been encountered in the zero stage rotor of the General Electric Frame 7 and 9 engine series. To correct the problem, a new R0 blade shape was designed with improved materials that reduce stresses along the exposed leading edge and detunes the vibration mode of the high cycle fatigue responsible for the fatigue cracks [28]. Two systems were developed independently by GE [29] and Turbotect [97] which both claim to reduce the droplet flow along the sensitive blade root area, reduce leading edge erosion and improve the mixing of water in the high speed air flow, thus allowing longer wash durations for units with the new blade design [50, 82]. The Turbotect system is documented to have satisfactory erosion properties for the GE 9F engines with a droplet size of 50 μm to 250 μm and a water-to-air ratio of 1.5 % [50, 97]. No further studies on erosion are done in this work.

Fogging systems for cooling the intake air of gas turbines installed in hot and dry regions, use atomized droplets that are injected at the air intake. The droplets evaporate before the air reaches the gas turbine, reducing the air intake temperature. Droplet size ($D_{v0.9}$) is typically less than 20 μm [61] although up to 40 μm are reported for inlet cooling [54].

Droplet evaporation rate is important to fogging and inlet cooling systems. Because evaporation occurs at the interface of air and water, the surface area is important for evaporation rates. In a spray of equal volumes of water, doubling the droplet diameter will halve the exposed surface area.

Aircraft engines must continue to operate when flying through precipitation and clouds. In meteorology, precipitation is categorized as cloud (fog), drizzle (mist), and rain according to the droplet size. The difference between cloud and drizzle is that drizzle drops fall to the ground rapidly enough to survive evaporative dissipation for a distance of several hundred meters. The free fall droplet speed is typically 0.7m/s for a 200 μ m droplet, which is considered the minimum size for drizzle; however, the exact survival distance for any droplet depends on the relative humidity of the atmosphere. Droplets much smaller than drizzle fall so slowly from most clouds that they evaporate before reaching the ground [1]. Aircraft flying through rain may encounter droplet sizes on the order of 100 μ m to 1,500 μ m, although 3,000 μ m size droplets have also been reported [95].

Figure 16 compares the different droplet sizes found in washing and fogging systems to the meteorological terms of precipitation.

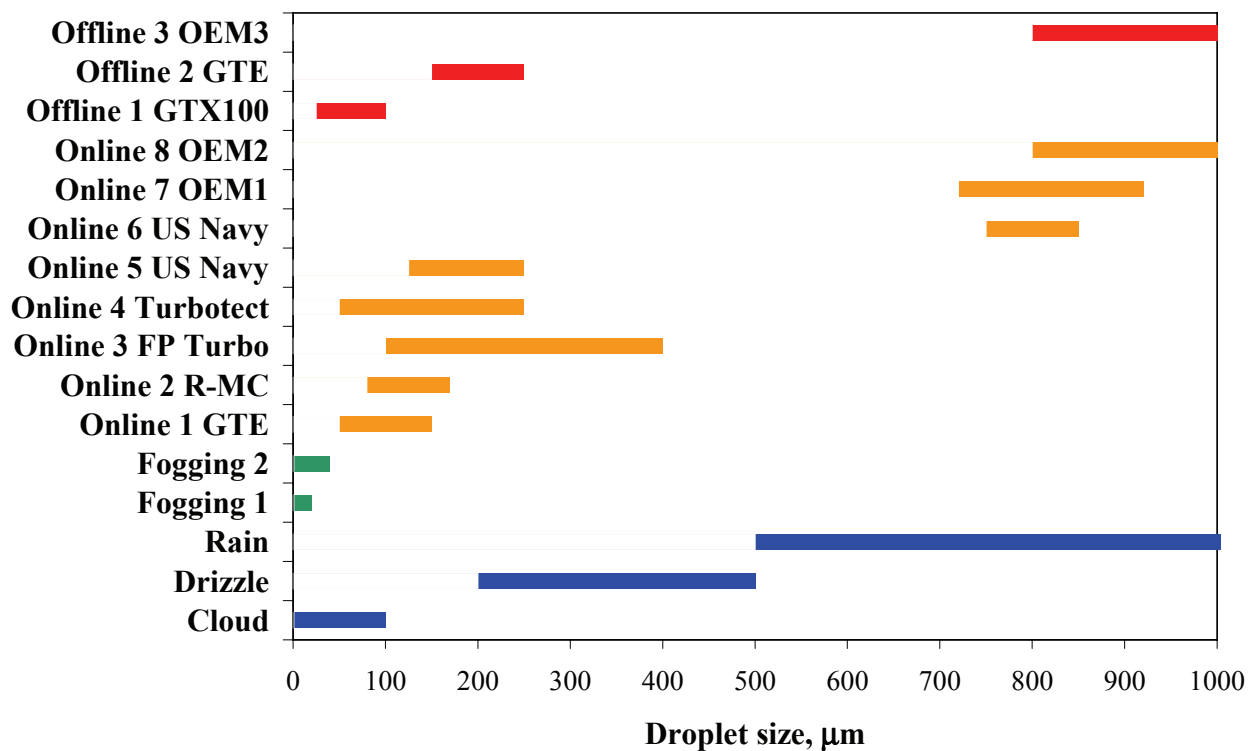


Figure 16 Droplet sizes applied in washing and fogging systems

In this work, the droplet size investigated is in the range of 25 μ m -200 μ m.

Three different categorizes are defined:

- 200 μ m droplets represent spray from single-phase low pressure systems
- 75 μ m droplets represent spray from single-phase high pressure systems and air-assisted low pressure systems
- 25 μ m droplets do not represent any online washing systems, but are used to check whether these small droplets will give improved penetration of water in the compressor

3.4 Droplet velocity and slip

The spray velocity from a nozzle depends on the nozzle type and the spraying pressure. The velocity efficiency is the ratio of the spray velocity at the orifice to the theoretical velocity through a solid stream orifice at the same spraying pressure. Correlations exist for the variation of velocity efficiency with nozzle spray angle, nozzle design and operating pressure. Flat spray nozzles will have a velocity efficiency of 80-85 % compared to 55 % for hollow cone nozzles [85]. Velocity efficiency decreases with spray angle and increases with operating pressure.

At a distance from the nozzle, the droplet velocity will be influenced by frictional effects of the air and gravity forces, and both effects are dependent on the droplet size. Fluid viscosity, specific gravity and surface tension will affect the spray break-up process. No correlations are offered for these effects.

The air flowing through the bellmouth has large velocity gradients accelerating from virtual stand-still to 110 m/s at the bellmouth and 180 m/s at the compressor face (see Appendix G). A numerical study of $\sim 70 \mu\text{m}$ (VMD) droplets in the bellmouth of an industrial engine showed that the droplets reached the air velocity in about 0.4 m [26].

The slip velocity is defined as the relative velocity between the flow field and the water droplet. High slip velocities will cause droplet break-up because of Rayleigh-Taylor instabilities occurring as the heavy fluid accelerates into the light air. Gas Turbine Efficiency claims that the spray should be introduced where the air velocity is at least 40 % of the final velocity, and that the slip ratio at the compressor face should be at least 0.9 [6].

Droplet break-up is correlated by the dimensionless Weber number which is a measure of the relative importance of the disruptive viscous drag forces on the droplet to its surface tension forces [74]:

$$We = \frac{\rho \Delta V^2 D}{\sigma}$$

where ρ is the free-stream air density, ΔV is the relative velocity between the air flow field and the water drop, D is the initial diameter of the water drop and σ is the surface tension of water. At subsonic speeds, droplet break-up due to slip will occur if the Weber number reaches 12 [74].

Three different droplet sizes were defined for this work. Any break-up of the droplets due to large velocity slips will result in smaller droplet sizes than desired. To avoid droplet break-up in the air intake during online washing, the water droplet velocity should be sufficient to maintain a Weber number below 12. Table 3 shows the minimum droplet velocity allowable to avoid slip induced droplet breakup in the flow field of the air intake.

Table 3 Minimum water droplet velocity

<i>Droplet size (μm)</i>	<i>Minimum velocity (m/s) Bellmouth</i>	<i>Minimum velocity (m/s) Compressor face</i>
200	45	115
75	< 5	74
25	< 1	< 1

It should be noted that this is a coarse approach to estimating the maximum slip for stable droplets and that other factors like droplet collisions and vibrational breakup can cause droplet breakup or coalescence at slip velocities at Weber numbers below 12. It is therefore advisable to keep the slip as low as possible at the compressor face.

Droplet velocity and droplet size are closely connected in the nozzle design and cannot be considered independently when the nozzle type is selected. Once the nozzle type is selected it is not possible to control droplet size and velocity independently. The only influence the designer can have on the slip velocity is in the positioning of the nozzles in the flow field of the air intake. Computational fluid dynamics may be used to optimize the position [68].

In this work, the droplet velocity is not measured in the air intake. To avoid large uncertainties in the size distribution due to break-up and coalescence, the droplets are introduced straight into the bellmouth to avoid cross-flows and to keep slip velocities as low as possible.

3.5 Duration and washing frequency

Wash duration and frequency are dictated by site specific issues like fouling solubility and gas turbine deterioration rate.

Test of chemical cleaners use 10 minute duration and tests conducted according to MIL-PRF-85704C [64] using lubricating oil and carbon black for soil [105]. Online detergent fluid evaluations have used 3 minute durations for salt deposits [43].

Engine manufacturers specify flow rates and total fluid so as the duration becomes 2-3 minutes [77]. However, for heavy-duty engines, up to 30 minute durations are used [50].

Frequent online washing is needed to avoid fouling to build up. However, the optimum schedule seems to depend on the gas turbine engine type and the type of fouling. Stalder reported online washing at time intervals between 700 and 120 hours and found that the shorter time interval gave significantly higher plant performance [86]. Within Statoil, several online wash frequencies have been tried. Daily online washing showed a slight improvement in overall performance at one installation [42]. A different reports show that online washing every 3rd day should be avoided as this significantly increases the degradation rate [22]. This is in direct conflict with other

findings that advocate online washing twice a week [39] or every 1 to 3 days [86]. In the absence of site-specific information, gas turbine manufacturers recommend daily online washing. Frequency should be determined from experience on site by balancing the cost of online washing to the engine capacity deterioration rate.

The effect of online washing is tested at duration up to 10 minutes total. Frequency is not relevant for this work because the engine is artificially fouled.

3.6 Spray pattern

The location of the nozzle will affect the spray pattern. A numerical study found the most uniform droplet distribution with 50 μm droplets for nozzles positioned in the bellmouth, and 300 μm for nozzles positioned in front of the air intake [68]. Flat spray nozzles are positioned to allow best penetration and wetting of the blades [6]. Others have targeted less fluid at the root because of erosion problems combined with high cycle fatigue [29].

The online washing system used in this work has uniform distribution of water nozzles at the air intake. Effects of non-uniform distribution of fluid at the inlet are therefore not considered.

3.7 Conclusions

This chapter supports goal D by identifying the fundamental parameters for online compressor washing from a review of the literature and industry practice.

The review determined fluid flow rate (water-to-air ratio), droplet size, and duration as the main parameters, while fluid temperature has secondary importance. Droplet velocity and spray pattern depend on the nozzle type and location and the selected droplet size. It is not possible to define the parameters individually. Duration is dependent on the solubility of deposits which is site dependent.

Table 4 summarizes the practical limits for online washing parameters and the range applied in this work.

Table 4 Limits for online washing parameters

	<i>Practical limit</i>	<i>Range applied in this work</i>
Water-to-air ratio	3 % by mass	0.4 % to 3 % by mass
Fluid temperature	Above freezing, fluid heating not required	15-20 °C
Droplet size	10 µm -400 µm avoid erosion	25 µm -200 µm (VMD)
Droplet velocity	Depends on nozzle design and position in air intake	See Table 3
Duration	Depends on deposit solubility 2-30 min industry practice	Up to 10 minutes
Frequency	Depends on deterioration rate	Daily to every 3 rd day
Spray pattern	As uniform as possible	Uniform

You cannot install temperature probes in the engine like that, it will never work!

(Dismayed colleague discussing gas path temperature measurements, Vienna 2004)

4 Test equipment and methods

This chapter gives an overview of the test equipment and methods used in this work.

The empirical data is taken from two sources:

- a) Online washing of an RB211-24G offshore installation at Statoil's Heidrun
- b) Deterioration testing and online washing of a GE J85-13 jet engine at the test facilities of the Royal Norwegian Air Force (RoNAF)

4.1 Test of RB211-24G gas turbine

The data from Statoil Heidrun were collected from 1998 to 2001 by the turbine operators using standard on-engine instrumentation. A total of 836 data series are analyzed in this work. Paper I covers all details of the RB211-24G tests, the site, the data verification and data correction.

4.2 Test of GE J85-13 jet engine

The General Electric J85-13 testing is a major part of this work and all testing, including test planning, instrumentation set-up and data gathering was done solely for the purpose of this research. Parts of the information on test equipment are published in Papers II, III and IV and are only repeated here if needed for clearness.

Engine testing was carried out from May to September 2004 at the Royal Norwegian Air Force test facilities at Kjeller, Norway. Kjeller is located inland, approximately 25 km east of Oslo, at an altitude of 119m above sea level.

4.2.1 GE J85-13

The GE J85-13 engine is a compact, lightweight, single-spool turbojet engine. This engine has been a successful engine in different applications since it first entered service in 1960. The J85 jet engine has a thrust-to-weight ratio close to 8 that was unmatched in subsequent GE designs until the F414 design came along 30 years later. [57].

The GE J85-13 compressor is an eight-stage axial-flow design with a 6.5:1 pressure ratio. The compressor is directly coupled to a two-stage turbine with variable exhaust nozzle and afterburner. The compressor holds a free-vortex design with high aspect ratio blades and transonic design conditions in the front stages. GE almost always used a modified NACA 65-Series thickness distribution with a circular arc mean-line for the subsonic blades, and NACA 65-Series are assumed in this work. The compressor geometry and stage characteristics are found from literature and are given in Appendix G.

Figure 17 presents the compressor stage work characteristics [63]. All characteristics are given in Appendix G. The compressor aerodynamic design is further discussed in Paper II and Paper IV Appendix A.

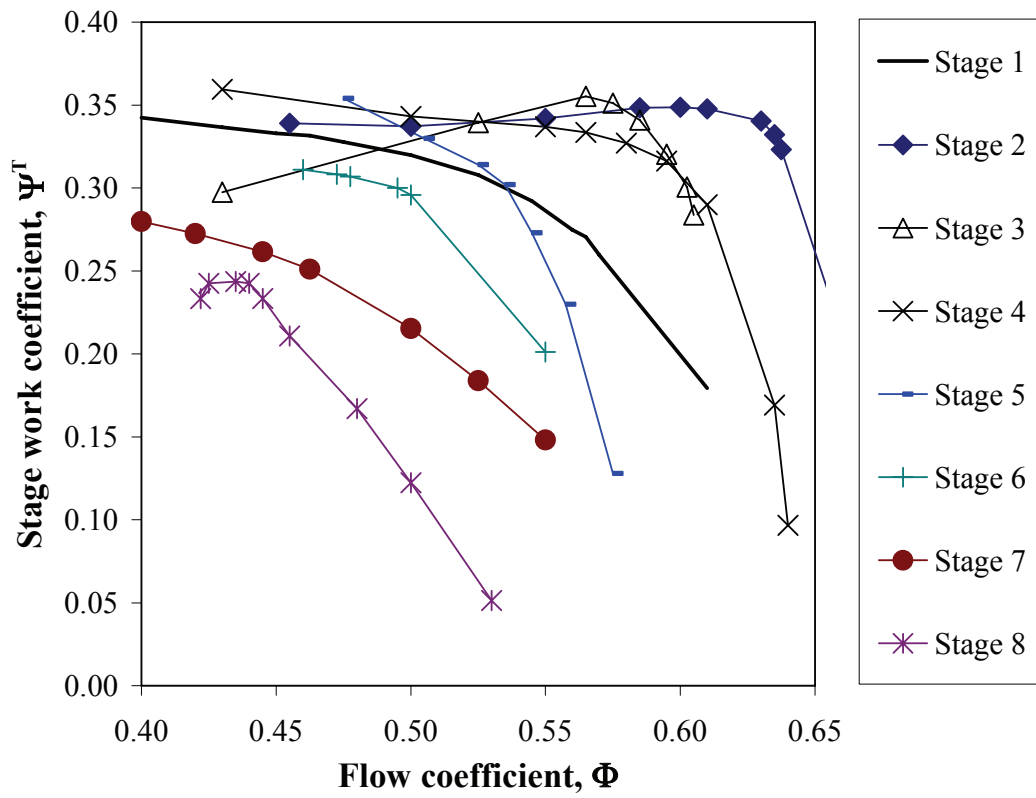


Figure 17 GE J85-13 stage work characteristics

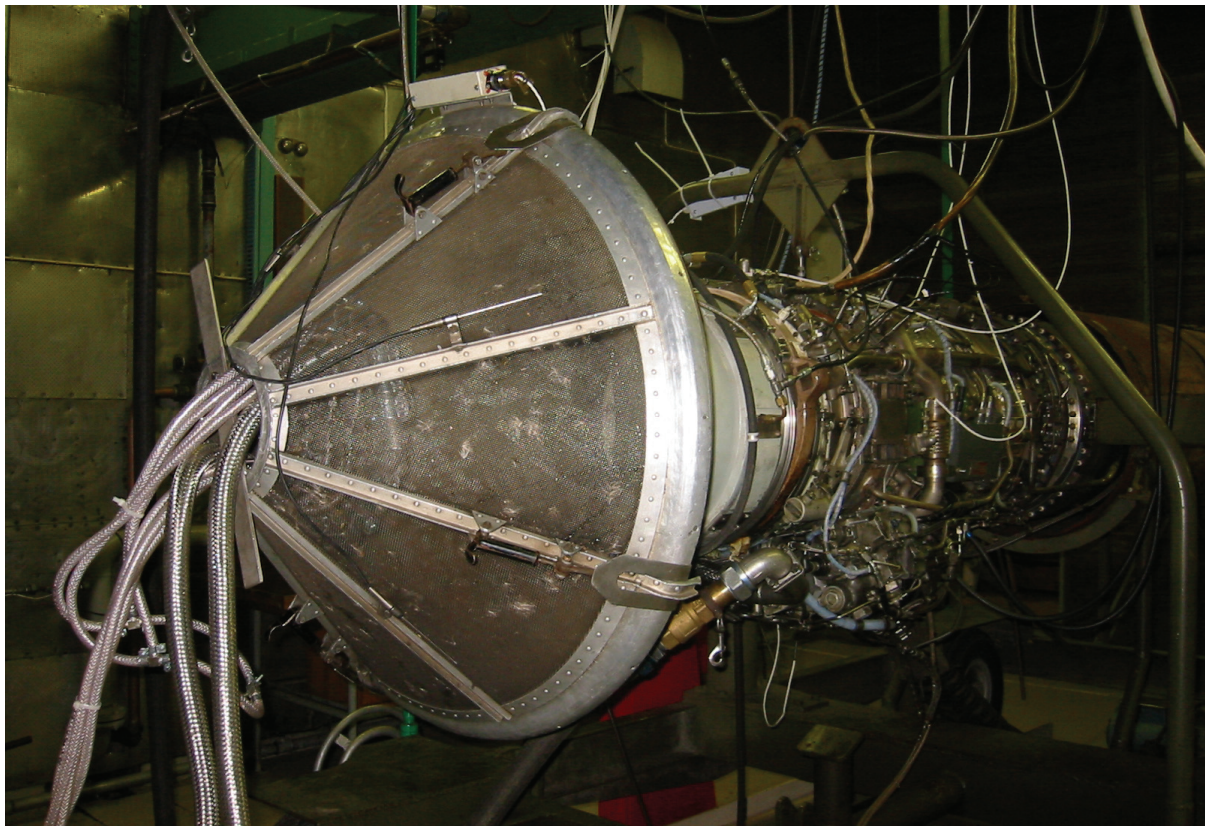


Figure 18 GE J85-13 with test equipment mounted in the inlet screen

GEJ85-13 off design operation is handled with variable inlet guide vanes, adjustable bleed-off-valves, and adjustable exhaust nozzle. Details are given in Paper II, in Appendix G, and by Brekke [18].

The GE J85-13 jet engine used in this project had approximately 300 hours onboard an aircraft and had been preserved, but not overhauled, before test. The engine was cleaned prior to testing, as given in Paper II.

4.2.2 Test equipment

Dedicated test equipment for salt deterioration and online water washing were installed in a single manifold inside the inlet screen at the front of the bellmouth, as seen in Figure 18.

Salt deterioration test equipment

The jet engine was deteriorated with atomized saltwater injected at the compressor inlet, similar to a method used by the United States Navy [21].

Four saltwater nozzles were installed on the online water wash manifold in front of the compressor inlet guide vanes. The nozzle type is Spraying Systems SU2A. The droplet diameter of the saltwater spray was measured according to ASTM Standard E799-92 [7] using a Malvern laser diffraction spray analyzer. This testing is reported separately [90].

The salt water was supplied at 0.2 l/min with droplet size of 23 μm (VMD). The salt composition is specified in Paper II.

Further details of the salt deterioration equipment are given in Paper II.

Online washing system

Compressor performance was restored using an online water wash system with water nozzles positioned on a manifold in front of the bellmouth. The manifolds are shown in Figures 2 and 3 of Paper III.

The nozzle types were Spraying Systems TN3, TN26 and QJ12. The droplet diameters were given by the manufacturer. Verification testing using a Malvern laser diffraction spray analyzer gave less variation between the different sprays than given by the manufacturer [90]. The results are compared in Table 1 of Paper III.

The online washing system was designed to meet the requirements determined in chapter 3. Table 5 summarizes the online washing system performance. To meet the droplet slip requirement, the water was introduced 0.3 m in front of the bellmouth or

0.77 m in front of the compressor inlet guide vanes. The water is sprayed uniformly into the bellmouth in the direction of the air flow.

Table 5 Online washing system data

	<i>Online washing system data</i>		
Water-to-air ratio (% by mass)	0.4, 0.8, 1.7 and 3		
Fluid temperature (°C)	15-20		
Droplet size (µm VMD)	25	75	200
Droplet velocity (m/s)	N/A	35	35
Duration	30 sec, 60 sec, 90 sec, 4 min and 10 min		

The water was analyzed by a laboratory, and the results are given in Table 2 of Paper III.

Further details of the online water wash system are given in Paper III.

4.2.3 Engine instrumentation

The standard test-cell instrumentation was extended with additional sensors to provide more information than is normally available in the test-cell. An overview of the engine instrumentation is shown in Figure 1, Paper II.

All instruments were calibrated prior to start up. During the course of the testing, three sensors were replaced. All replacement sensors were calibrated before testing continued. Pre-test and post-test measurement uncertainties were evaluated for all engine instrumentation using the ASME standards for performance testing and test uncertainty [3, 4]. The measurement uncertainties are given in Appendix E. The instrumentation specification is given by Brekke [18].

Ambient temperature and compressor inlet temperature

Ambient temperature was measured on the wall outside the test cell. Compressor inlet temperature was measured using four sensors located at the engine inlet screen. Due to test-cell recirculation, the recorded compressor inlet total temperature was higher than the measured ambient temperature and changed with engine load. The ambient temperature was used only for calculation of the specific humidity.

Humidity

Relative humidity and ambient temperature were manually recorded at the same location outside of the test-cell. The combined reading was converted to specific humidity. Although recirculation gave a slight increase in the compressor inlet temperature, the specific humidity was assumed to be unchanged in the air from the outside to the inside of the test cell.

Compressor inlet pressure

Total pressure in the bellmouth was measured using three pitot tubes in the bellmouth. The pitot tubes were connected providing one signal for compressor face total pressure. The pitot tubes are standard test-cell instrumentation for the GE J85-13.

Static pressure in the bellmouth was measured using three static ports of 1mm diameter. These static ports are located at the bellmouth circumference at the same axial position as the pitot tubes. The static ports were connected providing one signal for compressor static pressure. The static pressure measurements were added for the purpose of this work. Because of the three pitot tubes already installed in the bellmouth, it was assumed it would be better to install the static ports at equal distance from the pitot tubes. Recommended practice is four static ports along a circumference [49], although three ports are also found in use [92].

Throttle and nozzle position

Engine throttle and nozzle position setting was measured with the standard on-engine instrumentation and manually recorded at each setting.

Thrust

Thrust was measured with the standard test-cell instrumentation using two load cells.

Fuel consumption

F34 fuel consumption was measured with the standard test-cell turbine flow meter.

Air flow

Air flow was measured using the intake depression method [78, 83, 92]. The bellmouth depression, or deviation in the static pressure from the total pressure, is directly linked to the air velocity through the bellmouth. Assuming uniform flow across the bellmouth, the changing velocity is a measure of the mass flow rate through the engine [18].

Gas path pressure measurements

The static pressures at stage 5 were measured in the bleed channel using a 1 mm tap at a single point on the circumference. The compressor discharge pressure was measured using the standard on-engine instrumentation.

Gas path temperature measurements

The gas path temperatures were measured using one unshielded resistance temperature detector (RTD) at each stator rows 1, 3, 4, 6 and 8.

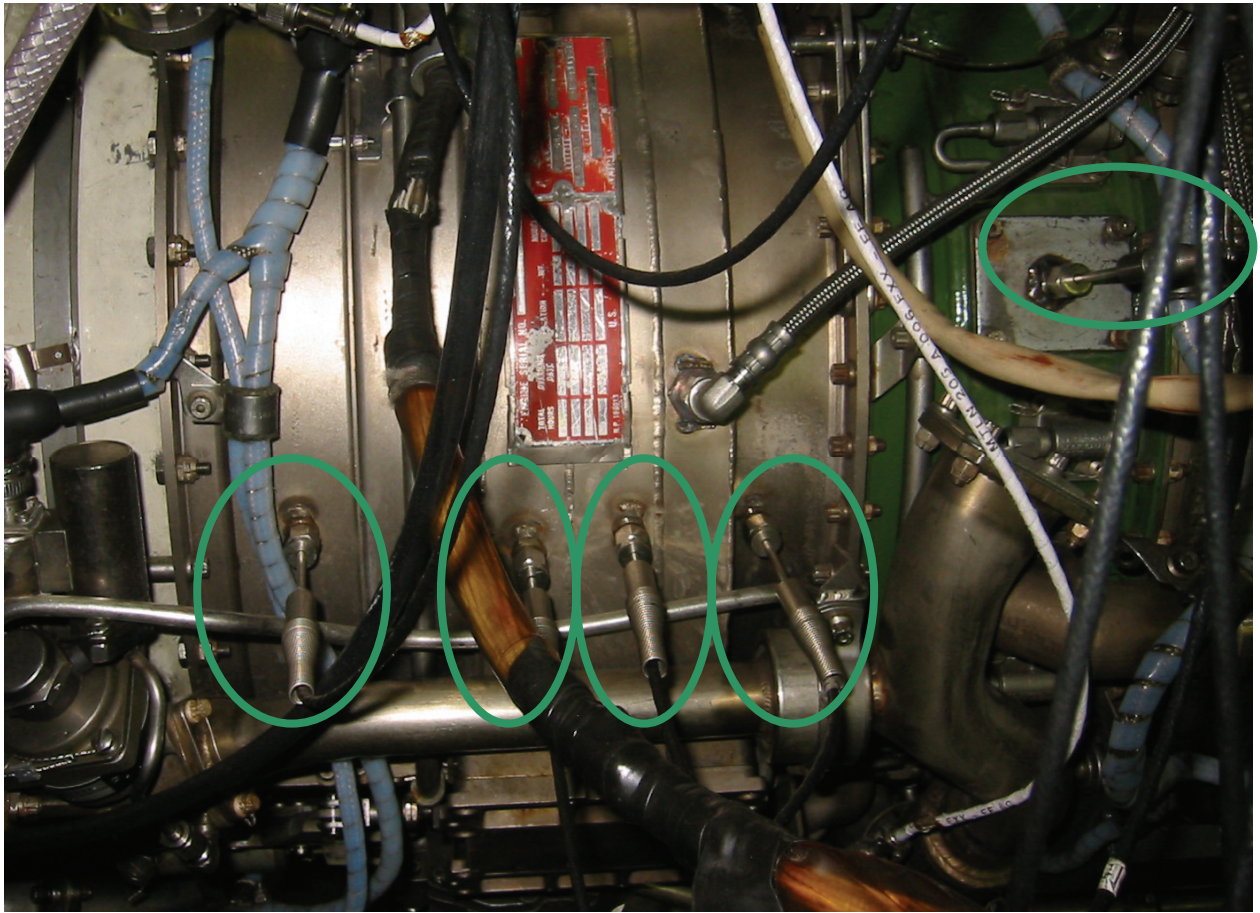


Figure 19 GE J85-13 casing with extra temperature sensors (top view)

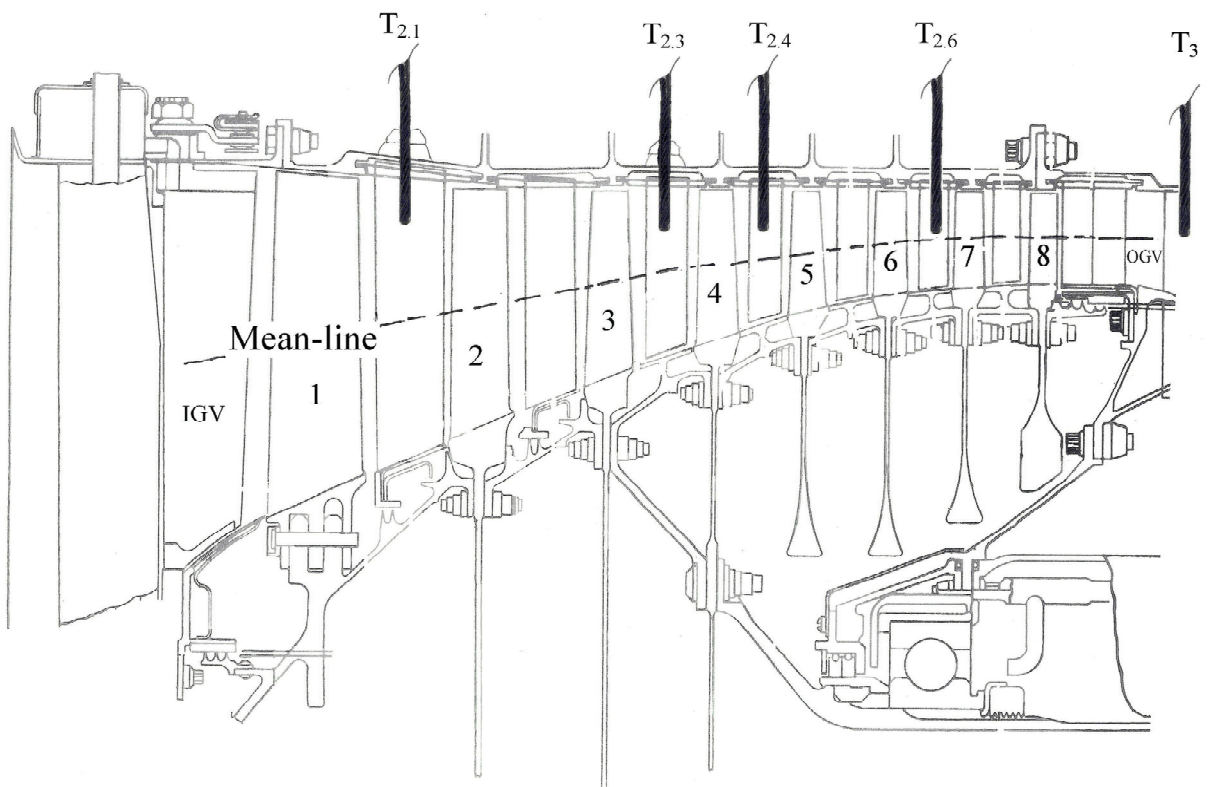


Figure 20 GE J85-13 compressor cross-sectional view with temperature sensors

Substantial work was necessary to modify the casing to accommodate the temperature sensors. The GE J85-13 casing is packed with instrumentation and only the top half casing had space available for additional sensors. The sensors were positioned as far as possible from the bleed valves to avoid additional errors in the measurement due to variations in the bleed valve position. Only one temperature sensor was installed at each gas path measurement station to reduce the risk of rotating stall due to partial gas path blockage. This single sensor approach requires stringent calibration procedures and low inherent measurement uncertainty to attain high repeatability in the measurements. The GE J85-13 gas path temperature instrumentation is shown in Figure 19.

All temperature probes were immersed 15mm which is the length of the sensing element. The shortest immersion length was selected to minimize the gas path blockage and to assure mechanical integrity of the sensor. Figure 20 shows the sensor elements drawn on the GE J85-13 cross-sectional drawing.

Measuring gas path temperatures in high velocity gas flow laden with salt and water droplets using unshielded sensors requires firm control of the associated errors. Temperature profile and gas velocity are significant sources of error in the absolute temperature measurements. To minimize errors, the data are analyzed for relative changes in the temperature measurements. The different error sources are discussed in detail in Appendix E.

Liquids in the flow

When liquid droplets are present in the flow the unshielded RTD probes will be wetted by the liquid droplets and the probe will act partially or completely as a wet bulb thermometer. The presence of evaporating liquid on the probe will cause an under-reading of the gas temperature. No reliable correction exists for these circumstances [34].

Figure 21 gives an example of stage 6 temperature measurements during water injection. For the higher water flow rates (high water-to-air ratios), the temperature drops to a steady state level similar to that observed in Figure 14 [96]. For the low water flow rates and small droplet sizes, the temperature drops to a steady state level which is the measured gas temperature. However, for the larger droplet size and the lower flow rates the temperature measurements are unsteady, showing a 5 °C to 10 °C variation in the measured temperature. This is believed to be due to droplets present in the flow and is used to analyze the penetration of liquids into the compressor at changing conditions.

In this work, test series with standard deviations larger than the measurement uncertainty are considered to be for two-phase flows, and are used as an indication of droplets present in the flow. All performance data are measured without water injection.

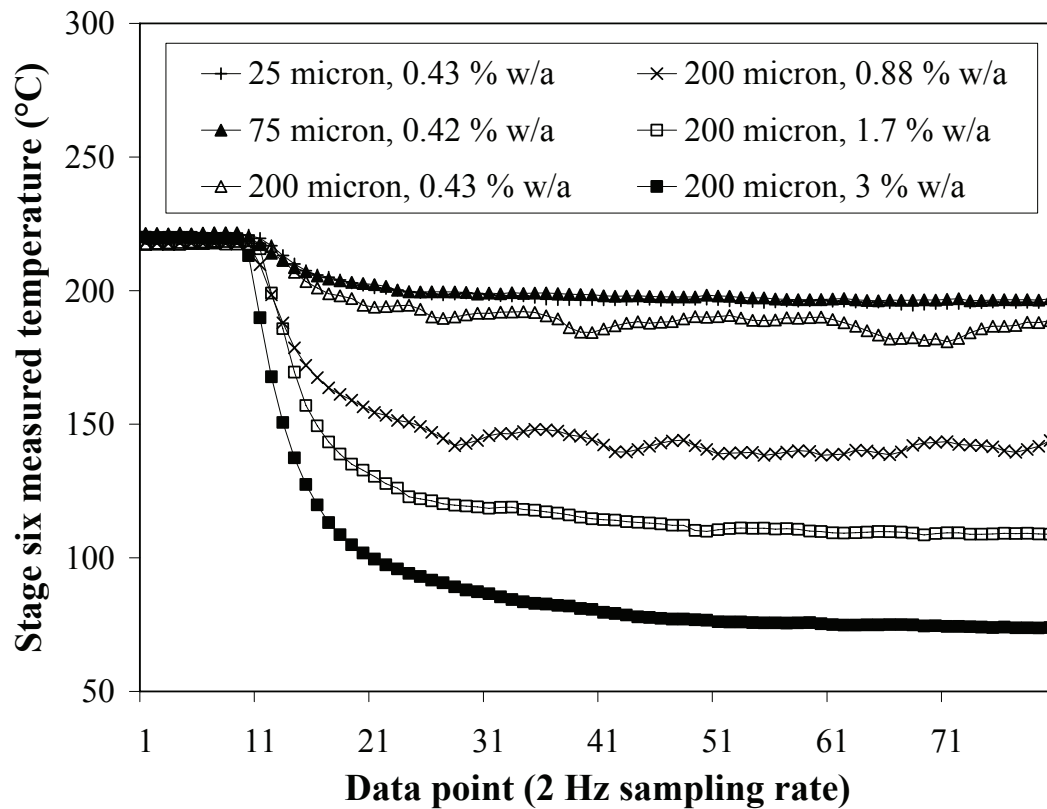


Figure 21 Stage six temperature measurements during water injection

4.2.4 Data acquisition and data correction

A total of 63400 data series were collected and analyzed for the GE J85-13. To reduce the data scatter, 60 data series (2Hz sampling rate) were collected at each setting. The average of these readings was taken as the steady-state data point. The original data acquisition system in the test cell used a 10 point rolling average for all data. This was also done in the online washing trials. The associated shift in mean value is analyzed in Appendix E. The largest shift in mean value is found for the compressor discharge pressure causing only partial overlap in the measurement uncertainties. This will have no influence on the conclusions of this work.

All thermodynamic performance measurements were corrected to standard ISO reference conditions of 15°C ambient temperature and 101,325 kPa barometric pressure. The ISO [47] and ASME [4] performance test codes recommend use of simulation programs for data correction. This was not available for any of the gas turbines used in this work. The applied corrections are therefore the classical equations for gas turbine performance data [100].

The compressor data were analyzed using a quasi-one-dimensional compressor model that applied the available measurements and calculated the missing data. The model is given in Paper II and III.

All test results published for the GE J85-13 are for a limited speed range of 95-98% of full speed. This is to avoid the effect of varying engine control on performance.

4.2.5 Test procedure

The GE J85-13 test procedure was written by Brekke [18]. This procedure was followed throughout the testing, except the engine baseline was recorded at constant throttle angle rather than constant engine speed. This is equivalent in practice, but reduces the need to calculate the corrected shaft speed for the given compressor inlet temperature. The speed line tests and transient performance tests given in the test procedure were only used for the initial testing. Because these tests gave little additional information and disturbed the engine baseline they were abandoned in the online washing program.

Engine performance was recorded prior to degradation, after salt degradation, and after each online water wash. The procedure is given in Paper II.

For all salt-deterioration cases, three liters of saltwater was ingested with a salt concentration of 1% (by weight). The engine was cleaned of salt deposits prior to each new deterioration test, as given in Paper III.

Test procedure for the online washing is given in Paper III.

4.2.6 Test matrix and test series repeatability

Seven deterioration and online water wash trials were completed at different droplet sizes and water flow rates. Some trials were repeated due to problems with clogging salt nozzles and reduced salt water ingestion which offset the deterioration signature. These tests results are not published. The test matrix is given in Appendix F.

The clean and deteriorated conditions for all tests are given in Appendix F. Deterioration reduced the intake depression by $3.5 \% \pm 0.05 \%$. The stage one work coefficient increased 0.1 ± 0.035 and the flow coefficient changed by 0.06 ± 0.015 . Representative test series were chosen for the reference clean and deteriorated conditions and is used throughout Papers II, III, IV and Appendix I and J.

4.2.7 Overall deterioration sensitivities

The overall GE J85-13 deterioration sensitivities were analyzed by Brekke [18] and his conclusion was used in Paper II and III. Table 6 presents the GE J85-13 monitoring parameters which were found to be consistent with compressor deterioration.

In this work, intake depression is used to display the overall GE J85-13 performance deterioration.

Table 6 Parameters for detecting GE J85-13 compressor deterioration [18]

<i>Dependent parameter (corrected)</i>	<i>Independent parameter (corrected)</i>	<i>Relative change (%)</i>	<i>Uncertainty</i>
Intake depression	Shaft speed	-18.1	Low
Air flow rate	Shaft speed	-8.1	N/A
Thrust	Exhaust gas temperature	-6.3	Low
Compressor discharge pressure	Exhaust gas temperature	4.2	Medium
Fuel flow	Exhaust gas temperature	-3.8	High
Stage 1 temperature	Shaft speed	3.1	Low
Thrust specific fuel consumption	Shaft speed	3.1	High

4.3 Methods for characterizing compressor fouling

The purpose of this section is to describe the four methods used to characterize the salt deposits in the GE J85-13 axial compressor.

All methods except visual inspection require disassembly of the engine and were applied to stator vanes only. Disassembly of the top casing takes two days, and was done twice during the test program, first after the initial salt deterioration testing, and second at the end of the test program.

4.3.1 Visual inspection

Visual inspection with a borescope provided a good method for observing the salt deposits inside the compressor. The method was used to determine clean conditions in the compressor. Figure 22 shows a typical view as seen through the bleed holes. Borescope inspection was possible through bleed holes in stages 3, 4, and 5. It was possible to observe deposits up to stage 6 stator and leading edge deposits up to stage 7 rotor.

The air intake, inlet guide vanes, stage 1 rotor and stator and stage 2 rotor were observed through the air intake.

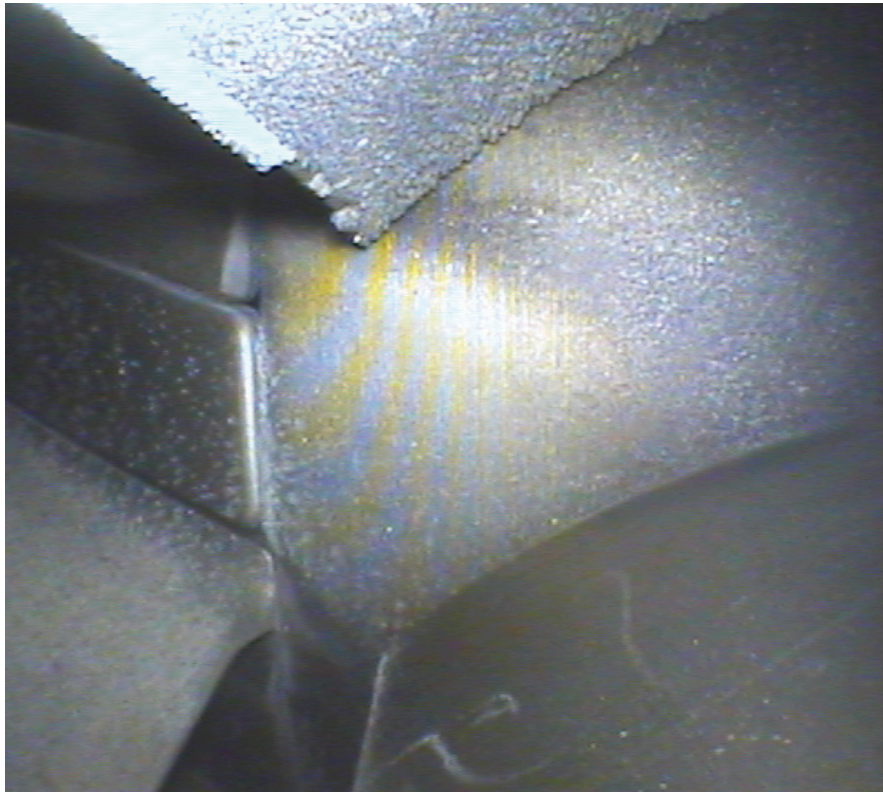
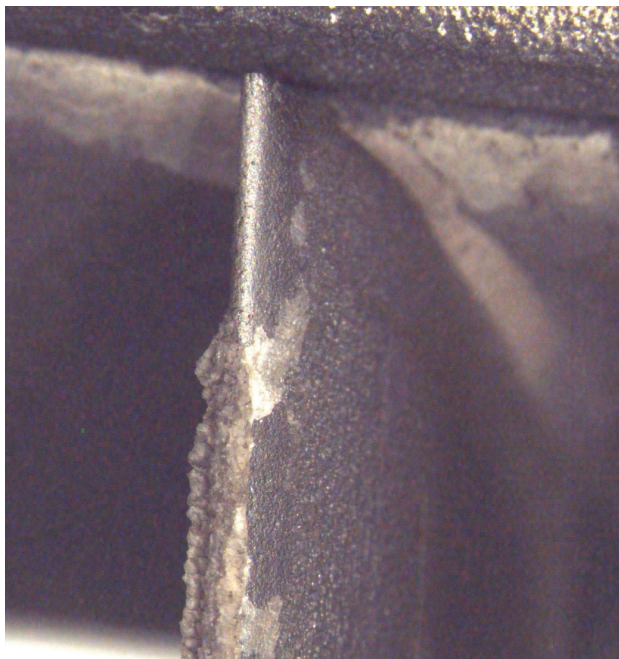
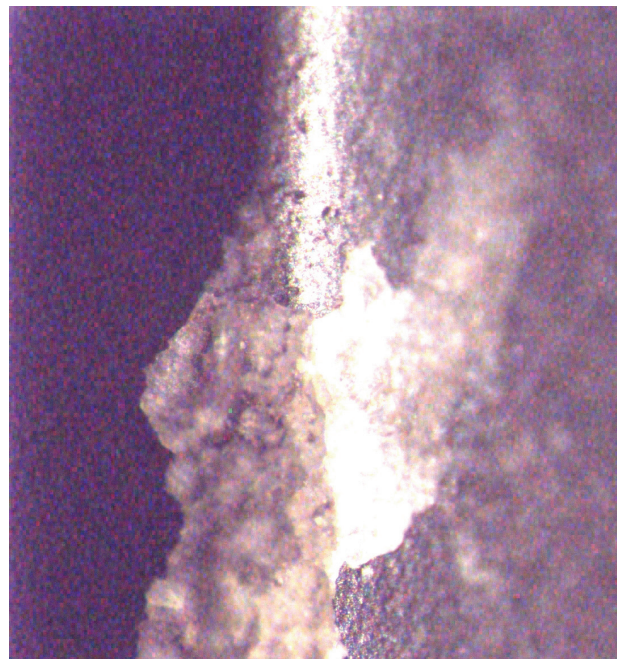


Figure 22 Salt deposits on the third stage stator vanes
(air flow moves from left to right)



a) 8x enlarged



b) 31x enlarged

Figure 23 Microscope images of second stage leading edge deposits

4.3.2 Leading edge deposit thickness

Leading edge deposit thickness was measured using electron microscopy. Figure 23 shows microscope images of the leading edge deposit thickness found on the second stage stator vanes.

4.3.3 Surface roughness along mean-line

The grain size and surface structure of the salt crystals along the mean-line of the first three stators were analyzed from Struers replicas using laboratory electron microscopes. Figure 24 shows application of Struers transcopy foil (reflective metallographic replica) on the 1st stage suction side. Further information is given in Paper II.

Microscope images of the grains were analyzed for stages one, two and three. A typical image is given in Figure 5 of Paper II. The arithmetic mean diameter of the salt grains in the sample is considered a measure of the grain size, k . The average distance between the salt crystals is calculated based on the number of crystals found in the sample.

The associated equivalent sand roughness, k_s , is estimated based on the average distance between the salt grains and by comparing the ratio of grain size to grain spacing with the associated equivalent sand roughness for regularly arranged spheres, as given in Table 1. Finally, the relative roughness is the ratio of equivalent sand roughness to the blade chord length.

4.3.4 Dissolved salt

To find the stage-by-stage salt distribution, the salt on the stator vanes was dissolved in water as seen in Figure 25. All top vanes in the top casing were used, and the salt in each stage was dissolved in 2 or 4 liters of boiling water. The stator vanes were continuously moved in the water for ten minutes. The water was analyzed for conductivity and chlorine content by Technological Institute Laboratory Services in Kongsberg, Norway and Buskerud Vann og Avløpscenter Laboratories in Drammen, Norway.



Figure 24 Application of Struer's replicas to collect salt grains (first stage suction side)



Figure 25 Dissolving salt on the first stage stator vanes

4.4 Conclusions

This chapter gave an overview of the test equipment and methods used in the experimental study, particularly for the GEJ85-13 experiments.

The online water wash system is designed to meet the requirements given in section 3.7.

The extra instrumentation added in the GE J85-13 allows collection of data which can verify fundamental issues of engine deterioration and recovery. The large number of unclassified reference sources provides a good basis for testing and modeling work for the GE J85-13.

The unshielded RTD sensors provide a good source of information on gas temperature change and the presence of liquids in the flow. The temperature sensors are only accurate for steady state measurements of single phase gas flow, and cannot measure the true phase temperatures in two-phase flow. Best accuracy is achieved when analyzing relative changes in the temperature at similar flow conditions. Care must be taken when comparing absolute gas temperatures because of gas velocity and temperature profile errors. Inter-stage temperature measurements can detect liquid propagation through the compressor.

Accelerated salt testing is an effective method to systematically deteriorate gas turbine compressor performance. Four methods are used for non-destructive characterization of the salt deposits in the engine. The methods can be applied to other water soluble deposits. The methods and their usage are given in Table 7. With the exception of borescope inspection, the methods require disassembly of the compressor section.

Table 7 Summary of methods to quantify compressor salt deposits

<i>Method</i>	<i>Applied to</i>
Visual inspection	Determine clean condition after washing
Leading edge deposit thickness	Quantify deposits at leading edge
Surface roughness along the mean-line	Quantify relative roughness along the mean-line
Dissolved salt	Stage-by-stage salt distribution

5 Performance Deterioration and Recovery

The purpose of this chapter is to summarize and discuss the main results of this work.

The main results are published in the papers. Stage characteristics published in Paper II were limited to four compressor stages, and a full set of data are given in Appendix I. Appendix J contains the online washing results for all stages for the cases published in Paper III. Previously unpublished data on liquid propagation in the GE J85-13 compressor are given in section 5.4.

The chapter is structured from the main issues defined in the scope of work:

- Section 5.1 covers character of fouling (goal C)
- Section 5.2 covers prediction accuracy of the loss models (goal A)
- Section 5.3 covers compressor deterioration signature (goal B)
- Section 5.4 covers sensitivity of online wash parameters (goal D)

5.1 Quantify fouling distribution and surface structure

This section summarizes results and discusses the salt deposits measured in the GE J85-13.

After the initial salt deterioration test, in which the GE J85-13 was deteriorated with 30g salt, the top casing was removed and the salt deposits were analyzed using the methods outlined in section 4.3. The data are published in Paper II.

The salt deposits in the GE J85-13 were found mainly in the front stages of the compressor. The stators were found to have more deposits than the rotor blades, and significant deposits were found both on the suction and the pressure side of the blades and along the hub and annulus.

Substantial leading edge deposits were observed particularly at the hub and annulus. These deposits are located at the leading edge stagnation point and are considered a visualization of the end-wall boundary layers.

Surface roughness was measured along the mean-line and corresponded to the scale of equivalent sand roughness. A maximum relative roughness of 0.0011 was found along the mean-line pressure side and 0.0008 along the mean-line suction side of the stator vanes (Table 2, Paper II). The roughness levels are sufficiently large to expect turbulent rough flow. The equivalent sand roughness levels imply less roughness than from a surface of emery grains 320. Although limited data are found in the literature (Paper II), the roughness levels found in this work are smaller than measured by others.

The weight distribution of fouling was measured after deterioration and repeated at the end of the test program after online wash after a 60 second online washing at low

flow rates and medium (75 μm) droplet size. The weight distribution in the deteriorated condition is similar to data found in the literature [91] (Figure 3, Paper II). Online washing re-deposits fouling in the aft stages, moving the peak fouling to stage 4 (Figure 14, Paper III).

The four methods for characterizing salt fouling in the stator vanes give valuable information on the location and character of the fouling in the engine. Visual inspection is important in defining a clean engine in between tests.

5.2 Validity of stage performance deterioration models

This section discusses the validity of the stage performance deterioration models.

The impact of fouling on stage performance is simulated using the loss models described in chapter 2 and applying the measured surface roughness given in Table 2 of Paper II. The results are compared to the measured stage performance losses of the fouled compressor to validate the applicability of the loss models. The results are presented in Paper IV, Figures 3 and 4.

The deviation model applies only to the design point and did not have any effect on the reduced stage performance shown in Paper IV. The deviation changes affect the stage velocity diagrams for deteriorated conditions given in Appendix I.

The deterioration loss models successfully reflect the degradation mechanisms although both models under-predict the relative changes from clean to deteriorated condition, particularly for total pressure and flow. Slightly better results are found for the isentropic efficiency modeled with the equivalent Reynolds correction method. The models under-predict the large variation in total pressure coefficient, but some of the deviation may be due to the unorthodox shape of the stage characteristics for the GE J85-13.

From the profile loss model, the fraction of hydraulic losses to total losses was found to be 38% at the design point for the GE J85-13. This number is reasonable compared to Howell's classic breakdown of losses for axial compressors given in Figure 4.

Reynolds corrections to the flow coefficient are not included in performance test codes. The modeling work shows the importance of the flow coefficient and necessitates a review of the current standards.

5.3 Compressor performance deterioration signature

This section discusses the deterioration signature for thermodynamic monitoring of compressor performance deterioration. Overall performance monitoring and stage performance monitoring are considered.

Overall performance monitoring

In Paper I, the overall performance deterioration parameters were identified for the RB211-24G installed on the Statoil Heidrun platform. For this three-spool engine, the best parameter was found to be the relative reduction in speed of the low pressure shaft compared to the shaft speed of the high pressure systems. The deterioration rate must be coupled with the deviation in compressor discharge condition to distinguish compressor fouling from other degradation sources. Although intake depression is recommended by the manufacturer for monitoring compressor fouling, the parameter was found to have too high of a data scatter because of inaccuracies in the estimation of bellmouth total pressure.

In Papers II and III, the overall GE J85-13 performance deterioration is displayed using the relative change in intake depression at constant corrected shaft speed. Sensitivity analysis (referred in section 4.2.7) showed intake depression to be the most sensitive parameter to engine deterioration, and the least affected by engine control, and is used to evaluate online washing effectiveness.

Compressor isentropic efficiency, given in Figure 9 of Paper II, showed a nonlinear shift in the degraded performance. The nonlinearity hampers the comparison of deterioration trends based on the calculation of percentage deviation at constant corrected engine speed.

In Paper I, the gas turbine was found to respond differently to fouling depending on the control mode. Fouling was found to be beneficial to the RB211-24G operating in speed control, due to the temperature compensation. In contrast, operation in temperature control (power turbine inlet temperature) resulted in rapid performance deterioration with fouling. In temperature control the accumulated cost of lost production was significant after only 400 hours. In speed control, the cost became significant after 800 hours of operation (Figure 10 of Paper I). ISO correction of data points did not account for the effect of varying control lines with ambient temperature.

The classic saw-tooth effect on engine capacity of offline and online washing is given in the introduction (Figure 3). This study shows that the engine control model may influence the power capacity. If the engine is running at different control modes during the course of the operation it would not be possible to duplicate the saw-tooth curve because the control mode will affect the output: The saw-tooth curve can only be duplicated at conditions in which the engine is running at the same exhaust gas temperature limitation.

In Paper IV, no narrowing of stall range is found in the combined compressor performance for the first three stages (Figure 5 of Paper IV). The narrowing of range found in Figure 11 may be due to the uniformly increased surface roughness applied in tests which was not found in the GE J85-13.

Stage performance monitoring

In Paper II, stage performance deterioration was monitored by analyzing the inter-stage temperature and pressure data measured in the engine. Full set of data for all stages are found in Appendix I.

The measurements for clean conditions are in good agreement with the published data. For stage 1, the maximum stage characteristic overshoots the published stage characteristics. However, the published stage characteristics are not validated at the surge point and the deteriorated condition measured in this work indicates that the maximum point of the characteristics is located at a higher point than reflected in the literature. For stages 6-8, the measured stage work coefficients are higher than in the published data. This is due to the inaccuracy of gas path temperature measurements.

Deterioration changes all aspects of the stage characteristics, reducing the stage work coefficient, the pressure coefficient, and the flow coefficient. The most significant effect of salt deterioration is the reduction in the flow coefficient. Stage efficiency was reduced for all stages. Stage work and pressure coefficient were unaffected by deterioration in the aft stages 5 to 8 where only traces of salt were observed.

The analysis of stage deterioration reveals performance deterioration in single stages and is used in this work to observe the relative movement of fouling and the stage performance recovery with online washing. This approach to measurement analysis is useful in determining performance recovery sensitivity with various online washing parameters.

5.4 Recovering performance with online washing

This section discusses the sensitivity of online wash parameters to performance recovery.

The results of the online washing tests were published in Paper I and Paper III. Paper III presents a limited set of data for the GE J85-13 tests, and the complete set is given in Appendix J.

In the following, the presence of liquids in the flow is analyzed by the gas path temperature variation from dry to wet conditions. These data are not previously published.

Fluid flow rate

The impact of increased fluid flow rate in terms of water-to-air ratio on the compressor performance recovery is published in Paper III. Data for all stages and including 0.87 % water-to-air ratio are given in Dataset 1 in Appendix J. Water-to-air ratio is found to be most significant for effective online water washing. For effective water washing of the entire compressor section the water-to-air ratio should be between 0.8 to 2%.

Figure 26 shows the temperature variation from dry to wet conditions in the GE J85-13 compressor. Liquid present in the gas path is indicated by a negative slope of the temperature change. For the lowest water-to-air ratio, liquids are present in the gas path up to stage 3, and seem to evaporate fully by stage 4. For larger water-to-air ratios, liquids are present in the aft stages at least up to stage 6. Increased water-to-air ratios allow liquids to penetrate further into the compressor section.

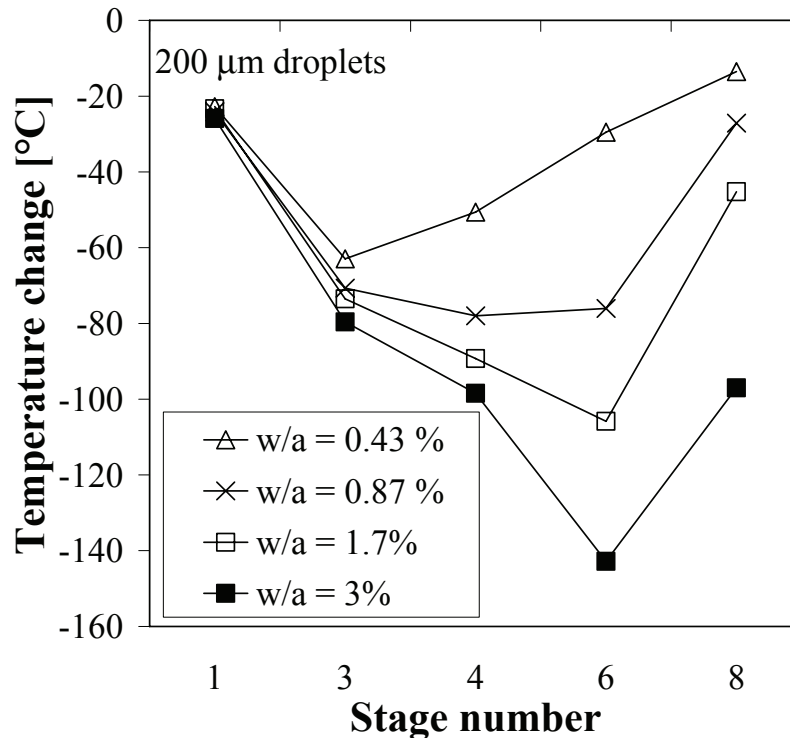


Figure 26 Temperature change from dry to wet conditions at different flow rates

The air temperature in stage six is above 200°C, as given in Appendix H. This shows that liquids penetrate further into the compressor section than expected from the water boiling point curve. The evaporation rate of the liquids must therefore be slower than the time to propagate through the compressor stages.

As shown in section 3.2, reports have concluded that online water washing can only be effective at air temperatures beyond the boiling point. By contrast, this work shows that liquids can propagate beyond the boiling point temperature of the compressor, and that the liquid propagation depends on the water-to-air ratio.

Duration

In Paper I, the effect of 3 minute and 6 minute online washing was tested with no significant variation in the deterioration rate.

In Paper III, the performance recovery was compared at equal water consumptions but different flow rates, hence at different durations. Dataset 3 in Appendix J gives

the stage work characteristics for all stages. Increased duration was found to have limited effect on performance recovery.

Washing frequency

In Paper I, the empirical data indicates that infrequent (less than once per day) washing intervals should be avoided due to increased deterioration rates.

Droplet size

In Paper I, two different nozzles were tested. The new nozzles provide the same flow rate, but the atomization of the droplets is improved. The two different nozzles gave no significant variation in the effectiveness of online washing in terms of limiting the engine deterioration rate.

In Paper III, the performance recovery with three different droplet sizes was tested at the lowest flow rate. Dataset 2 in Appendix J gives the stage work characteristics for all stages for 1 minute duration. The change in intake depression indicates a slightly better recovery with the 75 μm droplets, although from the stage characteristics the 200 μm and 75 μm droplet sizes give comparable recovery in all stages. The tests with smaller droplets of 25 μm shows less cleaning of the front stages and possible re-deposition of fouling beyond stage 4.

Figure 27 shows the temperature variation from dry to wet conditions with different droplet sizes. Liquids are present in the gas path up to stage 3. There is no observable change in the evaporation rate with the different droplet sizes. The increased re-deposition with the smaller droplets is therefore not caused by earlier evaporation.

The salt distribution tests discussed in section 5.1 showed fouling re-deposit with the 75 μm droplets. Based on data in Figure 27, the same picture is expected for the 25 μm droplet sizes at comparable water-to-air ratios.

System pressure levels are common to discuss when specifying online washing systems, advocating high pressure system because of smaller droplets and presumably better penetration into the compressor. This work shows that droplet size is not a predominant factor for performance recovery.

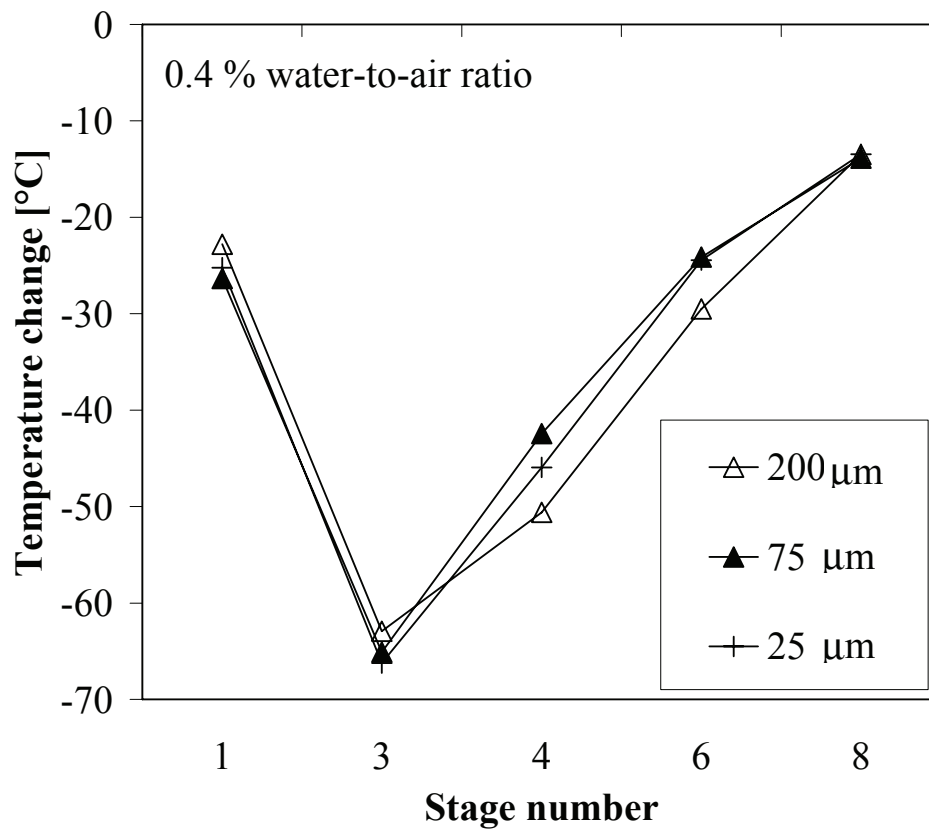


Figure 27 Temperature change from dry to wet conditions at different droplet sizes

Final note

A recent wind tunnel study of online washing effectiveness for carbon deposits supports the main conclusions of this work [19, 20]:

- Frequent intervals are necessary to clean off the deposits
- Online wash duration can be short, most of the cleaning occurs within 20 seconds.
- Increased water-to-air ratios reduce the level of re-deposit.

Use more water!

(Statoil gas turbine operator discussing test conditions, fall 2003)

6 Conclusions and Recommended work

The fundamental mechanisms of axial compressor performance deterioration and recovery were studied with three different approaches:

- a) Analysis of empirical data from a RB211-24G gas turbine installed at the Statoil Heidrun offshore platform.
- b) Accelerated salt deterioration and online water washing of a GE J85-13 jet engine at the test facilities of the Royal Norwegian Air Force at Kjeller, Norway.
- c) Development of a quasi-one-dimensional model for the GE J85-13 to aid in the test data analysis and to verify the applicability of deterioration loss models to fouled compressors.

6.1 Conclusions

The conclusions are derived directly from the scope of work given in section 1.3.

A: Performance deterioration mechanisms and loss models

- The literature review showed that profile loss, blockage, deviation, and 3D separation are the fundamental deterioration mechanisms of fouled axial compressors.
- Deterioration loss models are developed for all mechanisms except 3D separation and the results are validated based on empirical data from the GE J85-13.

The models successfully reflect the degradation mechanisms, although the models under-predict the relative changes from clean to deteriorated condition, particularly for total pressure and flow.

This work shows the importance of Reynolds correction in roughened compressors. Reynolds corrections to flow coefficient are not included in performance test codes.

B: Performance deterioration signature

- The empirical data collected at Heidrun successfully determined the overall performance deterioration signature of the RB211-24G.
- The GE J85-13 experimental program successfully demonstrated that performance recovery and relative movement of fouling can be detected by analyzing the stage work and pressure coefficients.

This work shows:

- Engine control mode will affect the deterioration rate and must be accounted for in the data analysis.

- Deterioration causes nonlinear changes to the compressor efficiency resulting in data scatter which hampers decision making.
- Fouling reduces the mass flow capacity of the compressor, and condition monitoring should include this parameter.
- Deterioration changes all aspects of the stage characteristics, reducing the stage work coefficient, the pressure coefficient and the flow coefficient. The most significant effect of salt deterioration is the reduction in the flow coefficient.

C: Deposit structure and distribution

- Surface roughness and weight-distribution were successfully measured for salt deteriorated stator vanes. The surface roughness elements were smaller than expected compared to data reported in the literature.
- Fouling was localized to individual stages by measuring weight distribution of salt deposits in the stages. The distribution of fouling was comparable to data in literature.

This work shows that fouling significantly increases the surface roughness on both the pressure side and the suction side of the stator vanes.

D: Fundamental parameters for online washing and performance recovery

- The literature review showed that water-to-air ratio, droplet size and duration are the most important parameters for online compressor washing.
- The empirical data collected at for the RB211-24G were not conclusive for establishing an optimized online washing method for the gas turbine.
- The GE J85-13 experimental program succeeded in highlighting the major parameters for online washing of axial compressors.

This work shows for online washing:

- Water-to-air ratio is the most sensitive online washing parameter for performance recovery. For effective water washing of the entire compressor section the recommended water-to-air ratio is between 0.8 to 2%. Lower flow rates cause re-deposit of fouling in the aft stages.
- Droplet size is of minor importance although the test data indicates that smaller droplets may increase the fouling in the aft stages.
- Longer durations cannot compensate for low flow rates.
- The evaporation rate inside the gas turbine is slower than the temperature increase of the air, allowing water to penetrate much further into the compressor section than is expected from the boiling point curve and the air temperature increase.

The work has determined the fundamental mechanisms of axial compressor performance deterioration and recovery through online washing and fulfils the overall project objective.

6.2 Recommended work

Inter-stage temperatures and intake depression should be reviewed to determine their suitability for field-testing and condition monitoring. Although the instrumentation used in this work is relatively easy to install, additional instrumentation should be tested in close cooperation with manufactures.

A fundamental review of the loss models and thereby a revision of the ASME and ISO standard codes on axial compressor testing is required to account for the effects of surface roughness and Reynolds number variation in axial compressors.

Online washing systems should be tailored to the gas turbine engine, the site and the fouling composition. Manufacturers should be challenged to allow for larger fluid flow rates during online wash.

New information is needed on actual fouling in industrial gas turbine engines. Fouling solubility, the associated surface roughness and stage-wise distribution are all important factors for the tailoring of online washing systems. The method used for characterizing the grain size of fouling should be improved for field applications. Further studies of fouling should be coupled with studies of the air intake filters in wetted conditions.

7 Perspectives of online washing

Online washing can decrease the deterioration rate in compressors, and regain most of the lost capacity seen in power plants. To be successful, online washing must be tailored to the gas turbine engine, and the water-to-air ratio must be increased from the current levels. Droplet size is not equally important as long as the droplets do not cause any secondary damage to the surfaces.

Ideally, online washing should remove the fouling from the compressor without increasing the level of re-deposit in the aft compressor stages or in the internal bleed channels. However, simply transporting the fouling to the combustion chamber may cause secondary problems depending on the nature of the fouling. Firstly, oily components may clog the combustor internals and cause coking. Secondly, salty components may cause hot corrosion of the turbine nozzle. Finally, liquids evaporating on the thin-walled combustor liner may cause temperature strains and subsequent liner cracking. Therefore, the best method for online washing may be to push the fouling from the front end of the compressor to an aft compressor stage, where severe fouling may not be detrimental to the gas turbine capacity and where the surge margin is sufficient to avoid compressor instabilities. Optimized online washing is therefore a compromise of hot corrosion resistance, combustor design, and stall margin of individual compressor stages. This optimized online washing can only be complimentary to offline washing.

Chemical additives that increase the fluid boiling point are not needed, because the evaporation rate inside the gas turbine is slower than the temperature increase of the air, allowing pure water to penetrate much further into the compressor section than is expected from the boiling point curve. Chemical additives may still be required to increase the solubility of the deposits.

Optimized online washing requires good monitoring practices to detect the small scale fouling of axial compressors. This work has shown that nonlinearities exist in the deteriorated performance signature. Future efforts to optimize online washing should carefully consider the deterioration signature of the individual gas turbine and the influence of engine control on the engine performance.

Final note and warning: Even the best-tailored online washing system design may fail its basic requirement of increased production capacity in the overall system. The great potential with online washing should be explored at sites where the engine capacity is limiting production and availability, bearing in mind that the engine control system may allow increased power capacity with compressor deterioration because the gas turbine is re-matched at a higher firing temperature.

8 References

- [1] American Meteorological Society, 2000, *Glossary of Meteorology* [online], Allen Press Inc., Second edition, <<http://amsglossary.allenpress.com/glossary/>> (Accessed 1 February 2007).
- [2] American Society of Mechanical Engineers, 1997, *Performance Test Code on Compressors and Exhausters*, ASME PTC 10-1997.
- [3] American Society of Mechanical Engineers, 1998, *Test Uncertainty*, ASME PTC 19.1-1998.
- [4] American Society of Mechanical Engineers, 1997, *Performance Test Code on Gas Turbines*, ASME PTC 22-1997.
- [5] Asplund, P., 1997, "Gas Turbine Cleaning Upgrade (Compressor Wash)," Proc. ASME ASIA'97 Congress and Exhibition, 30 Sept.- 2 Oct., Singapore, ASME Paper No. 97-AA-135.
- [6] Asplund, P. and Hjerpe, C.J., 2004, "A Method for Cleaning a Stationary Gas Turbine Unit During Operation," World Patent No. WO2004/055334.
- [7] ASTM, 1992, "Standard Practice for Determining Data Criteria and Processing for Liquid Drop Size Analysis," ASTM International, ASTM E 799-92 (Reapproved 1998).
- [8] Aungier, R.H., 2003, *Axial-Flow Compressors, A Strategy for Aerodynamic Design and Analysis*, ASME Press, New York, NY, USA, ISBN 0-7918-0192-6.
- [9] Badeer, G.H., 2000, "GE Aeroderivative Gas Turbines – Design and Operating Features" [online], GE Power Systems, GER-3695E, <http://www.gepower.com/prod_serv/products/tech_docs/en/downloads/ger3695e.pdf> (Downloaded 6 March 2003).
- [10] Baker, H.D., Ryder, E.A., Baker, N.H., 1975, *Temperature Measurement in Engineering Volume 2 – Deals with various methods of measuring low and very high temperatures in liquids, gases, flames and solid bodies*, Omega Press, Stamford, Connecticut, USA, LCCN 53-11565.
- [11] Bakken, L.E., Jordal, K., Syverud, E. and Veér, T., 2004, "Centenary of the First Gas Turbine to Give Net Power Output: a Tribute to Ægidius Elling", Proc. ASME Turbo Expo, 14-17 June, Vienna, Austria, ASME Paper No. GT2004-53211.
- [12] Balevic, D., Burger, R., Forry, D., 2004, "Heavy-Duty Gas Turbine Operating and Maintenance Considerations" [online], General Electric Company, GER-3620K, <http://www.gepower.com/prod_serv/products/tech_docs/en/downloads/ger3620k.pdf> (Downloaded 12 March 2007).
- [13] Bammert, K. and Milsch, R., 1972, "Boundary layers on rough compressor blades," Proc. ASME Gas Turbine and Fluids Engineering Conference & Product Show, 26-30 March, San Francisco, CA, USA, ASME Paper No. 72-GT-48.
- [14] Bammert, K. and Woelk, G.U., 1979, "The influence of the blading surface roughness on the aerodynamic behavior and characteristic of an axial compressor," Proc. ASME Gas Turbine Conference, 12-15 March, San Diego, Ca, ASME Paper No. 79-GT-102.

- [15] Birol, F., 2005, "World energy prospects to 2030" [online], In *The World Energy Book, Issue 1: Autumn 2005*, Published by Petroleum Economist Ltd on behalf of World Energy Council, London, UK, ISBN 1-8618-6290-3, pp. 2-5, <http://www.petroleum-economist.com/web/pdf/sect_1_world_overview.pdf> (Accessed 16 May 2006)
- [16] Bjørnås, F., 2000, *Optimal drift av gassturbinar*, Diploma Thesis, NTNU, Trondheim, Norway.
- [17] Borthne, M., 1993, *Fouling and on-line compressor cleaning of the Stal Laval GT35*, Diploma Thesis, NTH, Trondheim, Norway.
- [18] Brekke, O., 2004, *Gas turbine performance deterioration*, Master's thesis, NTNU, Trondheim, Norway.
- [19] Brun, K., Kurz, R., 2006 "Turbo myth busters," *Turbomachinery International*, 47, November/December.
- [20] Brun, K.(klaus.brun@swri.org), 18 January 2007, "Re: Online washing studies by SWRI," personal email to E. Syverud (elisabet.syverud@ntnu.no).
- [21] Caguiat, D.E., Zipkin, D.M., and Patterson, J.S., 2002, "Compressor fouling testing on Rolls Royce/Allison 501-K17 and General Electric LM 2500 gas turbine engines," Proc. ASME Turbo Expo, 3-6 June 2002, Amsterdam, the Netherlands, ASME Paper No. GT2002-30262.
- [22] Carstensen, C., Christiansen, A., Johansen, S., Puntervold, K., 1994, "Erfaringer med on-line vannvaskesytem på GFA," Statoil report.
- [23] Conntect, 2007, *Conntect Online*, Conntect Inc., Brookfield, CT, USA, <<http://www.conntect.com>> (Accessed 13 March 2007).
- [24] Cumpsty, N., 1989, *Compressor Aerodynamics*, Longman Scientific & Technical, Harlow, Essex, UK, ISBN 0-582-01364-X.
- [25] Dokka, A., Midttun, Ø. (editors), 2006, "FACTS, The Norwegian Petroleum Sector 2006," Norwegian Ministry of Petroleum and Energy, Oslo, Norway.
- [26] Engdar, U., Orbay, R.C., Genrup, M., Klingmann, J., 2004, "Investigation of the two-phase flow field of the GTX100 compressor inlet during off-line washing," Proceedings of ASME Turbo Expo, 14-17 June, Vienna, Austria, ASME Paper No. GT2004-53141.
- [27] Engine Cleaning Technology, 2007, *ECT Online*, Engine Cleaning Technology, Bridgeport, PA, USA, <<http://www.enginecleaningtechnology.com>> (Accessed 13 March 2007).
- [28] EPRI, 2006, "Combustion Turbine F-Class Life Management: Investigation of GE7FA R0 EPRI, Compressor Stage Blade: Investigation of GE7FA R0 Compressor Stage Blade", Electric Power Research Institute Report 1011490, EPRI Palo Alto, CA, USA, January 2005.
- [29] Erickson, D.M., Grove, G.W., Hu I.Z., Kight, M.S., Porter, L., Schott, C.G., 2007, "Gas turbine on-line compressor water wash system", US Patent Number US 2007/0028947 A1.
- [30] Faddegon, C.J., 1999, "Effective compressor cleaning as a result of scientific testing and field experience," FP Turbomachinery Consultants GmbH, Voorburg, the Netherlands.

-
- [31] Flashberg, L.S., Haub, G.L., 1992, "Measurement of Combustion Turbine Non-Recoverable Degradation," Proc. ASME International Gas Turbine and Aeroengine Congress and Exposition, Cologne, Germany, 1-4 June, ASME Paper No. 92-GT-264.
- [32] Foss, G., 1999, "On-line water wash test," Kværner Energy a.s., Test Cell, Report No. 690280.
- [33] FP-Turbomachinery, 2007, *FP-Turbo Online*, FP-Turbomachinery, <<http://www.fpturbo.com>> (Accessed 13 March 2007).
- [34] Garwood, K.R. (Chairman), 1995, *Recommended practices for the assessment of the effects of atmospheric water ingestion on the performance and operability of gas turbine engines*, North Atlantic Treaty Organization, Advisory Group for Aerospace Research & Development, Neuilly-Sur-Seine, France, AGARD-AR-332.
- [35] Gas Turbine Efficiency, 2007, *Optimized Gas Turbine Cleaning Technology*, Gas Turbine Efficiency, London, UK, <<http://www.gtefficiency.com/>> (Accessed 13 March 2007).
- [36] Gbadebo, S.A., Hynes, T.P., Cumpsty, N.A., 2004, "Influence of surface roughness on three-dimensional separation in axial compressors," Proceedings of Proc. ASME Turbo Expo, 14-17 June, Vienna, Austria, ASME Paper No. GT2004-53619.
- [37] Genrup, M., 2003, *Theory for turbomachinery degradation and monitoring tools*, Thesis for Degree of Licentiate in Engineering, Lund Institute of Technology, Lund, Sweden.
- [38] Ghenaiet, A., Tan, S.C., Elder, R., 2005, "Prediction of an axial turbomachine performance degradation due to sand ingestion," Proc. ImechE Part A: J. of Power and Energy, Vol.219, No.4, pp.273-287.
- [39] Gonzalez, F., Boyce, M.P., 2005, "A Study of On-Line And Off-Line Turbine Washing To Optimize The Operation of a Gas Turbine," Proc. ASME Turbo Expo: Power for Land, Sea and Air, 8-11 June, Reno NV, USA, ASME Paper No. GT2005-69126.
- [40] Hager, R.D., 1977, "Analysis of internal flow of J85-13 multistage compressor," NASA Lewis Research Center, Cleveland, OH, USA, NASA Technical Memorandum No. TM X-3513.
- [41] Halstead, D.E.; Wisler, D.C.; Okiishi, T.H.; Walker, G.J.; Hodson, H.P.; Shin, H.-W., 1997, "Boundary Layer Development in Axial Compressors and Turbines: Part 1 – Composite Picture," J. of Turbomachinery, Vol.119, January, pp. 114-127.
- [42] Hammersvik, A.K., Oltedal, H., 1999, "Langtidstest av høytrykks on-line vaskesystem på LM2500PE generatorturbin B på Sleipner A," Statoil Report.
- [43] Harris, H. and Calabrese, M., 1994, "On-Line Detergent Fluid Evaluation on a TF40B Gas Turbine Engine," Proc. ASME International Gas Turbine and Aeroengine Congress and Exposition, 13-16 June, the Hague, Netherlands, ASME Paper No. 94-GT-452.

- [44] Haub, G.L. and Hauhe, W.E. jr., 1990, "Field evaluation of on-line compressor cleaning in heavy duty industrial gas turbines," ASME Gas turbine and Aeroengine Congress and Exposition, 11-14 June, Brussels, Belgium, ASME Paper No. 90-GT-107.
- [45] Hayward, J., Winson, G., 2000, "Cleaning Method and Apparatus," US Patent No. 6,073,637, 2000.
- [46] Howell, A.R. and Calvert, W.J., 1978, "A New Stage Stacking technique for Axial-Flow Compressor Performance Prediction," J. of Engineering for Power, Vol.100, pp.698-703.
- [47] International Organization for Standardization, 1989, *Specification for gas turbine acceptance tests*, ISO 2314:1989.
- [48] International Organization for Standardization, 1992, *Turbocompressors – Performance test code*, ISO 5389:1992(E).
- [49] International Organization for Standardization, 2003, *Measurement of fluid flow by means of pressure differential devices inserted in circular cross-section conduits running full – Part 3: Nozzles and Venturi nozzles*, European Committee for Standardization, CEN, Brussels, Belgium, ISO 5167-3:2003.
- [50] Jeffs, E., 2007, "No more compressor was day blues", Power Engineering International, 15, Issue, 1 January/February.
- [51] Koch, C.C., Smith, L.H. jr., 1976, "Loss sources and Magnitudes in axial-flow compressors," J. of Engineering for Power, July, pp. 411-424.
- [52] Kolkman, H.J., 1993, "Performance of gas turbine compressor cleaners," J. of Engineering for Gas Turbines and Power, Vol.115, pp.674-677.
- [53] Lans, E., 2006, Camfil Farr Sweden, Private communication, April.
- [54] Lecheler, S., Hoffman, J., 2003, "The power of water in gas turbines: ALSTOMS's experience with air inlet cooling", Proc. POWER-GEN Latin America, 11 - 13 November, São Paulo, Brazil.
- [55] Lieblein, S., 1959, "Loss and Stall Analysis of Compressor Cascades", J. of Basic Engineering, September, pp.387-400.
- [56] Loud, R.L., Slaterpryce, A.A., 1991, "Gas Turbine Inlet Air Treatment" [online], GE Power Generation, GER-3419A, <www.gepower.com/prod_serv/products/tech_docs/en/downloads/ger3419a.pdf> (Downloaded 10 March 2004).
- [57] Maclin, H. M., 2003, "*Propulsion Technologies for Future Air Vehicles*" [online], Speech for the 2003 NASA/NIA Turning Goals Into Reality Conference, 10-12 June, Williamsburg, VA, USA.
- [58] Mal'tsev, Yu.N., and Shakov, V.G., 1989, "Influence of roughness of deposits in compressor cascade on flow lag angle (English translation)," Izvestiya VUZ, Aviatsionnaya Tekhnika, Vol.32, pp. 80-82.
- [59] Marson, E., 1992, "Effect of manufacturing deviations on performance of axial flow compressor blading," Proc. ASME Gas Turbine and Aeroengine Congress and Exposition, 1-4 June, Cologne, Germany, ASME Paper No. 92-GT-326.
- [60] McDermott, P.E., 1991, "Gas Turbine Compressor Fouling: The Case for On-Line Cleaning," Turbomachinery International, Jan/Feb.

-
- [61] Mee, T.R., 2004, "Droplet size affects fogger output", *Turbomachinery International*, Vol.45, March/April, pp.37-39.
- [62] Meher-Homji, C.B., Bromley, A., 2004, "Gas turbine axial compressor fouling and washing," Proc. 33rd Turbomachinery Symposium, Houston, TX, USA, pp. 163-192.
- [63] Milner, E.J., Wenzel, L.M., 1975, "Performance of a J85-13 compressor with clean and distorted inlet flow," NASA Lewis Research Center, Cleveland, OH, USA, NASA Technical Memorandum No. TM X-3304.
- [64] MIL-specification, 1998, *Performance Specification, Cleaning Compound, Turbine Engine Gas Path*, MIL-PRF-85704C.
- [65] Milsch, R., 1971, *Systematische Untersuchung über den Einfluss der Rauigkeit von Verdichterschaufeln auf den Gitterwirkungsgrad*, Doktor Ingenieur Dissertation, Technischen Universität Hannover, Germany.
- [66] Molinari, M., Dawes, W.N., 2006, "Review of evolution of compressor design process and future perspectives," *IMEchE Part C: J. of Mechanical Engineering Science*, Vol.220, pp. 761-771.
- [67] Mund, F., Pilidis, P., 2006, "Gas turbine compressor washing: Historical developments, trends, and main design parameters for online systems," *J. of Engineering for Gas Turbines and Power*, Vol.128, April, pp-344-353.
- [68] Mund, F.C., Pilidis, F., 2005, "Online compressor washing: a numerical survey of influencing parameters", *IMEchE Part A: J. of Power and Energy*, Vol. 219, pp.13-23.
- [69] NACA SP-36, 1965, "Aerodynamic design of axial flow compressors," NASA Lewis Research Center, Cleveland, OH, USA.
- [70] Nikuradse, J., 1933, "Strömungsgesetze in rauhen Rohren," *Forschungsheft 361*, VDI-Verlag GMBH, Ausgabe B, Band 4, Juli/August.
- [71] Norwegian Petroleum Directorate, 2006, *NPD fact pages 2006*, Heidrun Field [online], <<http://www.npd.no/engelsk/cwi/pbl/en/>> (Accessed 3 May 2007).
- [72] Oliver, J.S., 1992, "Review of on-line washing," Rolls-Royce PLC, Report No. RDR251.
- [73] Øverli, J., 1992, *Strømningsmaskiner 3*, Tapir forlag, Trondheim, Norway, 2nd ed., ISBN 82-519-1116-8.
- [74] Pilch, M., Erdman, C.A., 1987, "Use of breakup time data and velocity history data to predict the maximum size of table fragments for acceleration-induced breakup of a liquid drop," *Int. J. Multiphase Flow*, Vol.13, No.6, pp. 741-757.
- [75] R-MC, 2007, *R-MC Online*, R-MC Power Recovery Ltd, Stamford, UK, <<http://www.conntect.com>> (Accessed 13 March 2007).
- [76] Rochem, 2007, *Rochem Online*, Rochem Technical Services (USA) Ltd, Houston, TX, USA, <<http://www.rochemltd.com>> (Accessed 13 March 2007).
- [77] Rolls-Royce, 1996, "Fired compressor washing", RB211 Service Bulletin No. 087.

- [78] Rolls-Royce, 1997, "Performance assessment to study the effect of a 3000 hour interval between compressor washes on the Statoil Heidrun offshore installation", Technical Report No. CS052.
- [79] Saravanamuttoo, H.I.H. (Chairman), 1990, *Recommended practices for measurement of gas path pressures and temperature for performance assessment of aircraft turbine engines and components*, North Atlantic Treaty Organization, Advisory Group for Aerospace Research & Development, Neuilly-Sur-Seine, France, AGARD-AR-245.
- [80] Schäffler, A., 1980, "Experimental and analytical investigation of the effects of Reynolds number and blade surface roughness on multistage axial flow compressors," *J. of Engineering for power*, Vol.102, January, pp. 5-13.
- [81] Schlichting, H., 1979, *Boundary-layer theory*, McGraw-Hill Inc., New York, NY, 7th ed.
- [82] Schwieger, B. (ed.), 2006, "Compressor issues dominate discussion at annual conference" *Combined cycle journal*, PSI Media, Las Vegas, NV, USA, 3Q, pp.13-24.
- [83] Scott, J.N., 1979, "Axial compressor deterioration by measuring air intake depression," National Research Council, Third symposium on gas turbine operations and maintenance, Chapter 13.
- [84] Singh, D., Hamed, A., Tabakoff, W., 1996, "Simulation of performance deterioration in eroded compressors," *Proc. ASME International Gas Turbine and Aeroengine Congress & Exhibition*, Birmingham, UK, 10-13 June 1996, ASME Paper No. 96-GT-422.
- [85] Spraying Systems, 1989, "Datasheet 5838M," Spraying Systems Co., Wheaton, IL, USA.
- [86] Stalder, J.-P., 2001, "Gas turbine compressor washing state of the art: Field experiences," *J. of Engineering for Gas Turbines and Power*, Vol.123, April, pp. 363-370.
- [87] Stalder, J-P., Sire, J., 2001, "*Salt percolation through gas turbine air filtration systems and its contribution to total contaminant level*," *Proc. JPGC'01 International Joint Power Generation Conference*, 4-7 June, New Orleans, LA, USA, Paper No. JPGC2001/PWR-19148.
- [88] Statoil, 2006, *Statoil Annual report*, <<http://www.statoil.com>>.
- [89] Sturb, R.A., Bonciani, L., Borer, C.J., Casey, M.V., Cole, S.L., Cook, B.B., Kotzur, J., Simon, H., Strite, M.A. (ICAAMC working group), 1987, "Influence of the Reynolds number on the performance of centrifugal compressors," *ASME Gas Turbine Conference and Exhibition*, Anaheim, CA, USA, 31 May- 4 June, ASME Paper No. 87-GT-10.
- [90] Syverud, E., 2005, "Droplet size measurements of sprays used in GE J85-13 salt deterioration and online water wash test," NTNU Test report, 15 March.
- [91] Tarabrin, W.P., Schurovsky, V.A., Bodrov, A.I., and Stalder, J-P., 1998, "Influence of axial compressor fouling on gas turbine unit performance based on different schemes and with different initial parameters," *Proc. ASME Turbo Expo*, 2-5 June, Stockholm, Sweden, ASME Paper No. 98-GT416.

-
- [92] Taylor, D.H., 1993, "The use of air intake depression measurement for optimising compressor washing frequency," Rolls-Royce RB211 Service Information Letter 021.
- [93] Tesch W.A., and Steenken, W.G., 1976, "Blade row Dynamic digital compressor program, Volume 1, J85 clean inlet flow and parallel compressor models", General Electric Company Cincinnati, OH, USA, NASA Report No. CR-134978.
- [94] Thames, J.M., Stegmaier, J.W. and Ford, John J. jr., 1989, "On-line compressor washing practices and benefits," Proc. ASME Gas turbine and Aeroengine Congress and Exposition, 4-8 June, Toronto, Canada, ASME Paper No. 89-GT-91.
- [95] Tsuchiya, T. and Murthy, S.N.B., 1982, "Water ingestion into jet engine axial compressors," American Institute of Aeronautics and Astronautics, AIAA Paper No. 82-0196.
- [96] Tsuchiya, T., 1982, *Aerothermodynamics of axial-flow compressors with water ingestion*, PhD dissertation, Purdue University, Ann Arbor MI, USA.
- [97] Turbotect, "Innovative on line wash nozzle for large gas turbines", Turbotect Ltd, Baden, Switzerland, <<http://www.turbotect.com/product9.shtml>>, (Accessed 28 March 2007).
- [98] Turbotect, 2007, *Turbotect Online*, Turbotect Ltd, Baden, Switzerland, <<http://www.turbotect.com>> (Accessed 13 March 2007).
- [99] US Code of Federal regulations, 2007, "Paragraph 33.78 Rain and Hail Ingestion," in *Title 14: Aeronautics and Space, Part 33 – Airworthiness Standards: Aircraft Engines*.
- [100] Volponi, A., 1999, "Gas turbine parameter corrections", J. of Engineering for Gas Turbines and Power, Vol.121, October, pp. 613-621.
- [101] Walsh, P.P., and Fletcher, P., 1998, *Gas turbine performance*, Blackwell Science Ltd, Oxford, UK, ISBN 0-632-04874-3.
- [102] Wassell, A.B., 1968, "Reynolds number effects in axial compressors," J. of Engineering for Power, April, pp. 149-156.
- [103] Williams, J.C., Freeman, C., Day, I., 2005, "Rain ingestion in axial flow compressors at part speed," Proc. ASME Turbo Expo, June 2005, ASME Paper No. GT2005-68582.
- [104] World Energy Council, 2004, "Performance of Generating Plant – Synopsis: New Realities, New Needs," World Energy Council, London, UK.
- [105] Yan, L., Filipo, B.K., 2006, "Aqueous compositions for cleaning gas turbine compressor blades", United States Patent, US 7,018,965/B2.
- [106] Zaba, T., 1980, "Losses in gas turbines due to deposits on the blading," Brown Boveri Rev., Vol.67, No.12, pp. 715-722.

Appendix A

Paper I on Online washing at Heidrun

Syverud, E., Bakken, L.E., Langnes, K. and Bjørnås, F., 2003,
“Gas Turbine Operation Offshore; Online Compressor Wash at Peak Load”,
Proc. ASME Turbo Expo: Land, Sea & Air, 16-19 June, 2003, Atlanta, GA, USA,
ASME Paper No. 2003-GT-30871.

Paper I is not included due to copyright.

Appendix B

Paper II on Compressor Deterioration

Syverud, E., Brekke, O. and Bakken, L.E., 2007,
“Axial Compressor Deterioration Caused by Saltwater Ingestion”,
J. of Turbomachinery, Vol.129, No.1, pp. 119-126.

Errata:

Appendix B of paper, step (6)

Equation should read:

$$\tau = \frac{T_m - T_s}{T_t - T_s} \Rightarrow T_t = \frac{T_m - T_s}{\tau} + T_s$$

Paper II is not included due to copyright.

Appendix C

Paper III on Online Washing of GE J85-13

Syverud, E., and Bakken, L.E., 2007,
“**Online Water Wash Test of GE J85-13**”,
J. of Turbomachinery, Vol.129, No.1, pp. 136-142.

Paper III is not included due to copyright.

Appendix D

Paper IV on Modeling Losses Due to Surface Roughness

Syverud, E., and Bakken, L.E.

“The Impact of Surface Roughness on Axial Compressor Performance Deterioration,”

Proc. GT2006 ASME Turbo Expo: Power for Land, Sea and Air, 8-11 May, 2006, Barcelona, Spain, ASME Paper No. GT2006-90004.

Errata:

Table 2

Heading of column 3 is should read **$1-\eta_{\text{profile}}$ Eq. (13)**.

Frictional loss model (two off)

The assumed surface roughness in clean conditions is given as equivalent sand roughness, not relative roughness. For both models, step i) should read:

i) The Darcy friction factor for clean conditions, λ_{clean} , is calculated from Eq. (1) at given Reynolds number and assuming for the clean surface **an equivalent sand roughness of 5 k_s, 9 k_s, and 3 k_s** for stages 1, 2, and 3, respectively.

Paper IV is not included due to copyright.

Appendix E

GE J85-13 Measurement Error Analysis

This appendix contains measurement uncertainties for the GE J85-13 engine instrumentation and gives a measurement error analysis for the gas path temperature sensors.

Measurement uncertainty

Pre-test and post-test measurement uncertainties were evaluated for all data. The uncertainty analysis was based on the ASME Performance Test Codes on Gas Turbines [4] and Test Uncertainty [3]. Pre-test uncertainties were analyzed in full by Brekke [18] and are presented in Table 8. In the pre-test analysis, the random error was based on manufacturer's data and the systematic error was based on the highest deviation between enforced and measured values as observed during calibration.

Post-test review of all critical measurements is done for clean condition for a total of 26 data points at 98% shaft speed. The resulting confidence interval for the sample and the mean is given in Table 8. All data points used to assess the spread and confidence interval are raw data.

The measured test data consist of 60 datasets of 10-point rolling averages. When calculating the average of these 60 datasets, the initial and final nine data points are weighted differently than the middle points. This causes a shift in the mean value for the 60 datasets compared to the true mean of the 69 data points. The associated error in the mean value is given in Table 8 and is valid for all conditions (clean, deteriorated and recovered).

The post-test review shows a slightly larger sample spread for the gas path pressure data and the gas temperature at stage 4 and at compressor discharge.

The shift in the mean value due to rolling-average measurement is insignificant for all data except compressor discharge pressure.

The larger spread in the compressor discharge temperature is due to missing decimals in the measured data. This was not detected during testing.

The large deviation in exhaust gas temperature indicates burner deterioration due to coking. This was expected, because the engine was not overhauled prior to testing, and the F34 fuel is known to cause coking.

The spread in compressor discharge pressure is 3.5 times larger than expected. In addition, the mean is shifted significantly due to the rolling-average data sampling, and is caused by rapid variations in the measurements. To reduce the data scatter, more than one pressure tap should be installed to measure stage 5 and compressor discharge pressure. With only one pressure tap installed, the pressure measurements are the least accurate and most prone to instabilities of all measurements. The pressure data are used in the data analysis to determine polytropic efficiency. Increased inaccuracy in the pressure measurements is of minor importance to the data analysis.

Table 8 Measurement uncertainties

Measurement	Pre-test Measurement uncertainty	Sample spread	Post-test 95% confidence interval	Mean value shift
Ambient temperature (K)	0.506		Manual reading	
Relative humidity (%)	3.178		Manual reading	
Total pressure at compressor face (kPa)	0.305	0.203	0.018	$< \pm 0.005$
Static bellmouth depression (kPa)	0.433	0.765	0.041	$< \pm 0.01$
Compressor inlet temperature (total) (K)	0.368	0.150	0.009	$< \pm 0.07$
Temperature at station 2.1 (K)	0.394	0.400	0.029	$< \pm 0.02$
Temperature at station 2.3 (K)	0.604	0.500	0.033	$< \pm 0.01$
Temperature at station 2.4 (K)	0.604	1.13	0.073	$< \pm 0.01$
Pressure at station 2.5 (static) (kPa)	1.365	2.137	0.123	$< \pm 0.05$
Temperature at station 2.6 (K)	0.822	0.75	0.047	$< \pm 0.04$
Compressor discharge temperature (K)	0.846	1	0.108	$< \pm 0.07$
Compressor discharge pressure (static) (kPa)	2.738	9.58	0.602	$< \pm 0.4$
Exhaust gas temperature (K)	0.798	4	0.258	$< \pm 0.15$
Thrust (kN)	0.116	0.102	0.008	$< \pm 0.002$
Shaft speed (rpm)	37.03	33	2.48	$< \pm 1$
Fuel flow (kg/h)	32.57	19.3	1.04	$< \pm 0.5$

Uncertainty of dependent parameters

The uncertainties in the dependent parameters are calculated as the root-mean-square of the measurement uncertainty of the independent parameters [3].

Error analysis for the gas path temperature sensors

Measuring gas path temperatures in high velocity gas flow laden with salt and water droplets using unshielded sensors requires firm control of the associated errors. The following issues are discussed in detail:

- Gas path blockage
- Temperature profile errors
- Gas Velocity error
- Errors due to salt deposits
- Other aerodynamic and thermodynamic errors

Gas path blockage

According to recommended practices for gas path instrumentation, gas path blockage should be limited to 2 to 5% of flow path [79]. As seen in Table 9, the sensor installation fulfils the overall blockage recommendation although the single cell blockage is larger.

Table 9 Gas path blockage due to temperature sensors

<i>Stage</i>	<i>Sensor</i>	<i>Single cell blockage (%)</i>	<i>Overall blockage (%)</i>
1	T _{2,1}	2.5	0.053
3	T _{2,3}	7.6	0.080
4	T _{2,4}	11	0.096
6	T _{2,6}	19	0.13
Discharge	T ₃	N/A	0.14

In this work, measurement errors associated with gas path blockage are assumed insignificant.

Temperature profile errors

In this work, the measured temperature is regarded as a bulk mean temperature measurement at the stage. Any temperature profile may affect this assumption and cause deviations from expected performance.

The temperature profile of the GE J85-13 has been measured in tests at NASA [40]. Figure 28 shows the temperature profiles at compressor stages 1, 3, 4 and 6 at 100% of design speed in clean conditions. The data are measured at the inlet to the stage stator and are therefore representative of the measurement location used in this work. The hub, tip and mean-line radii are overlaid in the figure as well as the temperature sensor extremity. No temperature profile data are available for the compressor discharge condition, or for operation in fouled conditions.

The temperature sensor will measure the mean gas temperature of the immersed sensor height. This will be higher than the mean-line gas temperature. Table 10 gives the measurement errors due to temperature profile based on the data in Figure 28. The

temperature increases from stage 1 to 3 and from stage 4 to 6 are assumed to change linearly.

For direct comparison of measurements with published stage characteristics in clean conditions, the measured data will be higher than expected. The errors are particularly large at stages 1, 5 and 6 where the stage work coefficient may be 10 % to 20 % higher than expected. This is seen in Paper II and III where the stage six work coefficients are higher than the published data.

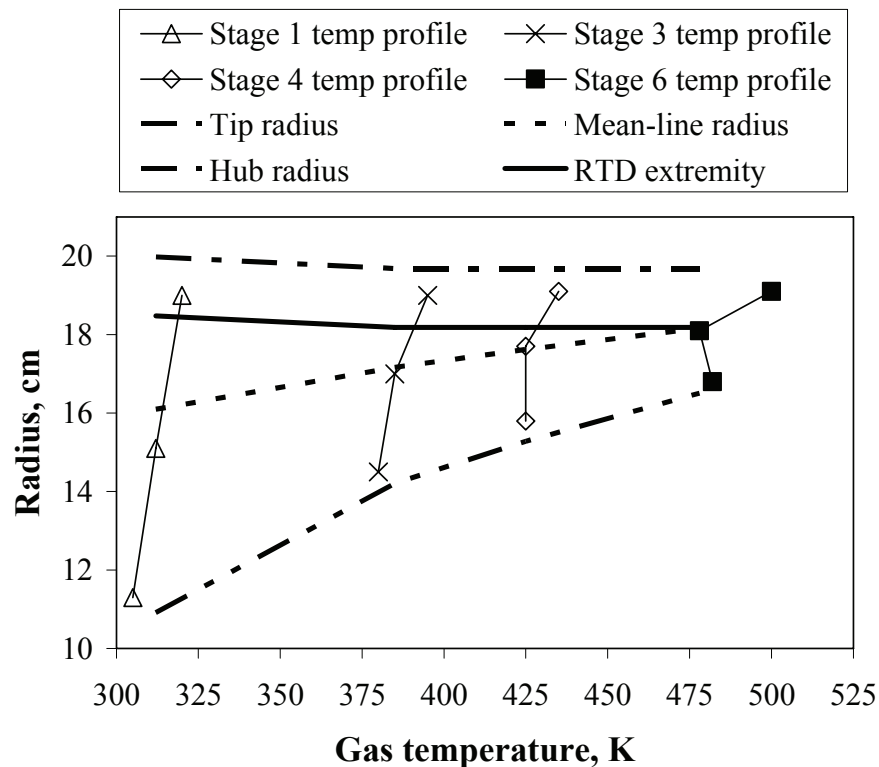


Figure 28 Gas path temperature profiles [40]

Table 10 Temperature profile error

<i>Stage</i>	<i>Sensor</i>	<i>Error in measured gas temperature error (K)</i>	<i>Error in stage temperature increase (K)</i>	<i>Error in stage work (%)</i>
1	T2.1	7.8	7.8	20
2	---	---	0.54	1.4
3	T2.3	8.9	0.54	1.4
4	T2.4	8.0	-0.9	-2.6
5	---	---	3.9	13
6	T2.6	16	3.9	13
7	---	---	---	N/A
Discharge	T3	Unknown	N/A	N/A

In this work, the gas path temperature measurements are not corrected for temperature profile. Because the analysis is based on the difference between the clean and deteriorated conditions, the deviation in measured stage work is insignificant to the conclusions.

Gas Velocity error

For a temperature sensor immersed in a gas, the gas stagnates against the sensor surface and equilibrates thermally with the sensor surface. However, the measured temperature generally does not indicate the thermodynamically ideal stagnation temperature because the gas is not brought to rest adiabatically. In addition, the viscous and thermal diffusion properties of real fluids are characterized by the Prandtl number, Pr . For an ideal gas of $Pr = 1.0$ the viscous heating effects generated by the stagnating real fluid are exactly diffused thermally so that the real dynamic temperature is the ideal. Air has a Prandtl number between 0.65 and 0.7, hence thermal diffusion effects are greater than the viscous effects and the dynamic temperature is less than the ideal [10].

When immersing unshielded RTD sensors in high velocity flow, the gas velocity will affect the flow measurement and one measures neither the total nor static temperature, but an in-between temperature. Gas velocities above 10 m/s or Mach numbers above 0.11 are expected to cause significant temperature errors (above 0.5 K) [2, 4, 47, 48]. As given in Appendix H, the gas velocities are above Mach 0.11 throughout the GE J85-13 compressor section.

The temperature recovery factor, r , is used to adjust for the gas velocity error. The factor is dependent upon gas properties, sensor shape, orientation in flow and the presence of turbulence in the stagnation process. To find the true recovery factor, a vigorous test program is needed to test the temperature probes under realistic conditions for pressure, temperature, velocity, flow orientation and turbulence. Recommended values for the temperature recovery factor for Mach numbers up to 1.0 is 0.68 ± 0.07 for bare thermocouple wires normal to flow [79]. The standards recommend a recovery factor of 0.65 for air velocities below 91m/s [2] or for cases where the recovery factor is not available or stagnation probes cannot be used [48]. No temperature recovery factor was available from the manufacturer of the RTD sensors used in the GE J85-13 tests.

In this work, a recovery factor of 0.65 is used for the gas temperature measurements. This is solely based on the above recommendations. Figure 29 shows the error in total temperature and stage work associated with changes in the temperature recovery factor from 0.65. Stage work is over-predicted if the temperature recovery factor is reduced.

The relative change in stage work due to salt deterioration is not affected by errors in the temperature recovery factor as long as the factor is kept constant throughout the data analysis, and the data are compared at similar Mach numbers.

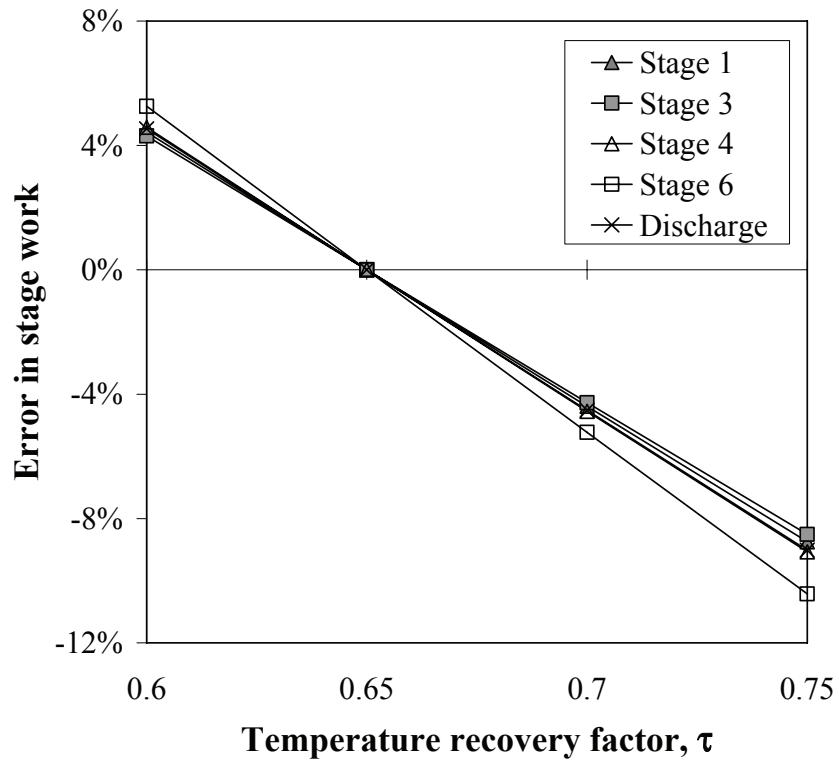


Figure 29 Effect of variation in temperature recovery factor on the stage work



Figure 30 Salt deposits on first stage temperature sensor

Errors due to probe salt deposits

Some salt deposits were present on the gas path temperature probes after deterioration. The probe with salt deposits is shown in Figure 30. A verification test showed no changes to the first stage temperature measurements after cleaning the stage 1 temperature probe.

In this work, the temperature measurements are considered to be unaffected by the small salt deposits on the probes.

Other aerodynamic and thermodynamic errors

In this work, the heat conduction errors are assumed negligible because the entire sensor is immersed in the flow. Any heat conduction from the probe to the test cell ambient air will not affect the measurement because this occurs in the part of the probe that does not have any sensor attached.

Heat radiation can occur from the internal surfaces of the stator vanes to the probe only if there is a temperature difference between the stator and the probe. The effect is greatest in low velocity gas flow. Because the compressor stators are uncooled and stationary, they should see the same air temperature as the probe itself, and the temperature difference between the probe and the stator will be negligible. Heat radiation errors are therefore considered negligible for the gas path measurements.

Appendix F

GE J85-13 Test Matrix and Test Repeatability

This appendix contains the test matrix and graphically displays the repeatability of the clean and deteriorated conditions.

Test matrix

A total of 7 configurations and 21 tests were run for the GE J85-13 online water wash tests. The test matrix is given below.

Table 11 GE J85-13 test matrix

<i>Nozzle type</i>	<i>Nozzle number</i>	<i>Flow rate, w/a (kg/kg)</i>	<i>Flow rate (l/min)</i>	<i>Droplet size VMD (μm)</i>	<i>Duration (log number if tested)</i>				
					<i>30 s</i>	<i>60 s</i>	<i>90 s</i>	<i>4 min</i>	<i>10 min</i>
TN26	7	3.0 %	30.9	200	8C	9C	---	---	---
TN26	4	1.7 %	17.6	200	10D	11D	---	---	---
TN26	2	0.87 %	8.8	200	9B	10B	---	---	---
TN26	1	0.43 %	4.4	200	17C	18C	---	19C	---
TN3	17	0.89 %	9.1	75	20	1B	2B	3B	---
TN3	8	0.42 %	4.3	75	4D	5D	---	6D	7D
QJ12	12	0.43 %	4.4	25	3E	4E	---	5E	6E

Repeatability of clean and deteriorated condition

In this work, the clean and deteriorated conditions are represented by reference data series. The same data series are used for all GE J85-13 cases.

Figure 31 shows the intake depression for all cases. The data series with highest intake depression are chosen for both the clean and the deteriorated conditions. All data series are -5% of the reference conditions at constant corrected shaft speed, indicated by the 5% error bars.

The repeatability of stage work coefficient for clean and deteriorated conditions is given in Figures 32 and 33.

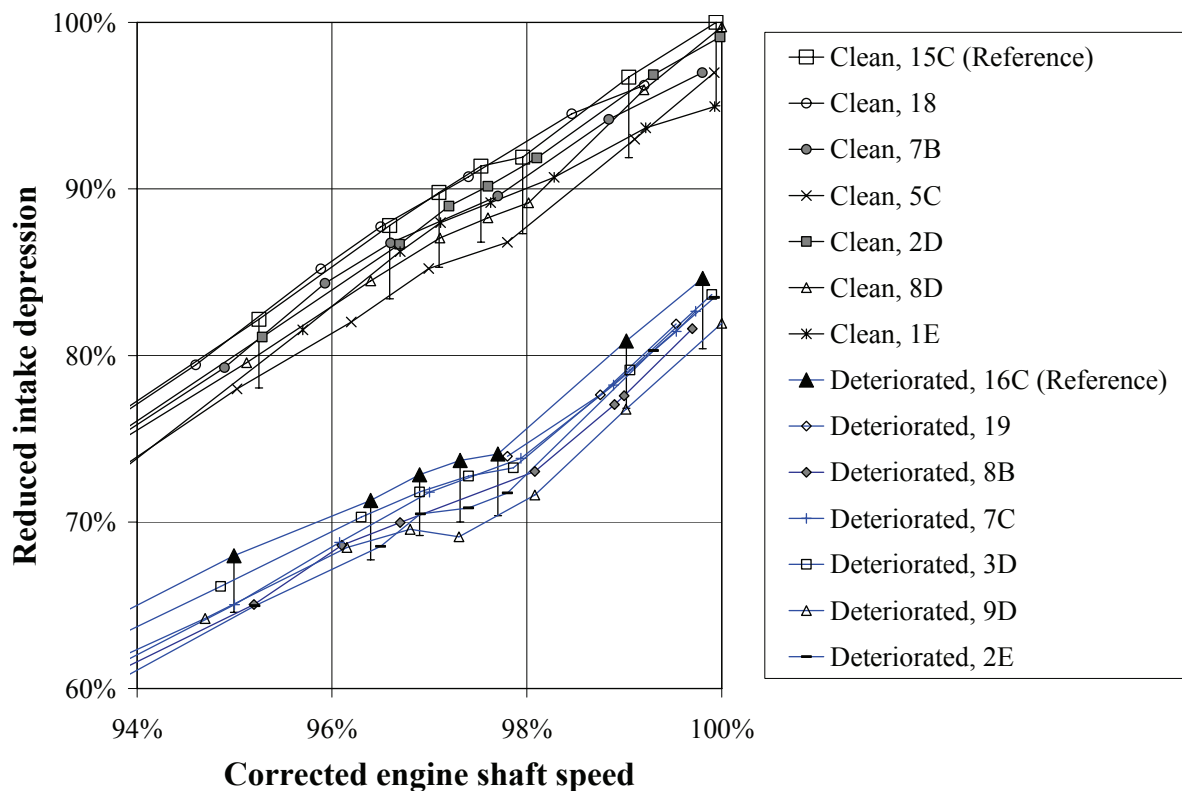


Figure 31 Repeatability of clean and degraded condition

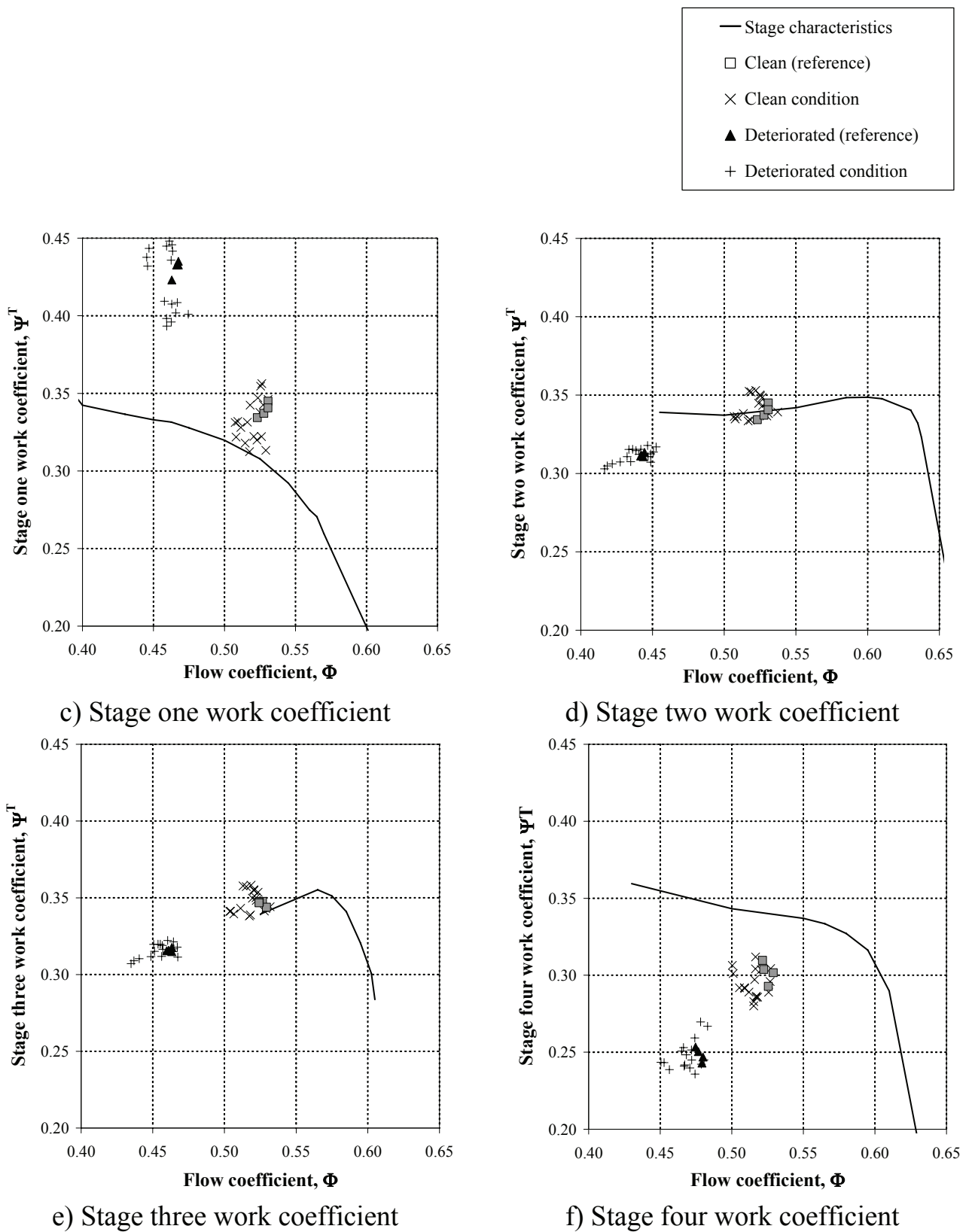


Figure 32 Repeatability of stage work coefficient, stages one to four

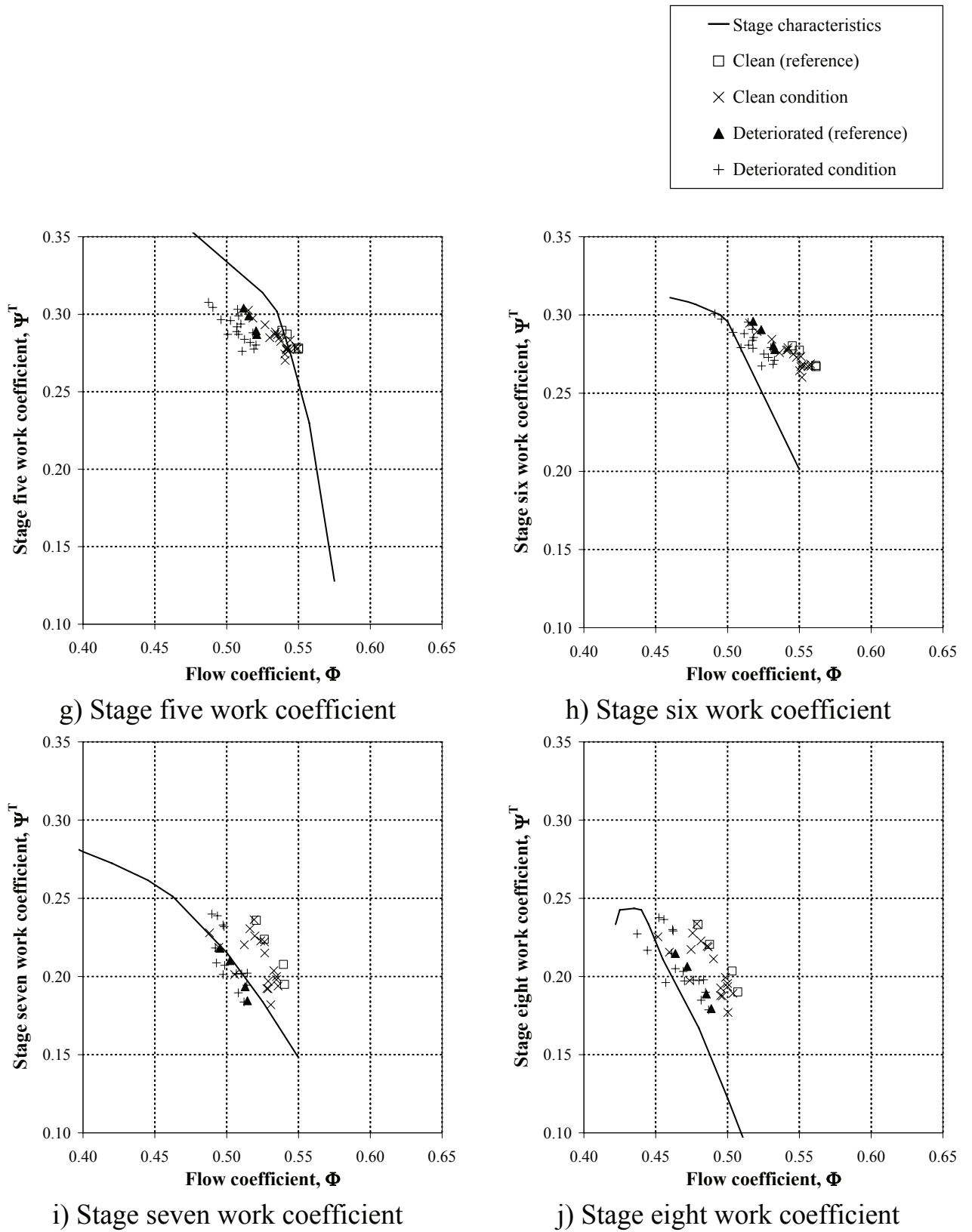


Figure 33 Repeatability of stage work coefficient, stage five to eight

Appendix G

GE J85-13 Compressor Geometry and Stage Characteristics

This Appendix contains data on GE J85-13 compressor geometry and stage characteristics as applied in the models. The data are intended as a database for GE J85-13 compressor geometry for future reference and to simplify comparison to other engines.

The axial compressor geometry is given in NASA reports [63, 93] and verified from drawings and measurements. The effective flow area includes a 0.97 blockage factor as recommended by NASA CR-134978 [93]. The geometry is given in Figures 34-39.

According to NASA CR-134978 [93], the stator deviation angles are assumed constant independent of incidence angle or corrected speed. This assumption is based on the results of cascade testing which shows little variation in deviation angles for a wide range of incidence angles and Mach numbers less than 0.7.

Details on the variable geometry are given by Brekke [18].

Stage characteristics are given in Figures 40 and 41, in addition to stage work given in Figure 17.

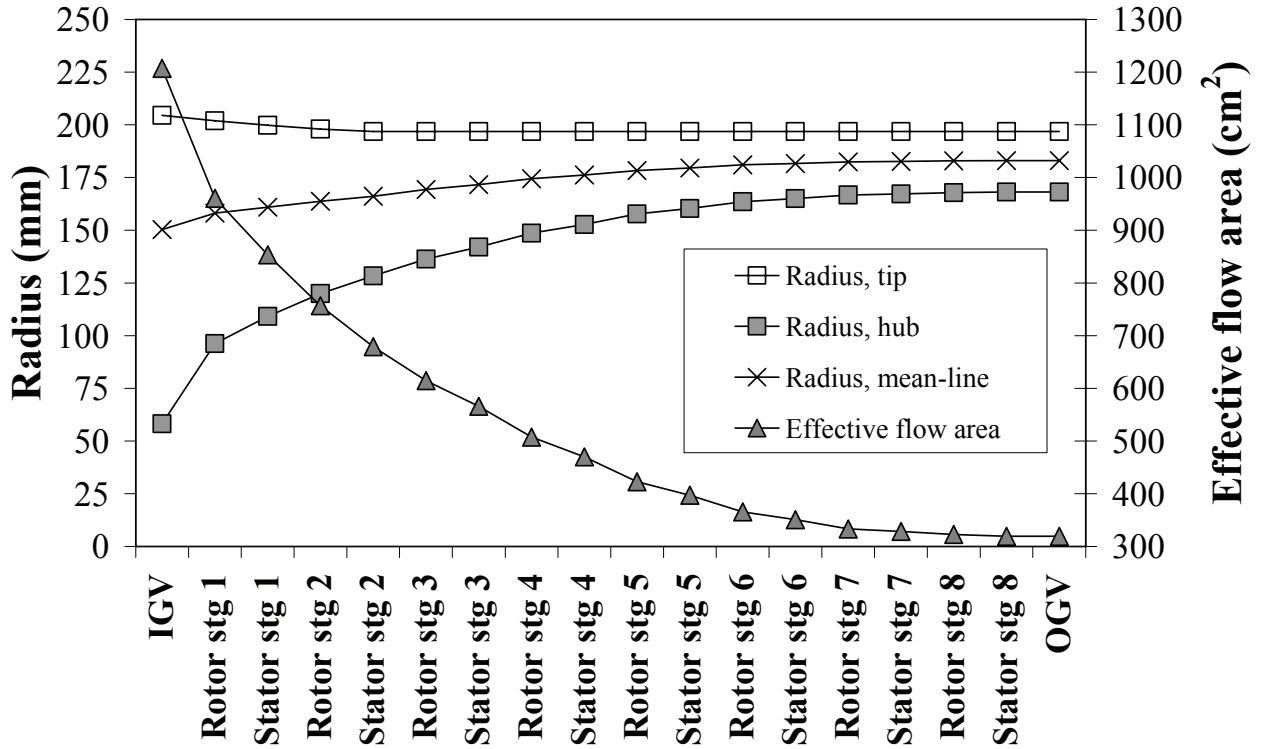


Figure 34 GE J85-13 compressor geometry

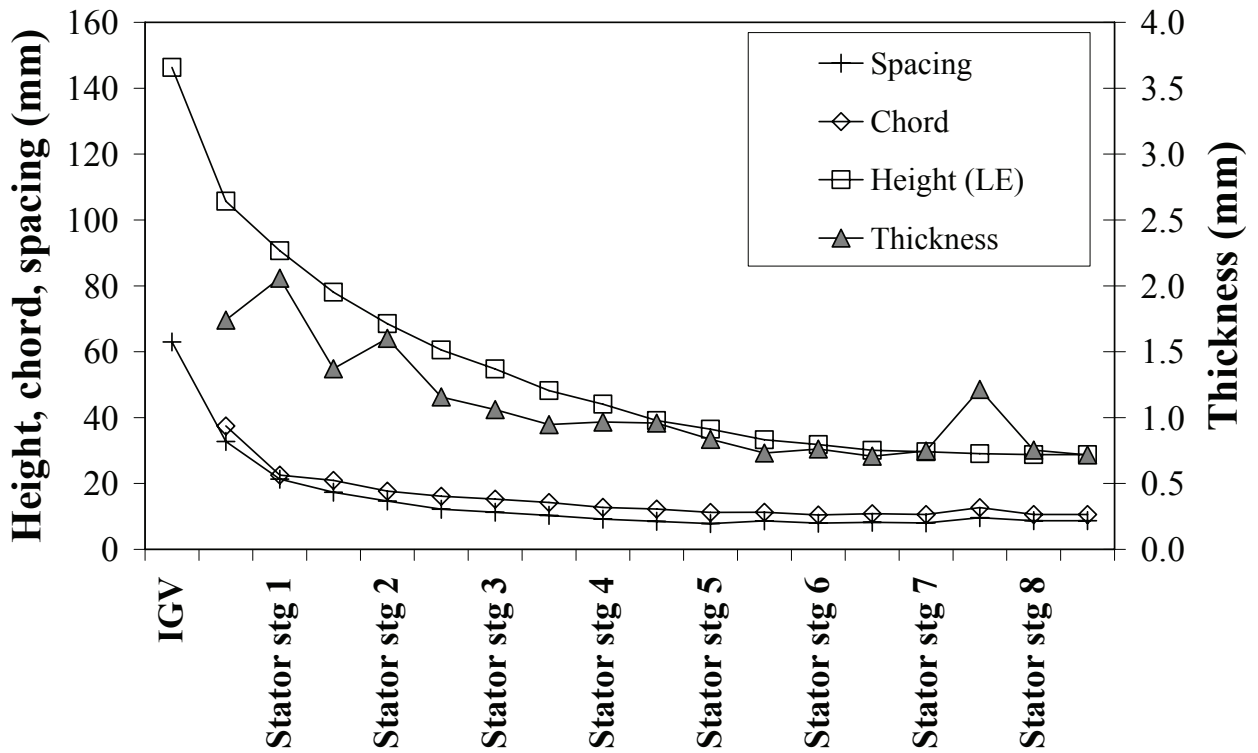


Figure 35 GE J85-13 mean-line geometry

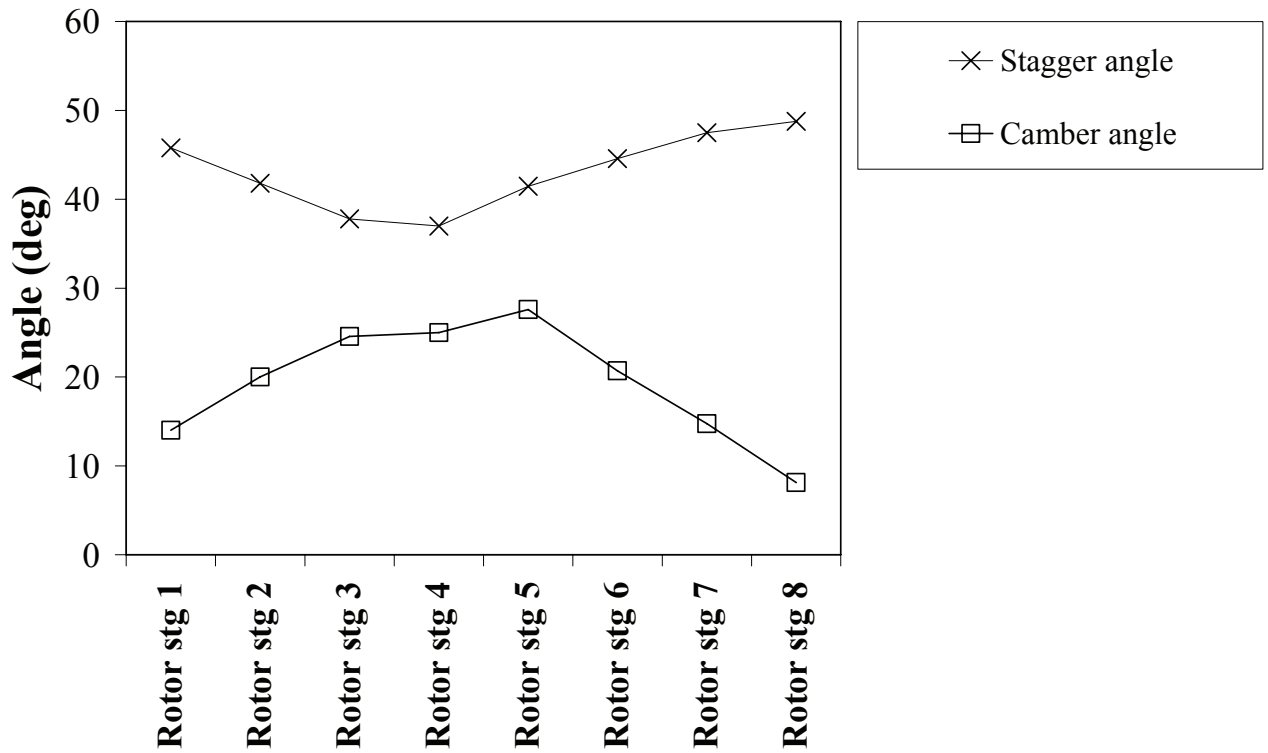


Figure 36 GE J85-13 mean-line rotor blade geometry

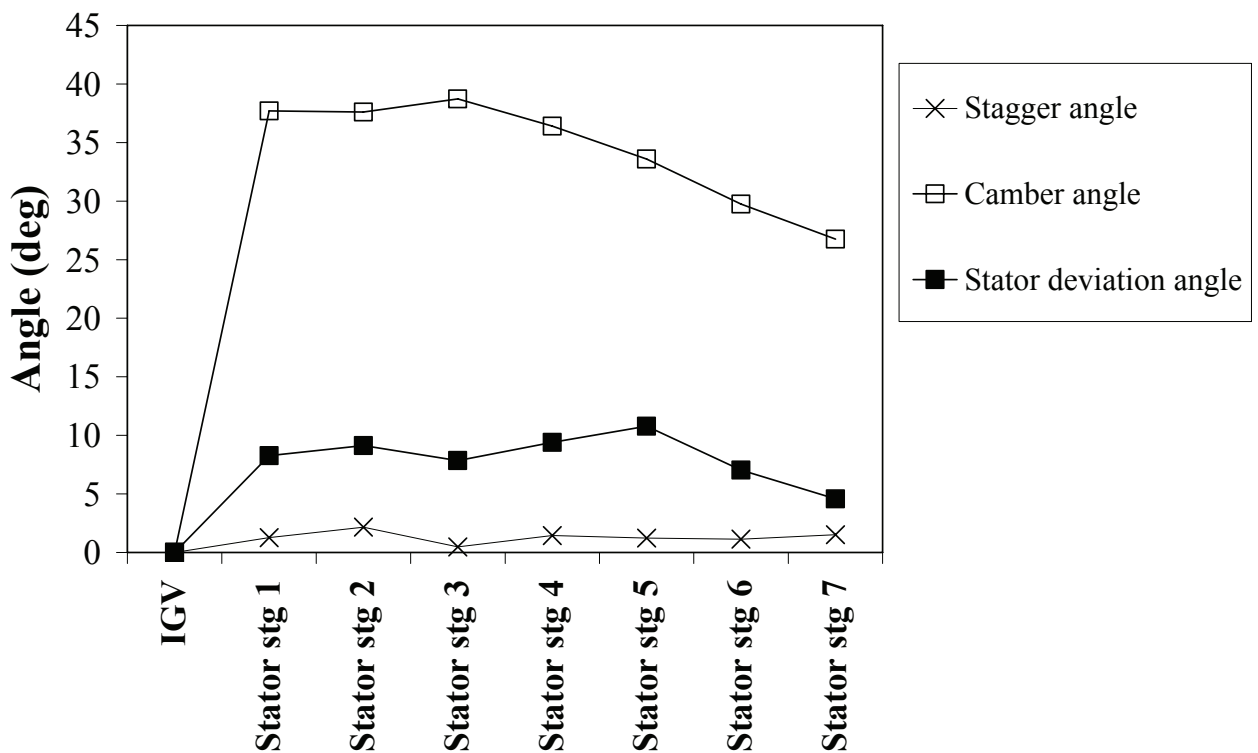


Figure 37 GE J85-13 mean-line stator vane geometry

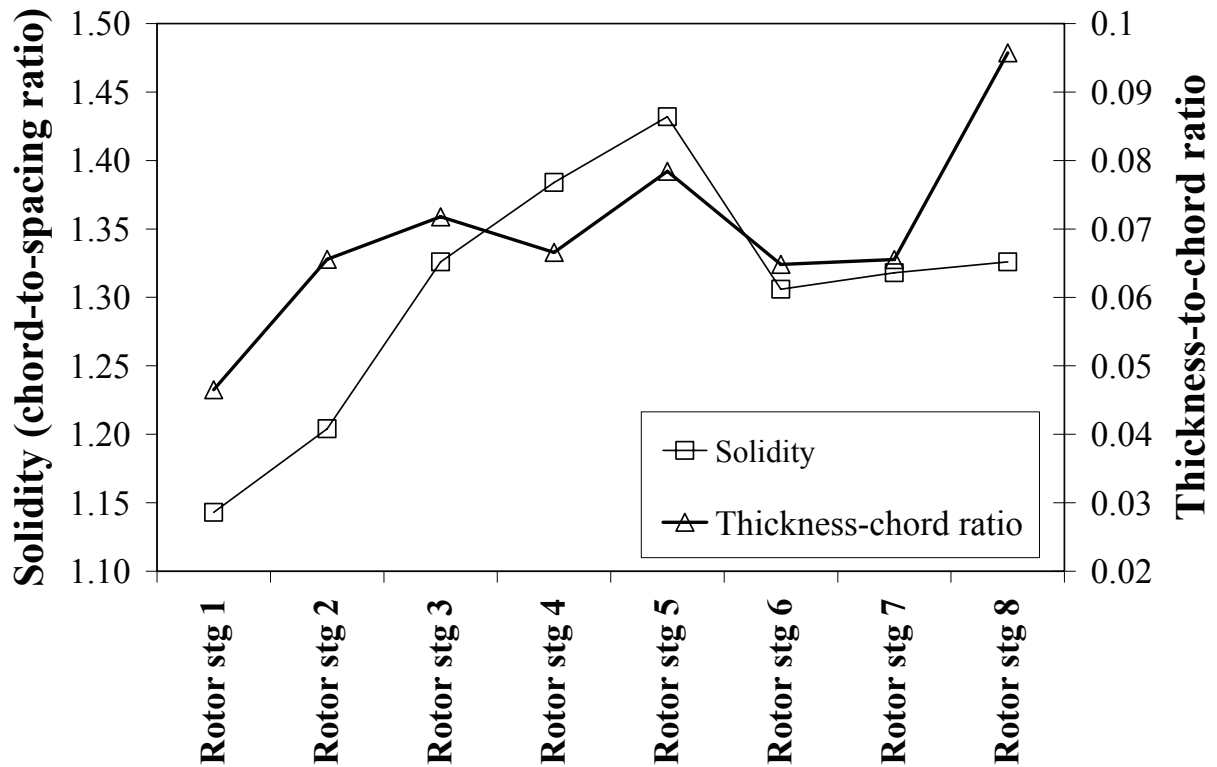


Figure 38 GE J85-13 mean-line rotor blade solidity and thickness-to-chord ratio

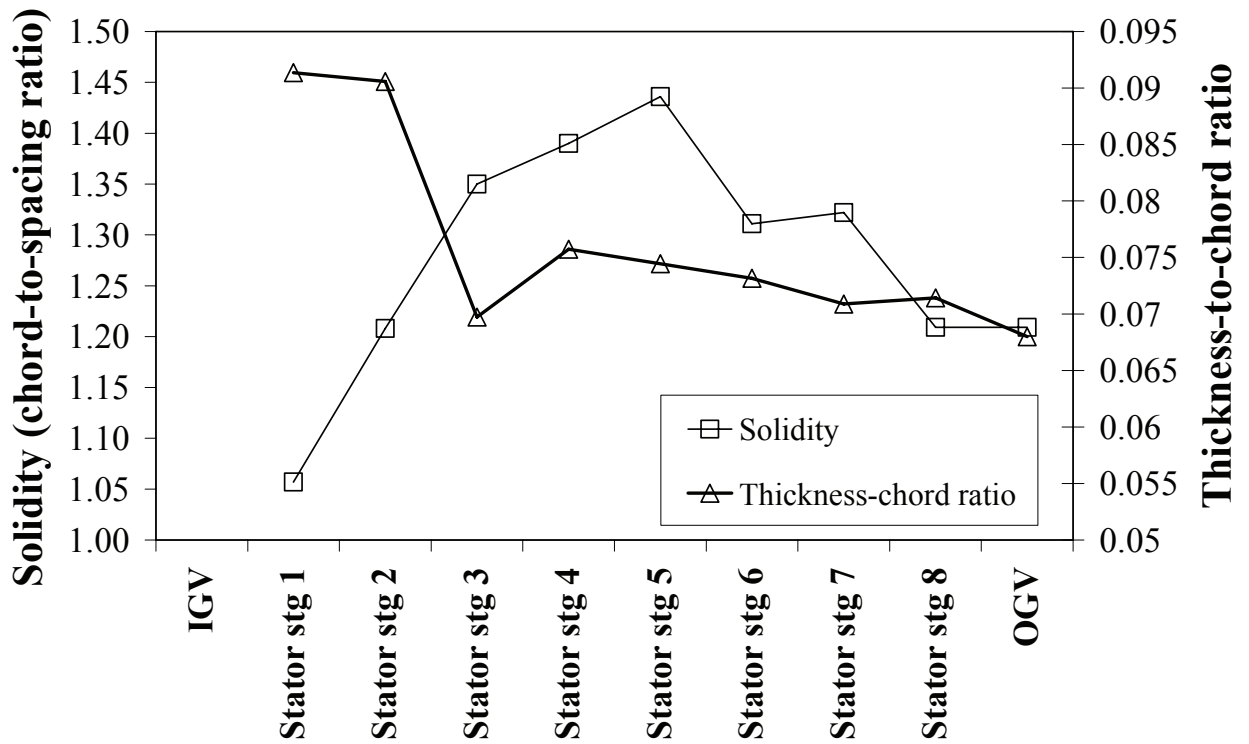


Figure 39 GE J85-13 mean-line stator vane solidity and thickness-to-chord ratio

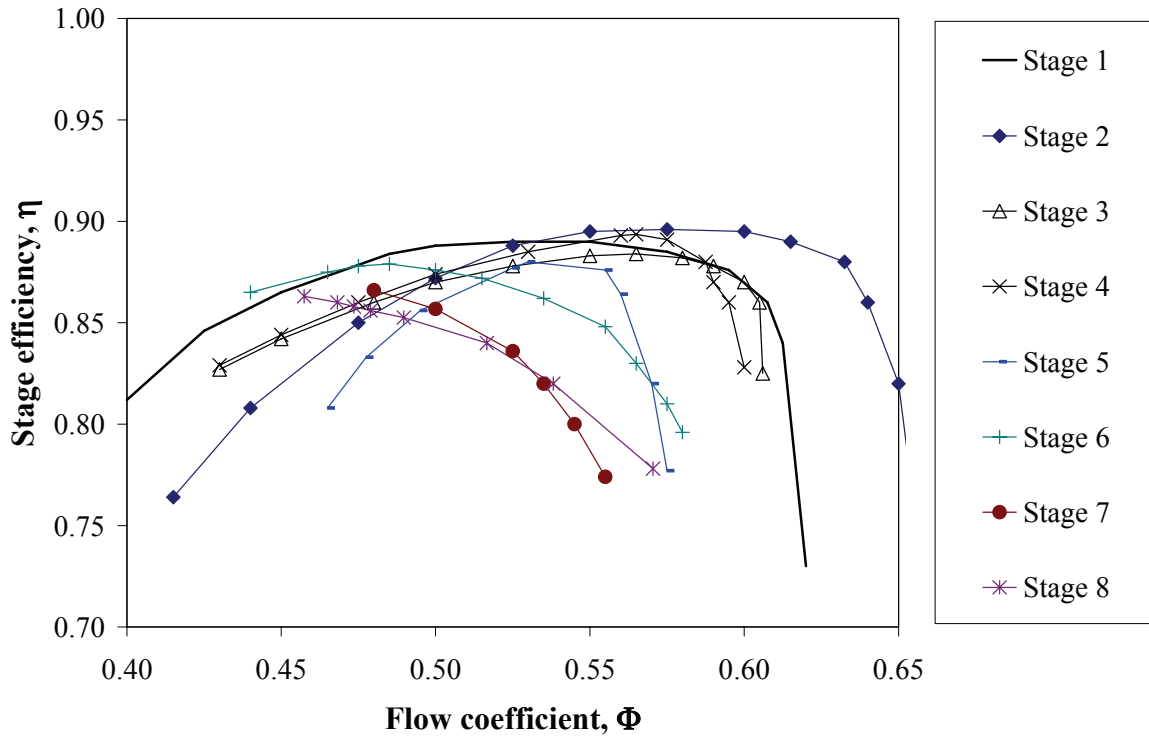


Figure 40 Stage efficiencies

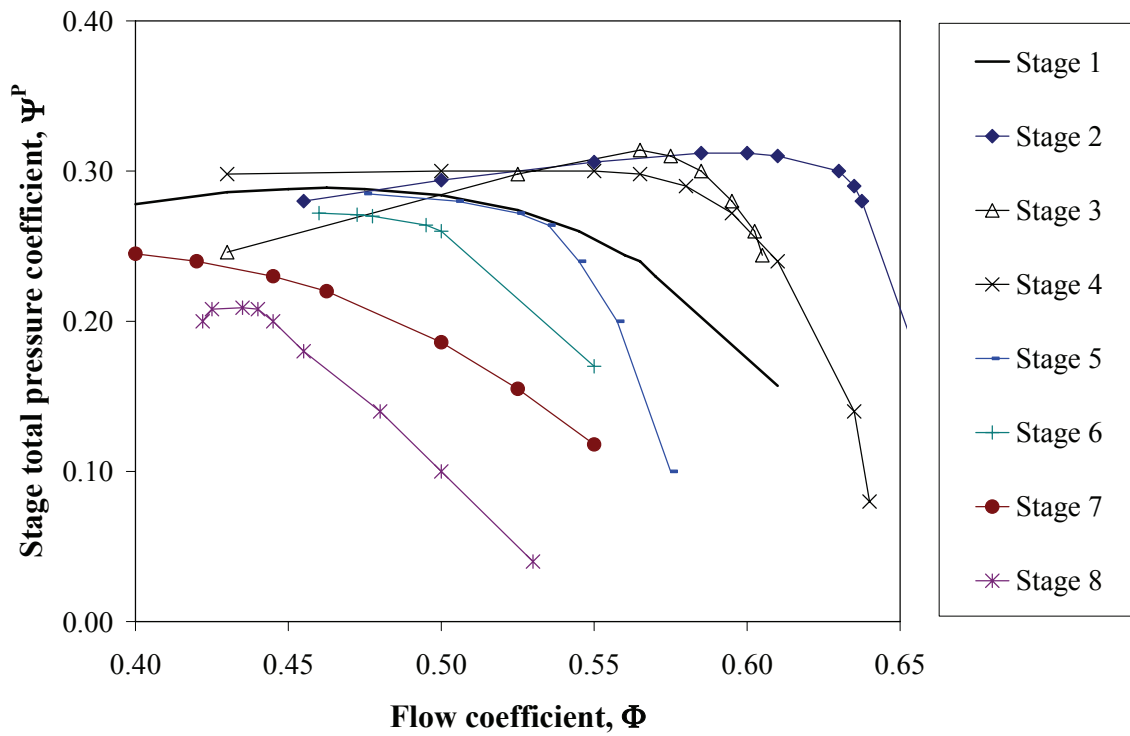


Figure 41 Stage total pressure coefficients

Appendix H

GE J85-13 Compressor Performance in Clean Conditions

This Appendix contains the calculated data on GE J85-13 compressor performance in clean conditions. The data are included to simplify comparison to other engines.

The GE J85-13 model calculates the stage performance and forces the solution to fit the measured stage temperatures and the outlet static pressure. The model is given in Paper II, Appendix A and B and Paper III, Appendix A.

The figures below show the stage-by-stage variation for a clean GE J85-13 operated at 16539 rpm (full load) at 60% relative humidity, 98.42kPa inlet total pressure and 21°C ambient temperature.

The total-to-static stage isentropic efficiency is 0.821 in all stages to fit the overall measurements.

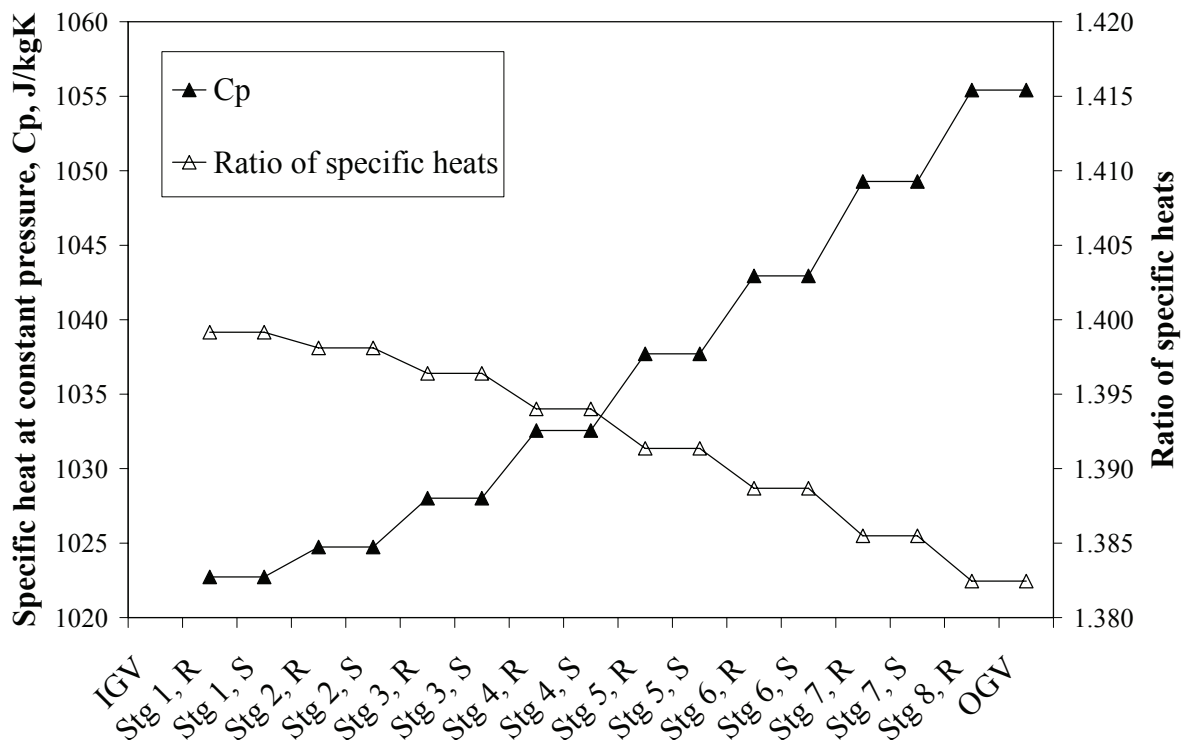


Figure 42 Gas properties (air and vapor mixture)

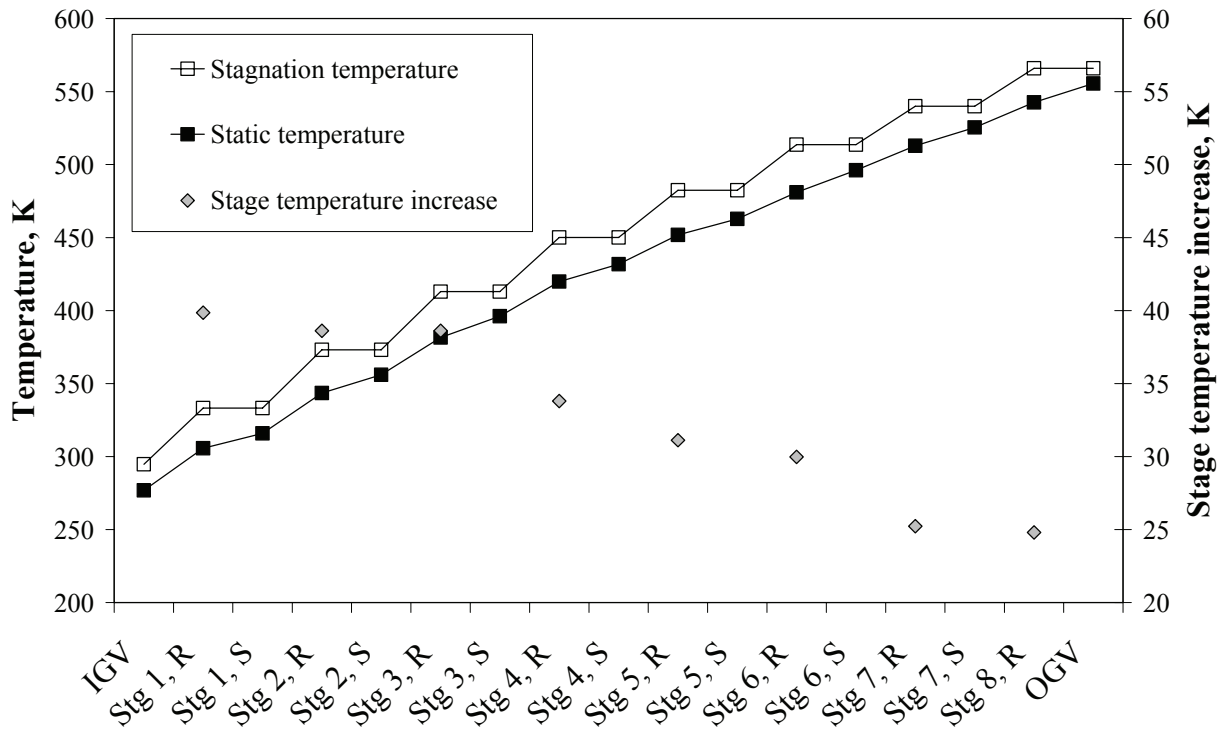


Figure 43 GE J85-13 compressor temperatures (clean condition)

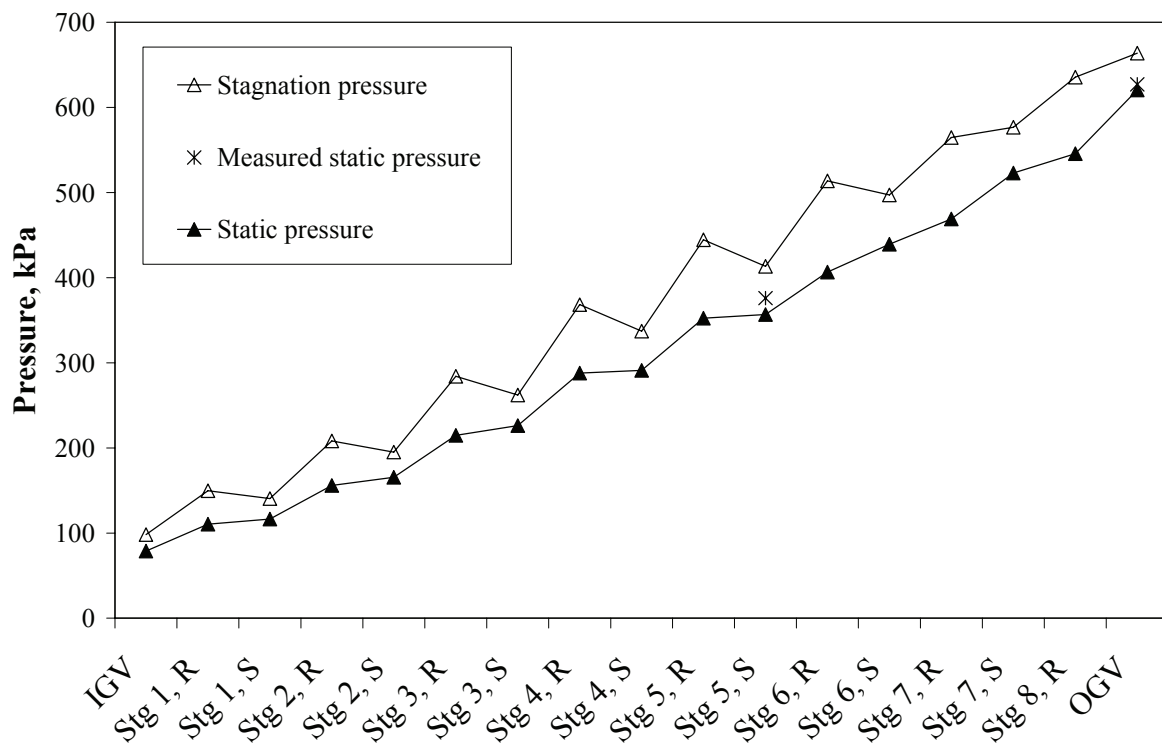


Figure 44 GE J85-13 compressor pressures (clean condition)

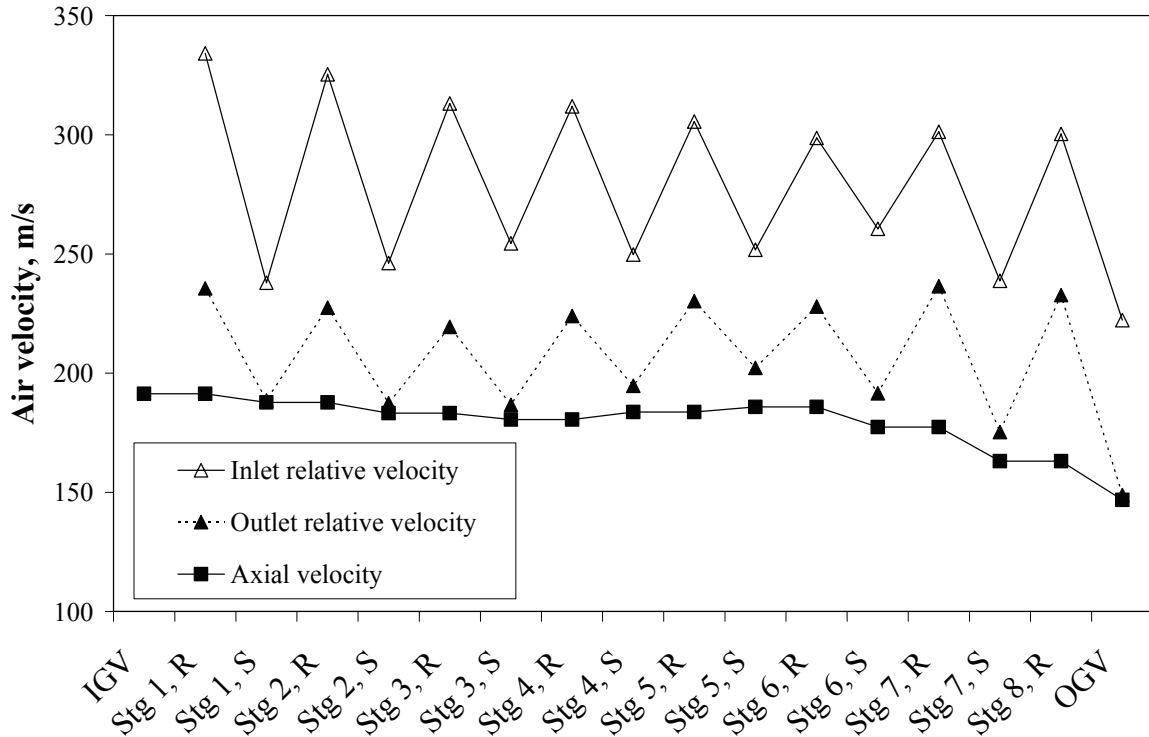


Figure 45 GE J85-13 compressor air velocities (clean condition)

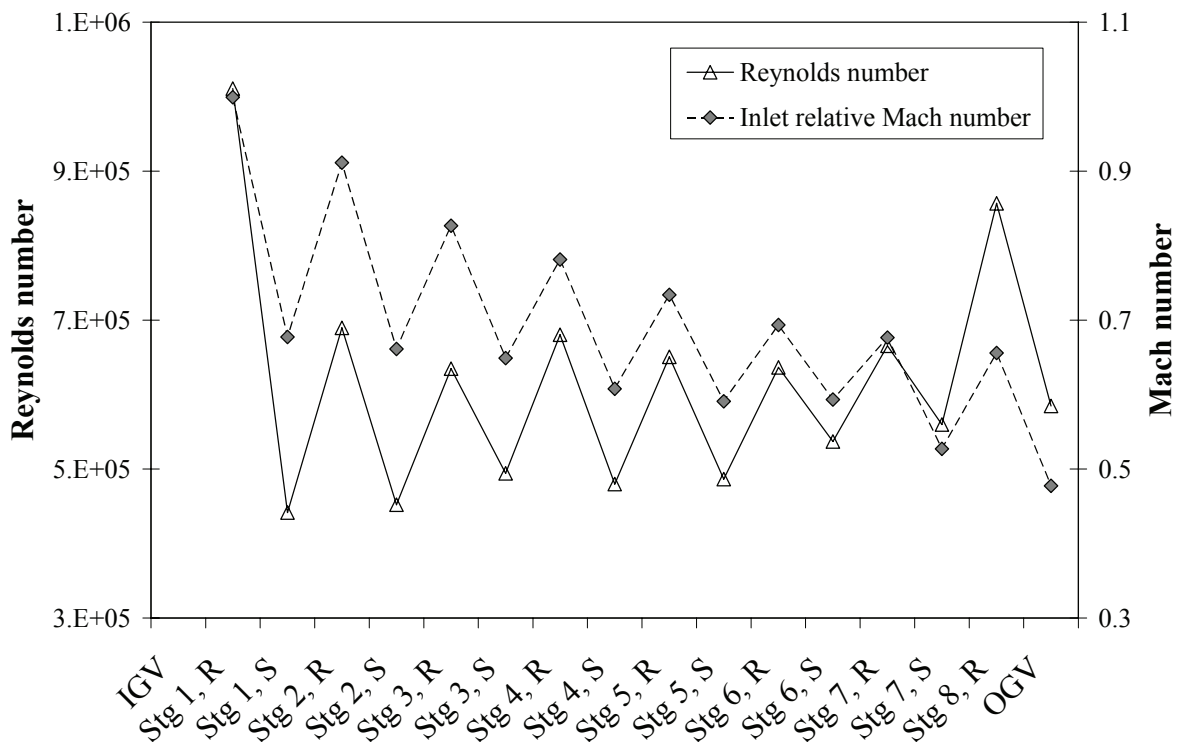


Figure 46 GE J85-13 Reynolds number and Mach number (clean condition)

Appendix I

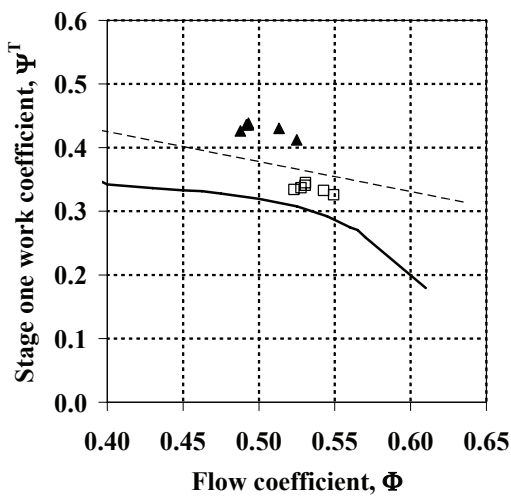
GE J85-13 Deteriorated Stage Performance

This appendix contains the clean and deteriorated stage performance for all compressor stages.

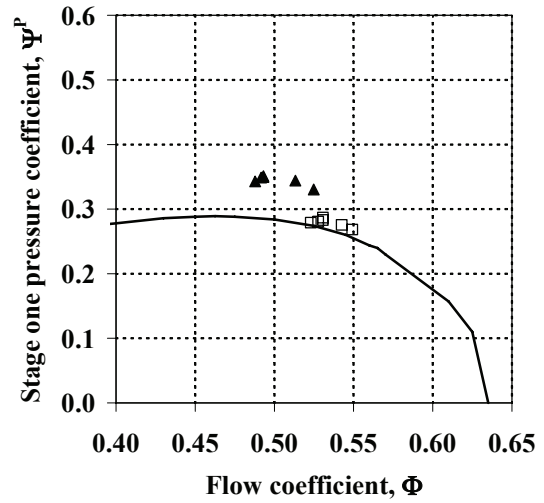
The data are based on measurements at 96 % to 100 % shaft speed. Unknown data are calculated by the quasi-one-dimensional model assuming constant axial velocity in the stage. For the deteriorated conditions, a 96% blockage is applied in the model and the deviation model is applied for the first three stages where the surface roughness is measured.

Parts of the stage characteristics are published in Paper II.

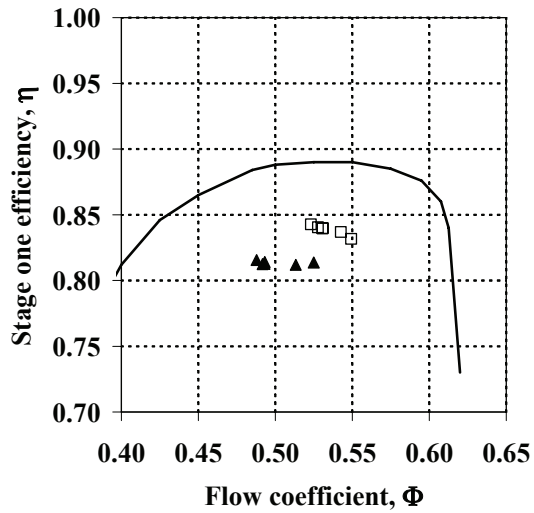
The velocity diagram published in Paper III does not include the deviation model.



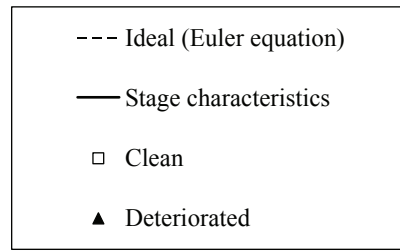
a) Work coefficient



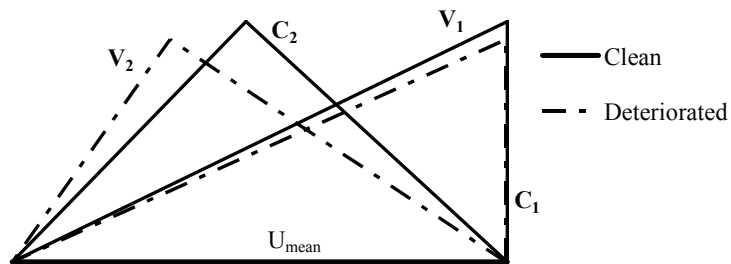
b) Pressure coefficient



c) Efficiency

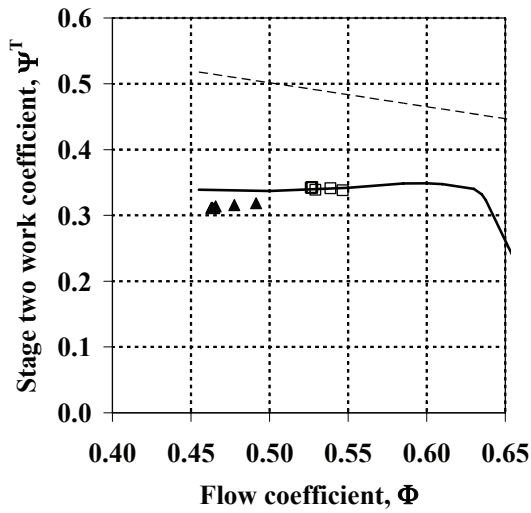


Legend for a), b) and c)

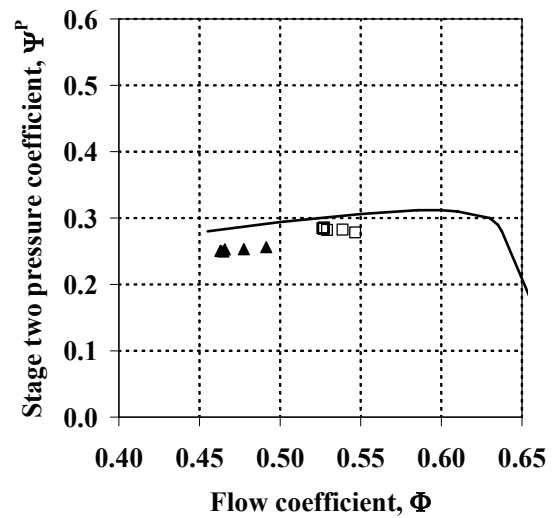


d) Mean-line velocity diagram at 98% speed

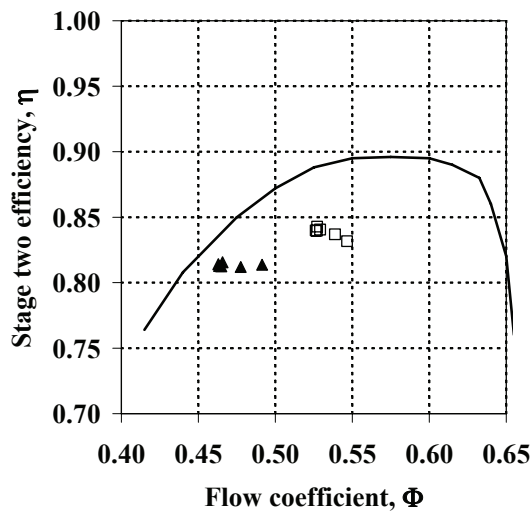
Figure 47 Stage one deteriorated performance



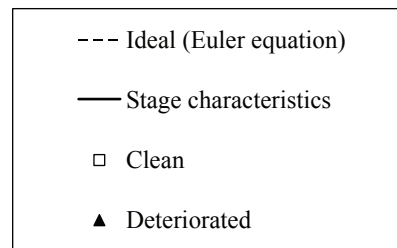
a) Work coefficient



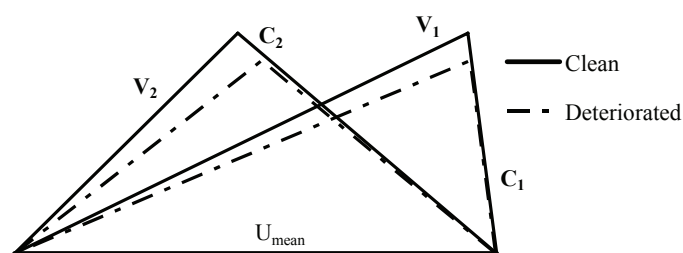
b) Pressure coefficient



c) Efficiency

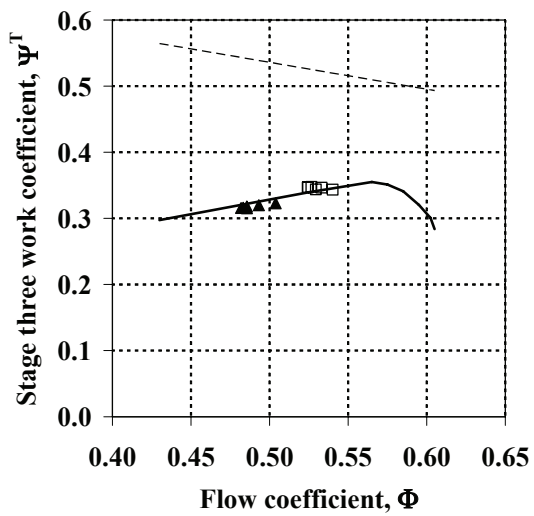


Legend for a), b) and c)

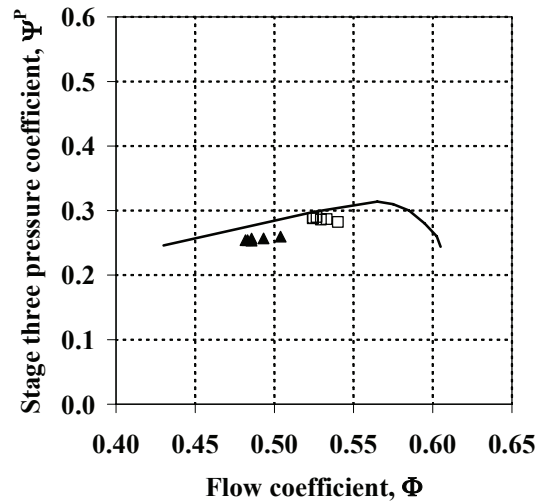


d) Mean-line velocity diagram at 98% speed

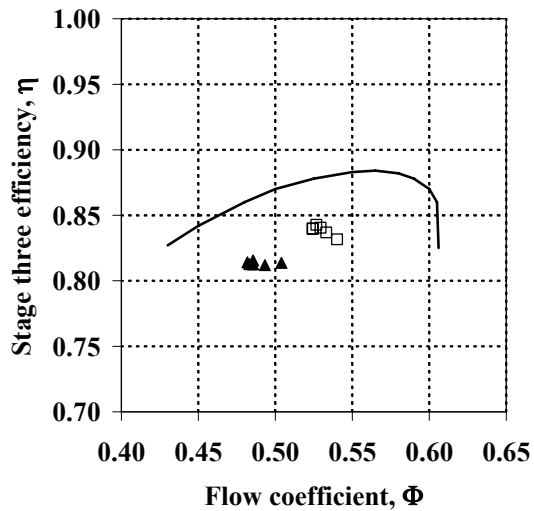
Figure 48 Stage two deteriorated performance



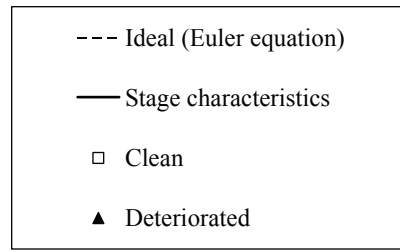
a) Work coefficient



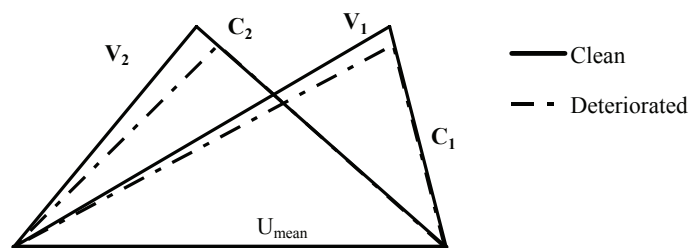
b) Pressure coefficient



c) Efficiency

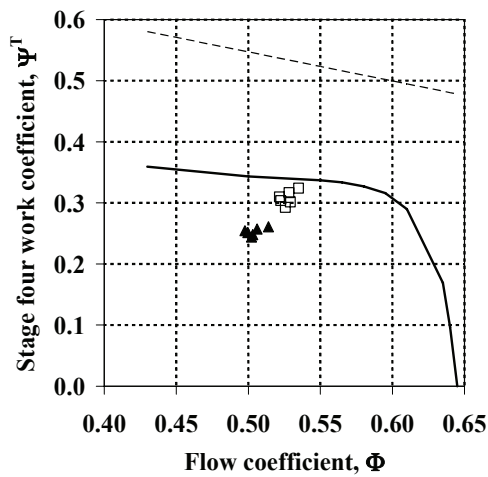


Legend for a), b) and c)

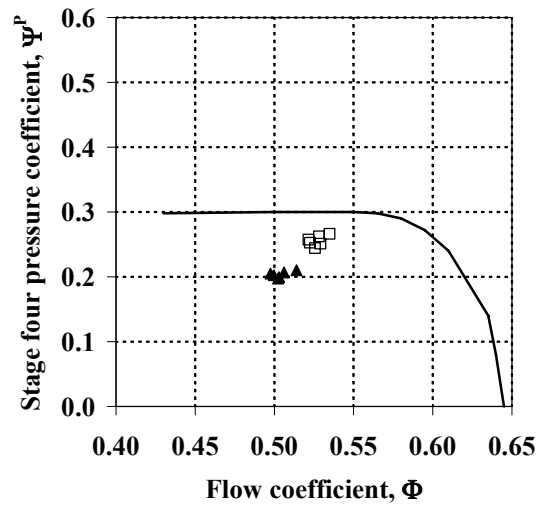


d) Mean-line velocity diagram at 98% speed

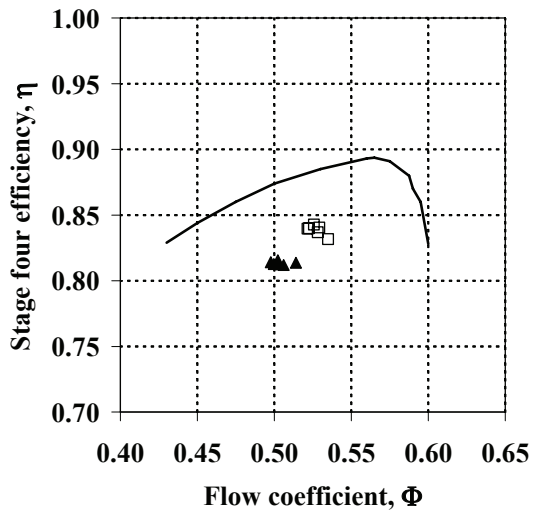
Figure 49 Stage three deteriorated performance



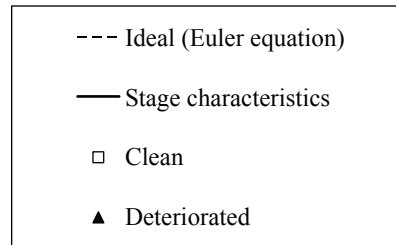
a) Work coefficient



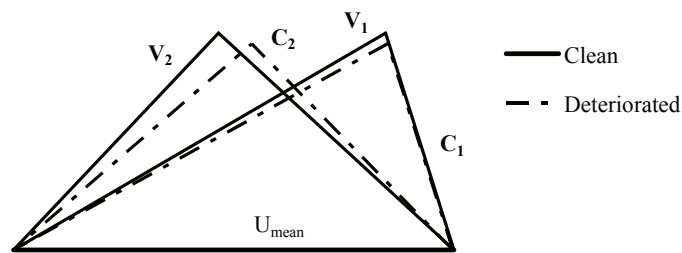
b) Pressure coefficient



c) Efficiency

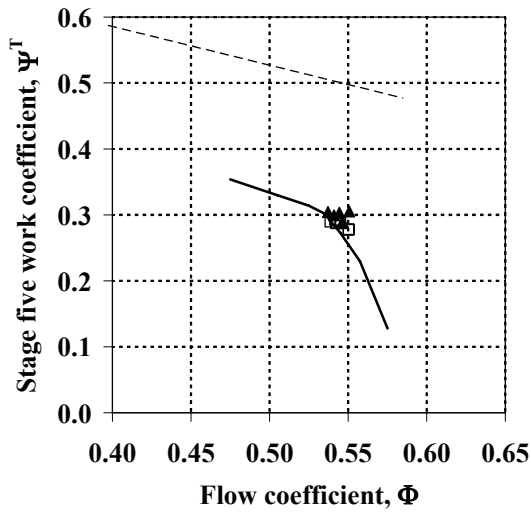


Legend for a), b) and c)

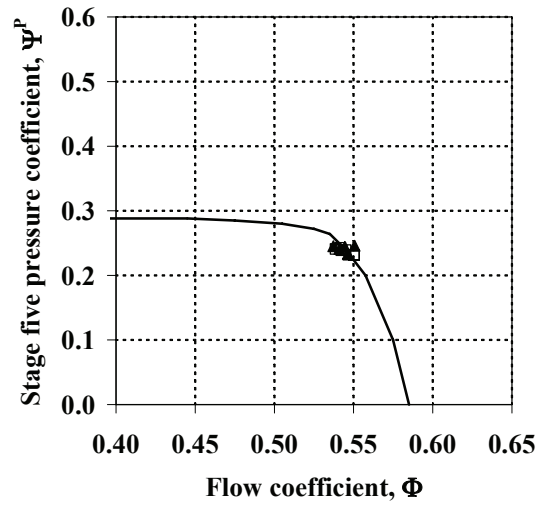


d) Mean-line velocity diagram at 98% speed

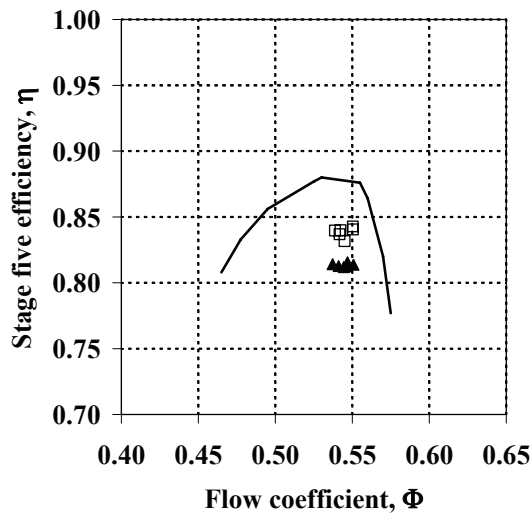
Figure 50 Stage four deteriorated performance



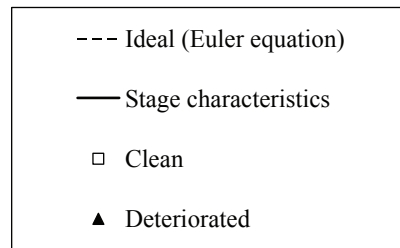
a) Work coefficient



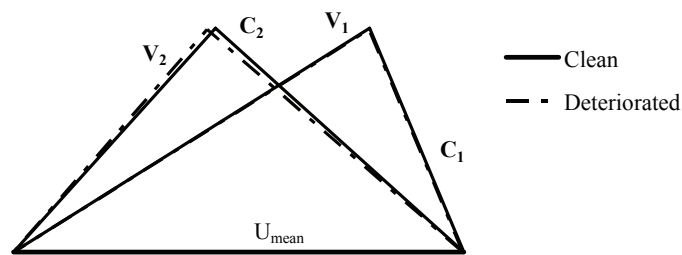
b) Pressure coefficient



c) Efficiency

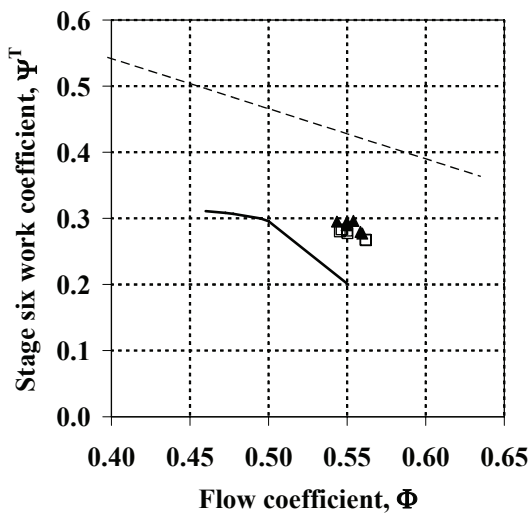


Legend for a), b) and c)

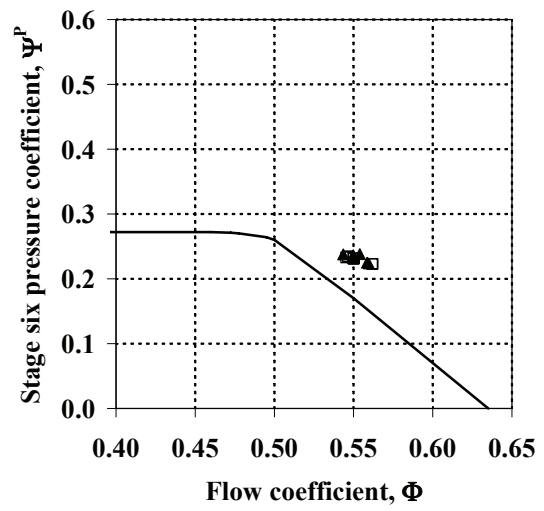


d) Mean-line velocity diagram at 98% speed

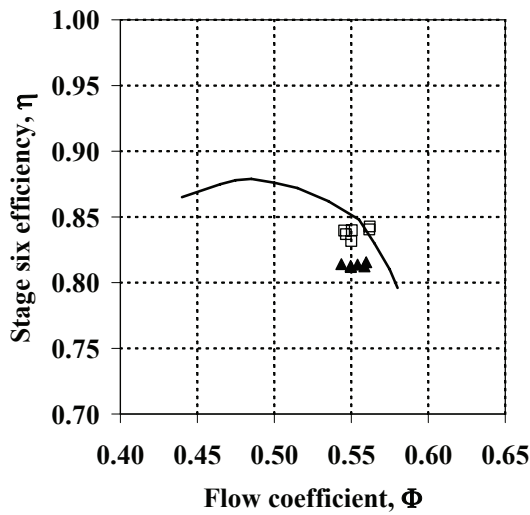
Figure 51 Stage five deteriorated performance



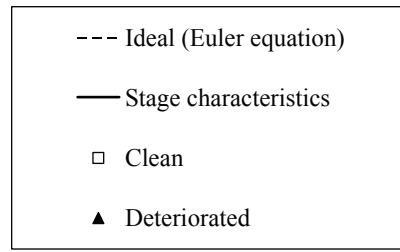
a) Work coefficient



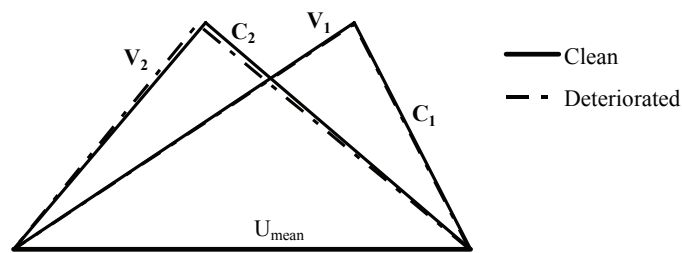
b) Pressure coefficient



c) Efficiency

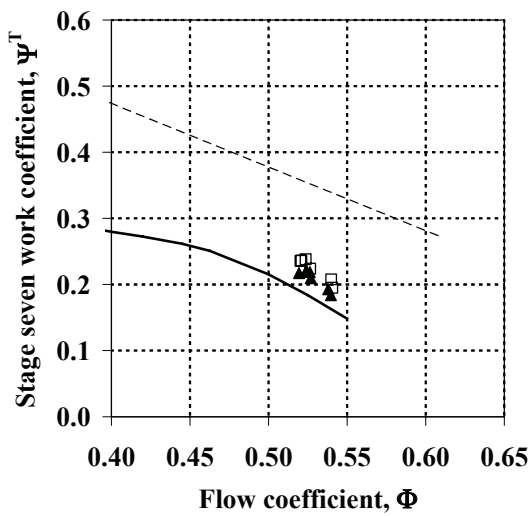


Legend for a), b) and c)

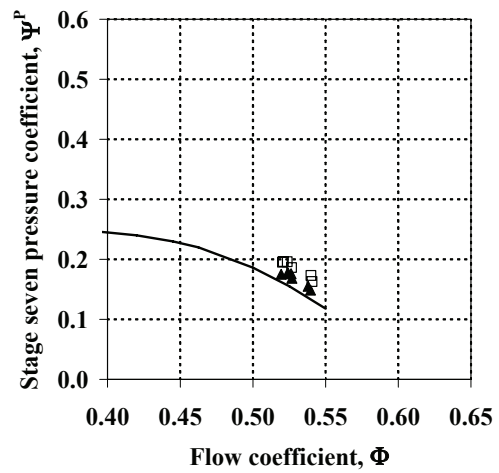


d) Mean-line velocity diagram at 98% speed

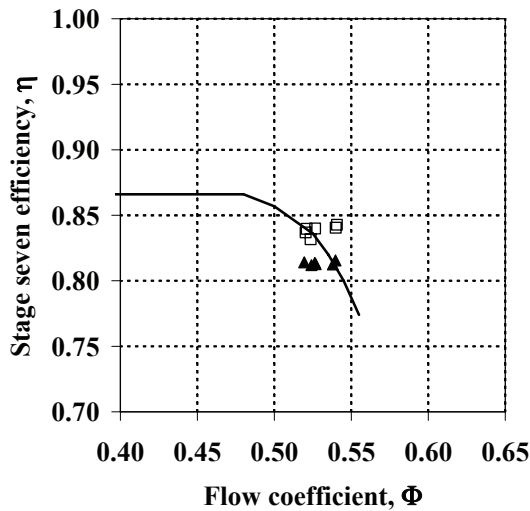
Figure 52 Stage six deteriorated performance



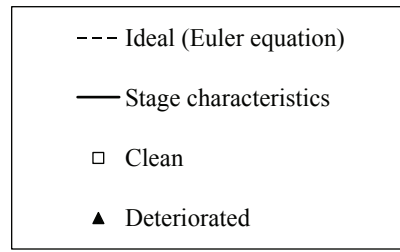
a) Work coefficient



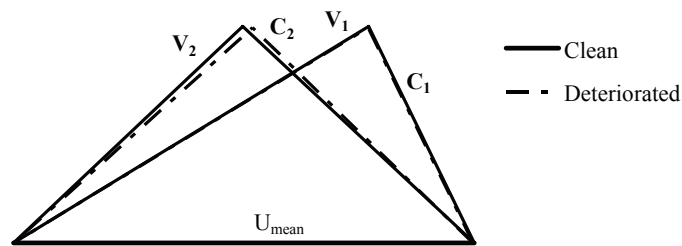
b) Pressure coefficient



c) Efficiency

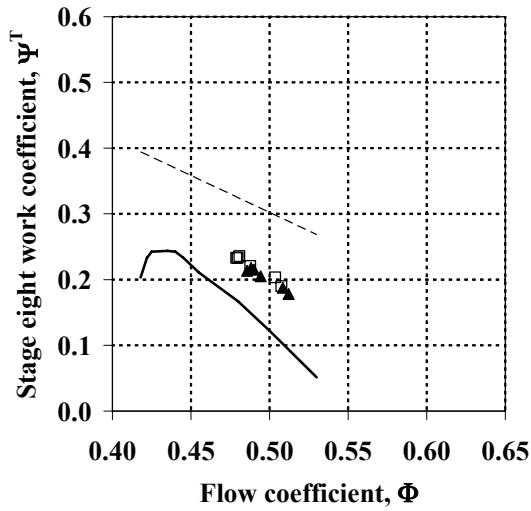


Legend for a), b) and c)

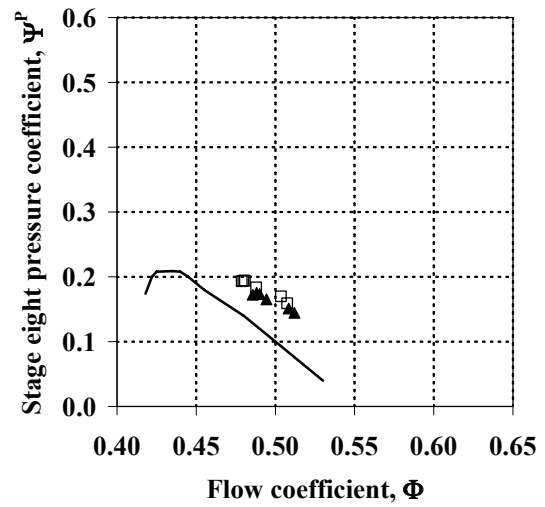


d) Mean-line velocity diagram at 98% speed

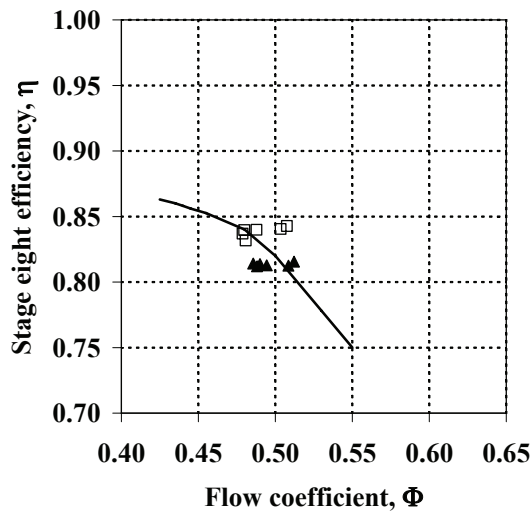
Figure 53 Stage seven deteriorated performance



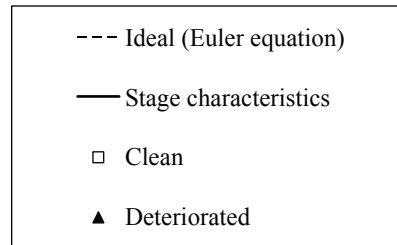
a) Work coefficient



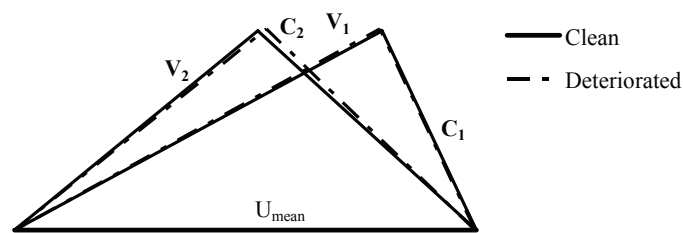
b) Pressure coefficient



c) Efficiency



Legend for a), b) and c)



d) Mean-line velocity diagram at 98% speed

Figure 54 Stage eight deteriorated performance

Appendix J

GE J85-13 Recovered Stage Performance

This Appendix holds all the stage work characteristics for the online washing tests. Parts of the data are published in Paper III. The reference cases for clean and deteriorated conditions are also included. The data are based on measurements at 96 % to 99 % shaft speed, except for intake depression where a larger range is included.

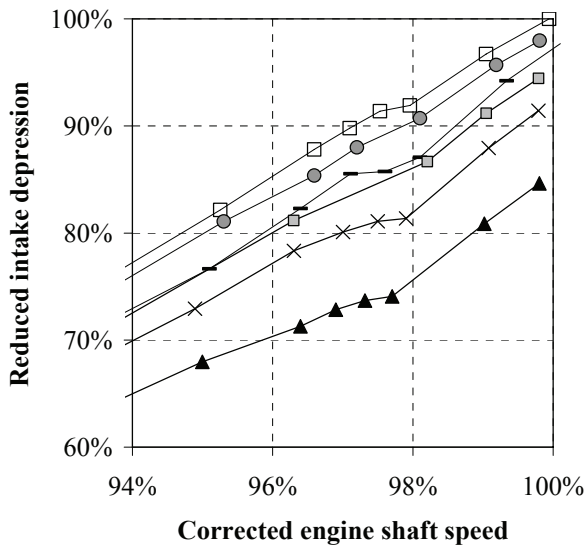
Unknown data are calculated from the quasi-one-dimensional model assuming constant axial velocity in the stage, zero deviation due to fouling and zero blockage.

The following datasets are given in this Appendix:

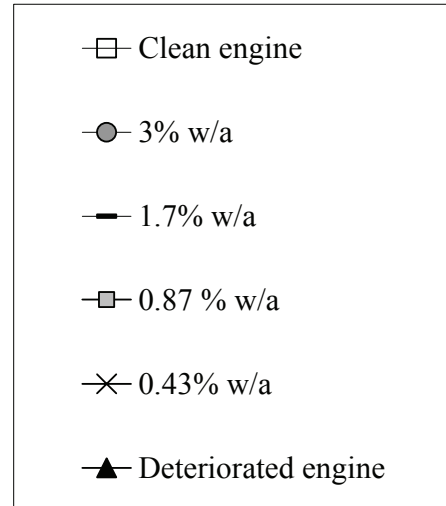
Table 12 Specification of datasets for recovered performance

<i>Dataset</i>	<i>Water-to-air ratio</i> (%)	<i>Droplet size</i> (μm)	<i>Duration</i> (min)
1	0.43 - 3	200	1
2	0.43	25, 75, 200	1
3	0.43, 1.7	200	0.5 - 4

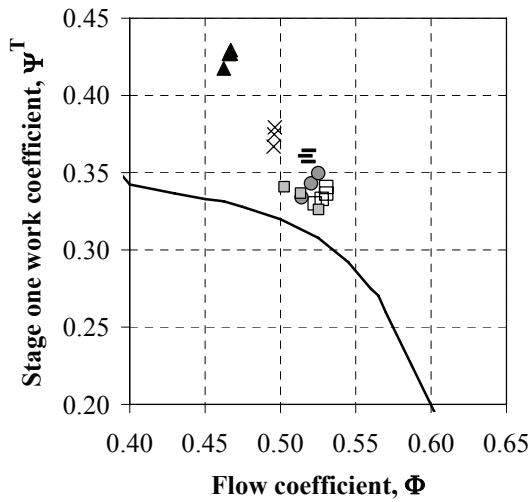
The data series for 3% water-to-air ratio published in Paper III are based on erroneous compressor inlet temperature which further offsets the data from the clean condition. The correct data series is given in Dataset 1. The overall conclusions are not affected by this error.



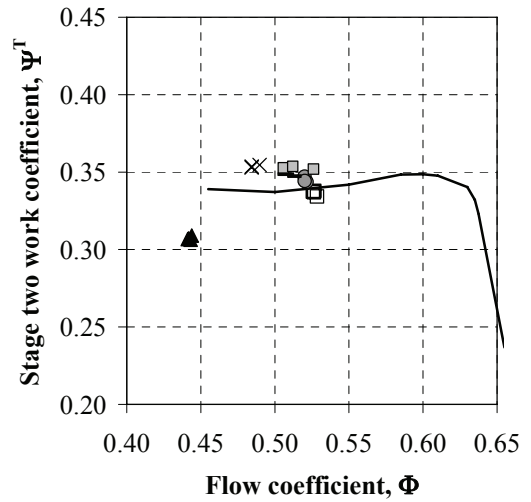
a) Intake depression



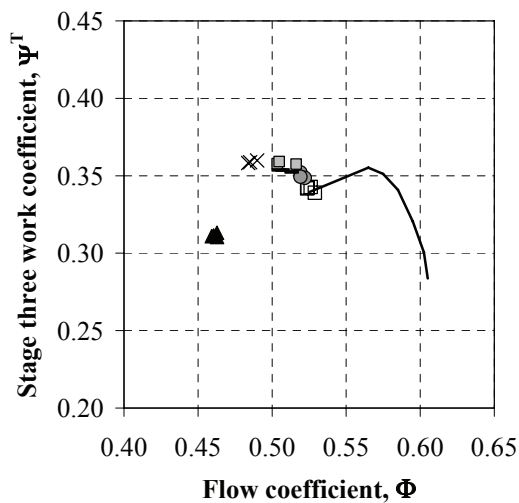
b) Dataset 1 legend



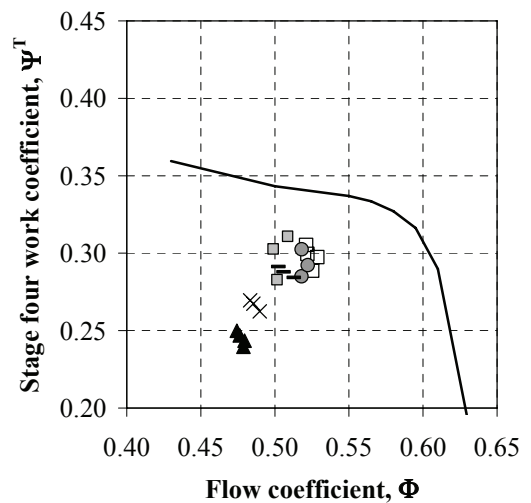
c) Stage one work coefficient



d) Stage two work coefficient

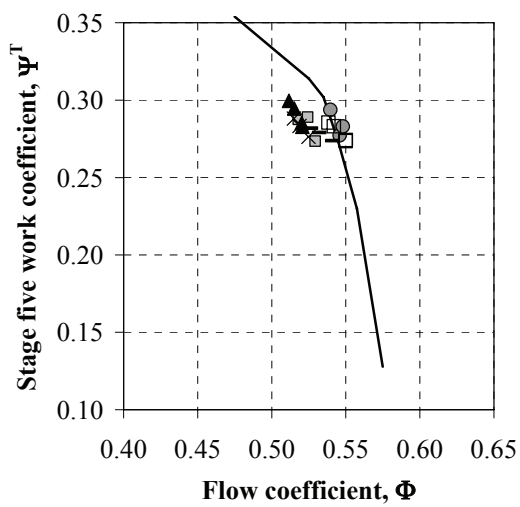


e) Stage three work coefficient

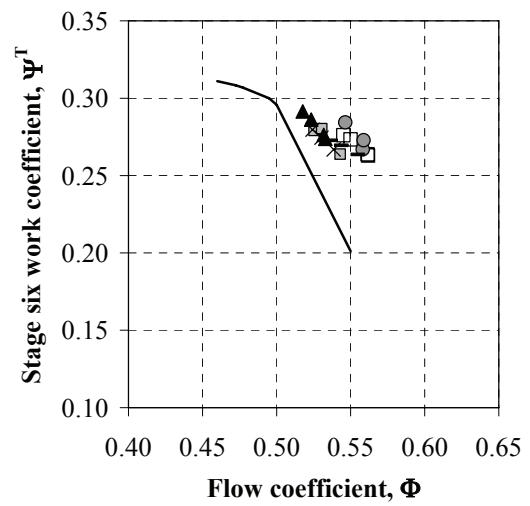


f) Stage four work coefficient

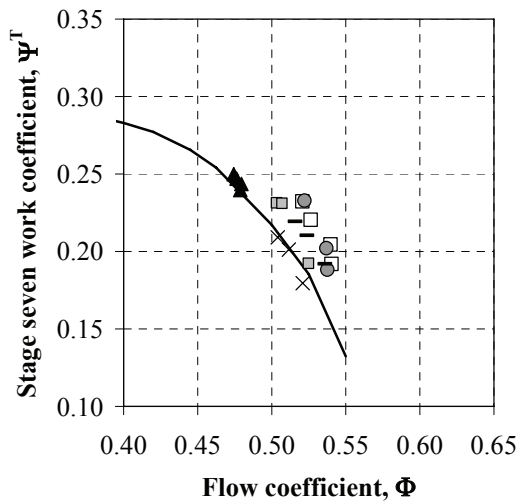
Figure 55 Dataset 1, stage one to four



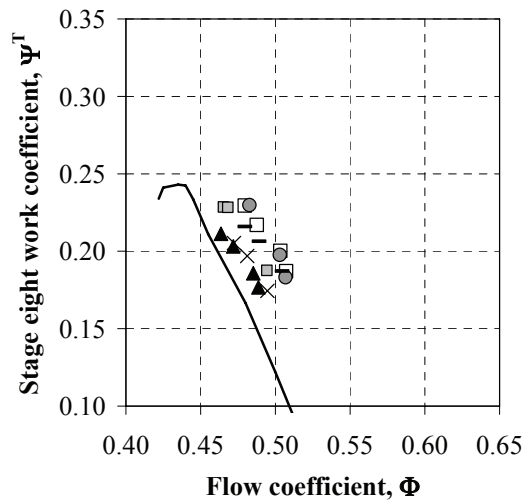
g) Stage five work coefficient



h) Stage six work coefficient

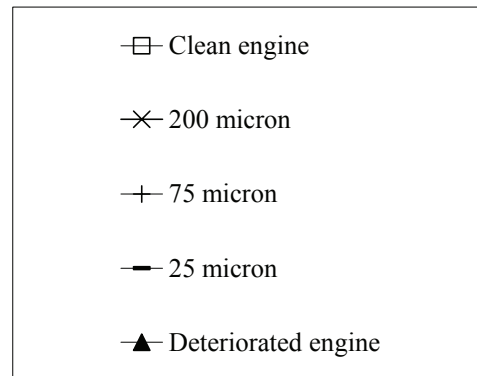
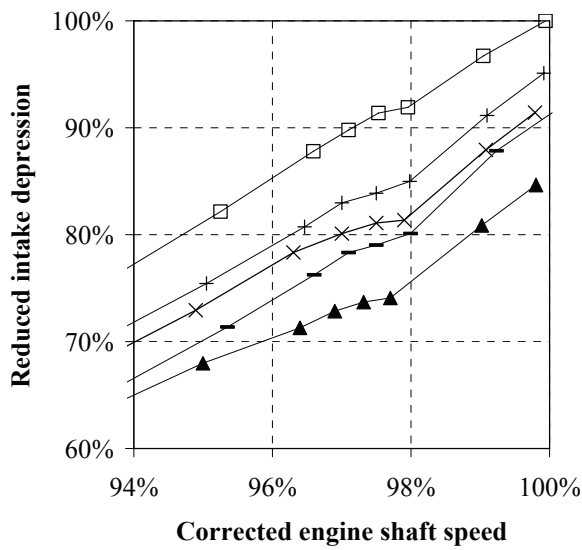


i) Stage seven work coefficient



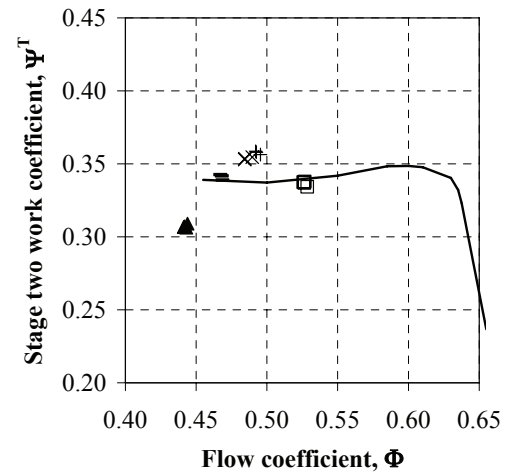
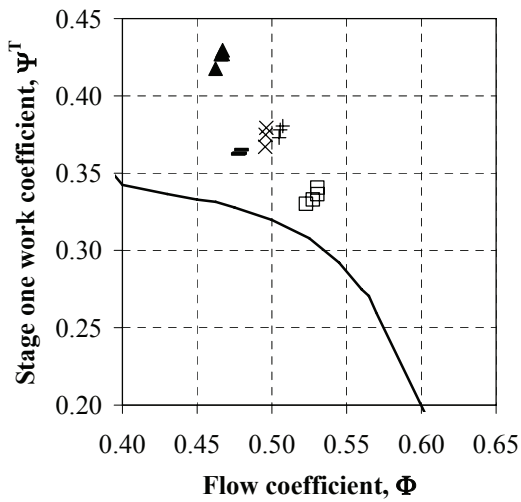
j) Stage eight work coefficient

Figure 56 Dataset 1, stage five to eight



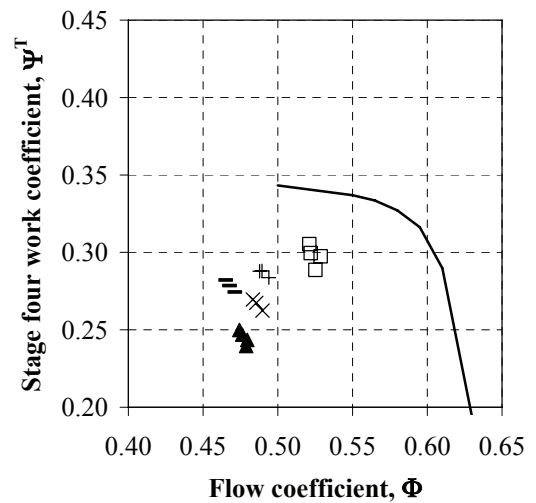
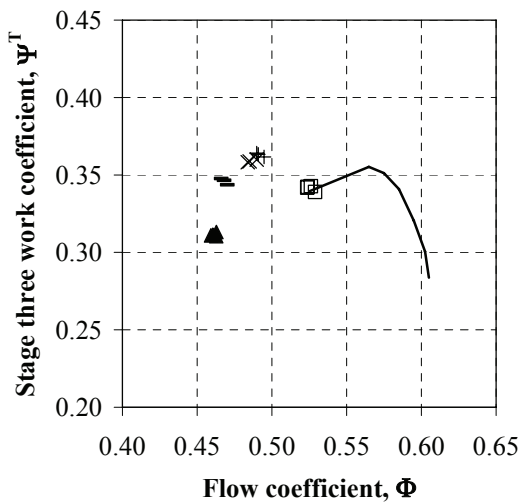
a) Intake depression

b) Dataset 2 legend



c) Stage one work coefficient

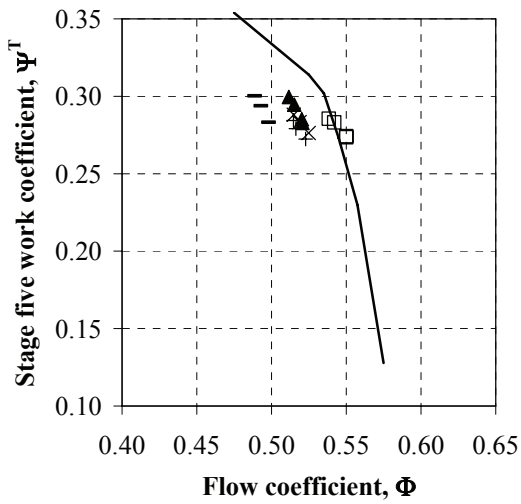
d) Stage two work coefficient



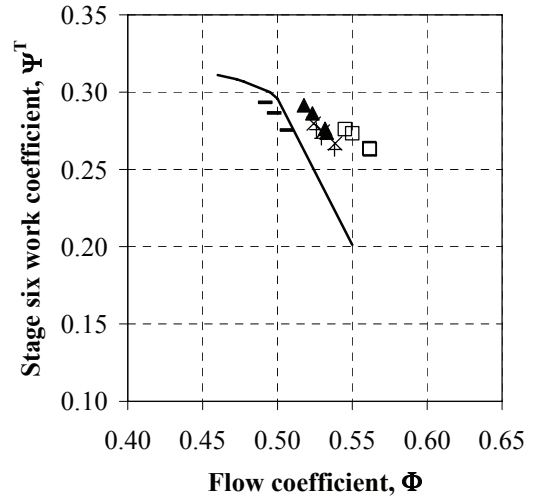
e) Stage three work coefficient

f) Stage four work coefficient

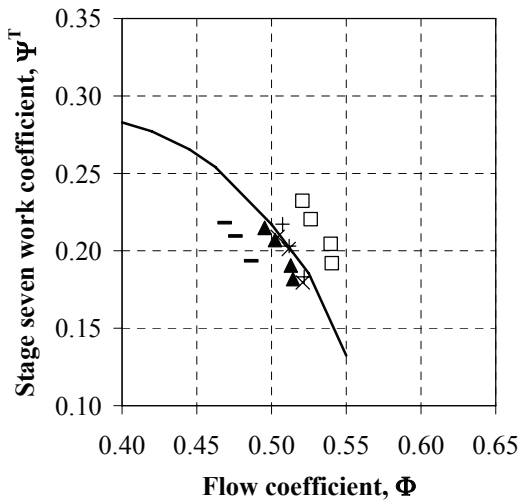
Figure 57 Dataset 2, stage one to four



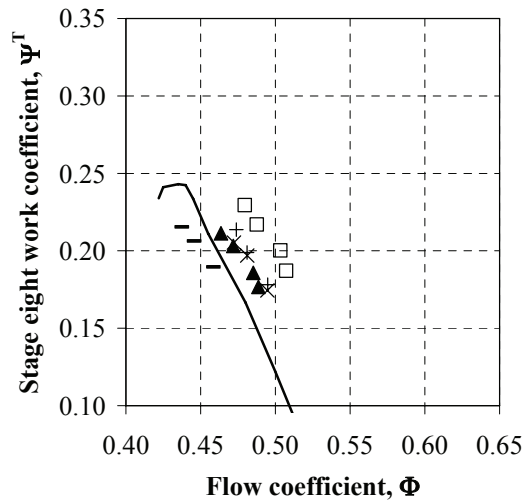
g) Stage five work coefficient



h) Stage six work coefficient

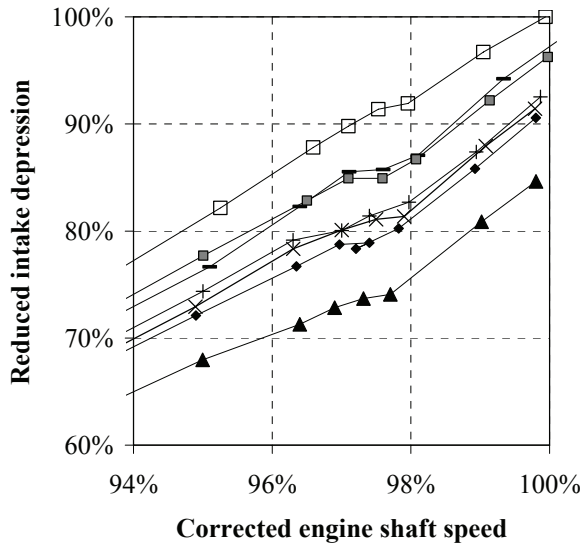


i) Stage seven work coefficient

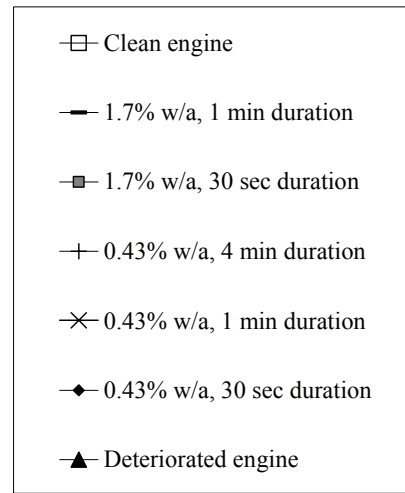


j) Stage eight work coefficient

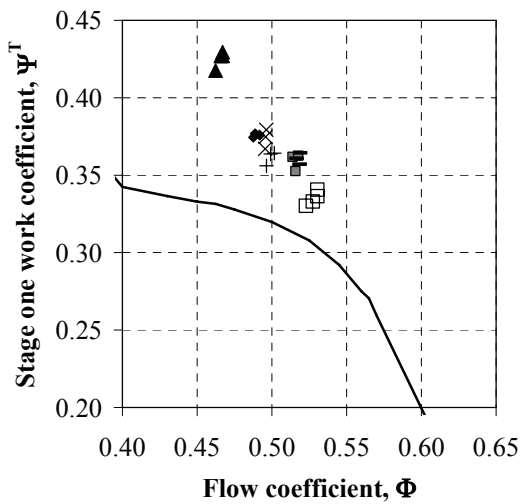
Figure 58 Dataset 2, stage five to eight



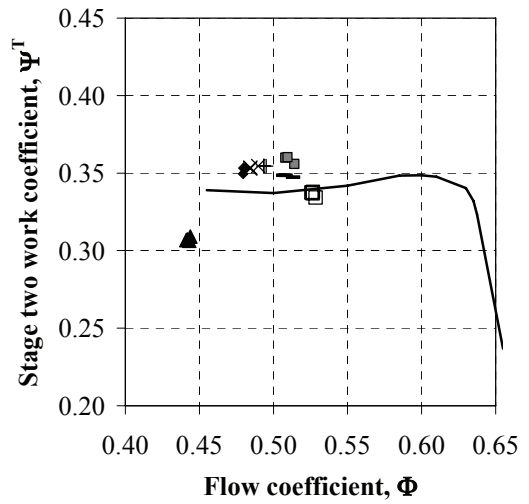
a) Intake depression



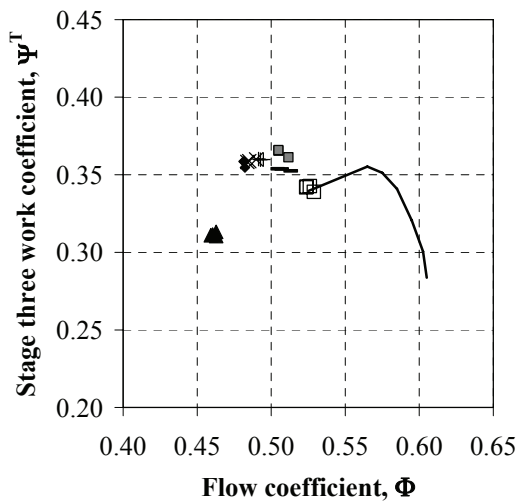
b) Dataset 3 legend



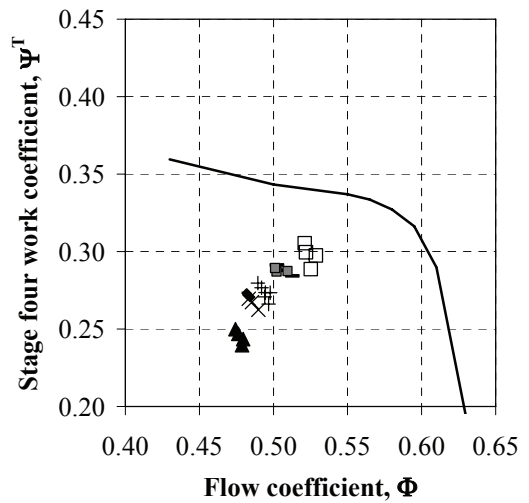
c) Stage one work coefficient



d) Stage two work coefficient

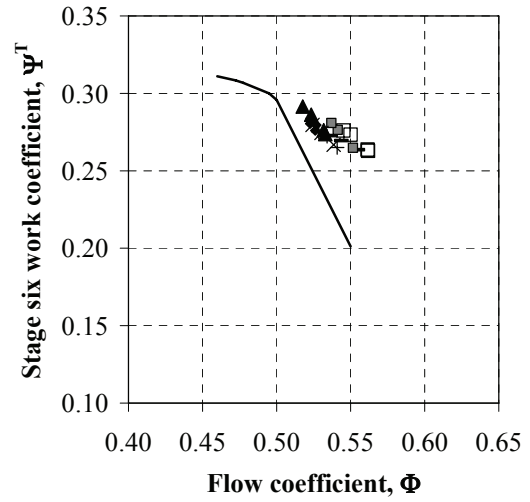
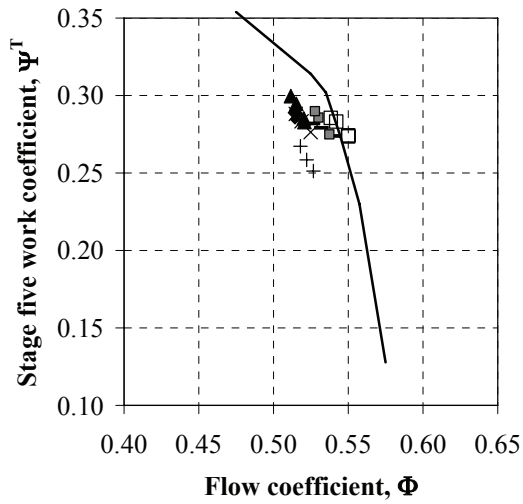


e) Stage three work coefficient



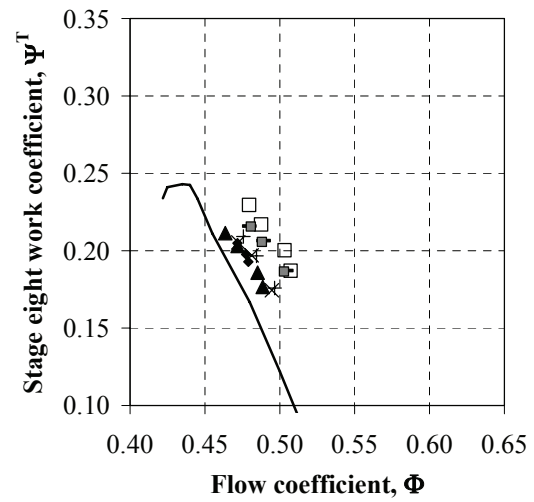
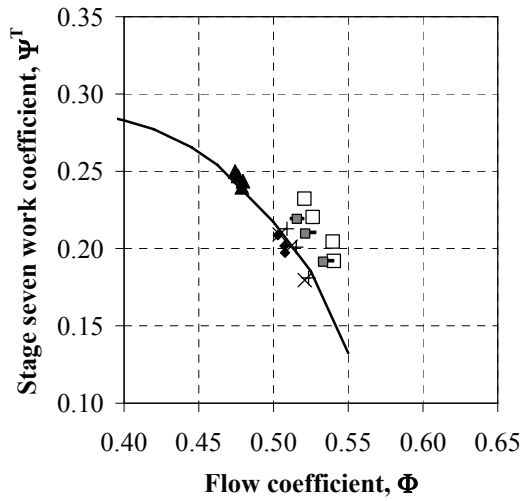
f) Stage four work coefficient

Figure 59 Dataset 3, stage one to four



g) Stage five work coefficient

h) Stage six work coefficient



i) Stage seven work coefficient

j) Stage eight work coefficient

Figure 60 Dataset 3, stage five to eight